UNIVERSITY OF OKLAHOMA

GRADUATE COLLEGE

BAYESIAN APPROACHES TO DETECT AND MITIGATE GROUND CLUTTER MIXED WITH WEATHER SIGNALS

A DISSERTATION

SUBMITTED TO THE GRADUATE FACULTY

in partial fulfillment of the requirements for the

Degree of

DOCTOR OF PHILOSOPHY

By

YINGUANG LI
Norman, Oklahoma
2013

BAYESIAN APPROACHES TO DETECT AND MITIGATE GROUND CLUTTER MIXED WITH WEATHER SIGNALS

A DISSERTATION APPROVED FOR THE
SCHOOL OF ELECTRICAL AND COMPUTER ENGINEERING

BY

Dr. Guifu Zhang, Co-chair

Dr. Richard Doviak, Co-chair

Dr. Robert Palmer

Dr. Xuguang Wang

Dr. Mark Yeary

Acknowledgements

First, I would like to thank my advisors Drs. Richard J. Doviak and Guifu Zhang, who are insightful and inspirational guides during my Ph.D. study. Their kindness and support will never be forgotten. Their stimulating suggestions, ideas, and encouragement help me persevere with my research. I also appreciate the valuable discussions with Drs. Qing Cao and Boon Leng Cheong, who are always ready to help. In addition, I would like to thank Drs. Robert Palmer, Xuguang Wang, and Mark Yeary for being my committee members.

For other friends and colleagues in the group, I would like to acknowledge their friendship: Dr. Shang Wang, Dr. Xinyi Shen, Dr. Youcun Qi, Dr. Zhengzheng Li, Fanxing Kong, Ying Bai, Qing Zhao, Dr. Shaya Karimkashi, Dr. Brad Isom, Benjamin Root, Dr. Sheng Chen, Dr. Xianwu Xue, Krysta Bruehl, Jo Ann Mehl, David Bodine, Tim Bonin, Petar Bukovcic, Jim Kurdzo, Feng Nai, Serkan Ozturk, Eric Jacobsen, Yu Pan, Hernan Suarez, and Yu Zhang.

Finally, I want to give my most gracious gratitude to my family, especially my wife, Lei Lei, and my one-year old son, Xunze. It’s them who make my life meaningful and promising. Their unwavering support and encouragement make all of this possible.

Table of Contents

List of Tables

List of Figures

Abstract

Ground clutter is a long standing issue in radar meteorology, considering that it can bring significant bias to the estimations of weather moments, polarimetric parameters, rainfall rate, hydrometeor identification, etc. Bayes' theorem is introduced and applied to signal processing of weather radar signals which distinguishes it from existing empirical methods to improve data quality. Five ground clutter detection algorithms are discussed, which are the Spectrum Clutter Identification (SCI), Simple Bayesian Classifier applied to the Dual-Scan discriminants (SBC-DS), test statistic obtained from the Generalized Likelihood Ratio Test (GLRT), Simple Bayesian Classifier applied to the Dual-Pol discriminants (SBC-DP), and Simple Bayesian Classifier applied to the Dual-Pol Dual-Scan discriminants (SBC-DPDS). One ground clutter filtering algorithm is developed, which is the Bi-Gaussian Model Adaptive Processing (BGMAP). The BGMAP algorithm will be applied to the clutter contaminated gates identified by ground clutter detection algorithms. The performances of the clutter detection and filtering algorithms are evaluated using the data collected by the OU-PRIME (University of Oklahoma-Polarimetric Radar for Innovation in Meteorology and Engineering) 5-cm polarimetric radar and PX-1000 3-cm polarimetric transportable radar.

Chapter 1: Introduction

Ground clutter is received when the mainlobe or sidelobes of the antenna illuminate objects on the ground. Weather data can be highly contaminated by ground clutter if the radar is measuring precipitation near the ground using elevation angles θ_e less than a beamwidth. Data at low θ_e are required to have accurate estimates of rainfall for long ranges. But clutter power can strongly bias the estimated spectral moments of the weather signal. The estimated reflectivity of the weather signal will be biased high, and the estimated mean radial velocity of the weather signal will be biased toward zero, but the estimated spectrum width bias has a more complicated dependence on the Clutter to Signal power Ratio (CSR), mean radial velocity, and spectrum width of the weather signal.

Because the spectrum of ground clutter is located around zero mean radial velocity, a band-stop filter centered at zero is commonly used to remove the effect of ground clutter according to Groginsky and Glover (1980). However, if power spectral components of weather fall into the stopband, a band-stop filter will bias the weather estimates. This can be more severe for narrow-band zero-velocity weather signals because most of the weather power components are suppressed by the filter. Thus, in order to avoid the potential bias, the efficient way is to first detect the locations of ground clutter and then apply ground clutter filter on those contaminated gates.

Resolution volumes that echo weather signals contaminated by ground clutter can be identified using a static clutter map determined from data collected in

clear-air conditions according to Meischner (2002). However, static clutter maps do not identify clutter locations that appear only under anomalous propagation (AP) conditions. Thus, an adaptive ground clutter detection algorithm is needed to detect ground clutter under both normal propagation (NP) and AP conditions.

One such adaptive approach is the decision tree algorithm introduced by Lee et al. (1995), which makes a clutter/non-clutter decision using radial velocity, spectrum width, minimum detectable signal, one-lag and two-lag signal fluctuations, the vertical gradient of reflectivity, and a continuously updated clutter map. A Radar Echo Classifier (REC) proposed by Kessinger et al. (2003) was deployed within the National Weather Service's WSR-88D ORPG (Open Radar Product Generator) build 2 and it uses fuzzy logic to classify the source of radar echoes including ground scatters seen via AP, precipitation, insects, and clutter associated with sea waves. Another approach introduced by Steiner and Smith (2002) uses the three dimensional reflectivity structure to detect ground clutter observed under both NP and AP conditions. The clutter mitigation decision (CMD) algorithm introduced by Hubbert et al. (2009a and 2009b) and tested by Ice et al. (2009) combines three discriminants: clutter phase alignment (CPA), texture of reflectivity (TDBZ), and SPIN (Steiner and Smith, 2002) using a fuzzy logic approach to determine the existence of clutter; it is currently used in the RDA (WSR-88D's Radar Data Acquisition subsystem) build 11 with GMAP (Gaussian Model Adaptive Processing) filter introduced by Siggia and Passarelli (2004) and has been tested by WSR-88D's Radar Operation Center to replace the bypass map according to Torres et al. (2012). The CLEAN-AP (CLutter Environment ANalysis using Adaptive Processing)

algorithm introduced by Warde and Torres (2010) combines a ground clutter detection algorithm and a ground clutter filter; it uses the phase of the auto-correlation spectral density, and it is shown that CLEAN-AP has better ground clutter mitigation (detection and filtering) than the current CMD/GMAP (Torres et al., 2012). A spectrum clutter identification (SCI) algorithm introduced by Li et al. (2013a) and tested by Cao et al. (2012) combines four discriminants: spectral power distribution, spectral phase fluctuations, spatial texture of echo power, and spatial texture of spectrum width to make decisions as to the presence of clutter; it is focused on detecting ground clutter mixed with weather signals, even if the clutter to signal ratio (CSR) is low but can still significantly bias the weather moment estimates.

A multipattern technique proposed by Zhang et al. (2011) demonstrated the potential of phased array radar (PAR) in detecting/mitigating ground clutter as well as moving clutter. Recently Li et al. (2013b) introduced a scan-to-scan correlation method to identify ground clutter, which takes advantage of the fact the correlation time of echoes from hydrometeors is typically much shorter than that from ground objects.

In addition to the clutter detection algorithms based on single polarization radar data introduced above, many ground clutter detection algorithms based on polarimetric radar data were also introduced. A fuzzy logic algorithm introduced by Gourley et al. (2007) combines horizontal reflectivity (Z_h), differential reflectivity (Z_{DR}), copolar correlation coefficient ($|\rho_{hv}(0)|$), mean radial velocity (v), pulse-to-

pulse variability of Z_h, and textures of Z_{DR} and differential propagation phase ϕ_{DP} to classify three classes: clear air echoes, ground clutter, and precipitation. A hydrometeor classification algorithm (HCA) proposed by Park et al. (2009) and Schuur et al. (2003) discriminates ten classes of weather radar echoes using fuzzy logic by combining six discriminants: Z_h, Z_{DR}, $|\rho_{hv}(0)|$, specific differential phase K_{DP}, and the textures of Z_h and ϕ_{DP} fields. Rico-Ramirez and Cluckie (2008) introduced a polarimetric classification algorithm in which eight input measurements are used to detect ground clutter received via NP and AP conditions; the eight measurements were combined by using both fuzzy logic and Bayesian classifiers. A clutter recognition algorithm using polarimetric spectral analysis introduced by Melnikov et al. (2008) combined polarimetric variables obtained from three central lines of the Doppler spectrum to determine the existence of ground clutter; the focus of this method is clutter recognition in a single range gate and the textures of polarimetric parameters are not used.

After the locations of ground clutter are detected, a ground clutter filter needs to be applied to the clutter contaminated gates to mitigate clutter effects and restore weather estimates. Considering that ground clutter is located around zero mean radial velocity, a band-stop filter (notch filter) centered at zero is commonly used to remove the effect of ground clutter (Groginsky and Glover, 1980) in the time domain. Recently, clutter filtering in the velocity (spectral) domain has received attention by the weather radar community considering the fact that the weather and clutter can be well separated in the spectral domain if their spectra are not heavily overlapped. Siggia and Passarelli (2004) introduced the Gaussian Model

Adaptive Processing (GMAP) method, which is capable of recovering the weather spectrum after notching the spectrum around zero Doppler. The limitation of spectral filtering is that the spectral leakage, caused by finite number of samples, might bias the spectral moment estimations. Nguyen et al. (2008) introduced the Parametric Time Domain Method (PTDM) algorithm; indicated by its name, PTDM algorithm is based on the estimation of signal properties in the time domain, the results are not affected by spectral leakage and therefore it performs well even in cases of strong clutter contamination. The main drawback of the PTDM is that it is roughly 10 times slower than the spectral filter.

In the detection section of this dissertation, the Simple Bayesian Classifier (SBC) is used to combine the discriminants derived from radar measurements to make decisions as to the presence of ground clutter. The SBC distinguishes itself from existing empirical classification algorithms such as fuzzy logic and decision tree (Lee et al., 1995; Kessinger et al., 2003; Hubbert et al., 2009a, 2009b) commonly used in the weather radar community, because the SBC is a statistical classifier based on Bayes' theorem and it can predict class membership probabilities such as the probability that a given tuple belongs to a particular class. In order to simplify the computations involved in the SBC, the assumption of class-conditional independence is made. In spite of its naïve design and over-simplified assumptions, the SBC has worked quite well in many complex real-world situations (Clark and Niblett, 1989). In the filtering section of this dissertation, the Maximum A Posteriori (MAP) approach based on the Bayes' theorem (Papoulis, 1991) is used to obtain the cost function. By minimizing the cost function, the weather spectral moments can be

estimated. The MAP approach was also used by Waldteufel (1976) to fit the tornado spectrum.

This dissertation is structured as follows. Five different ground clutter detection algorithms will be discussed in Chapter 2 and their performance will be evaluated using the radar data collected by the 5-cm dual-pol OU-PRIME (University of Oklahoma-Polarimetric Radar for Innovations in Meteorology and Engineering) radar (Palmer et al., 2011) and 3-cm dual-pol transportable PX-1000 radar. The ground clutter filtering algorithm, BGMAP (Bi-Gaussian Model Adaptive Processing), and its performance evaluation will be discussed in Chapter 3. In Chapter 4, conclusions and future work are given.

Chapter 2: Ground Clutter Detection Algorithms

To avoid potential bias caused by applying a ground clutter filter to uncontaminated weather signals, ground clutter contaminated weather signals are detected first and then the clutter filter is only applied to those weather signal samples having significant contamination. In this chapter, five different algorithms are discussed. In Section 2.1, the background of the Simple Bayesian Classifier (SBC) is discussed. In Section 2.2, a single-pol based Spectrum Clutter Identification (SCI) algorithm is introduced, which combines four discriminants using the SBC to make decisions as to the presence of ground clutter. In Section 2.3, the SBC-DS (Simple Bayesian Classifier applied to the Dual-Scan discriminants) algorithm is discussed, which takes advantage of the fact that the correlation time of

radar echoes from hydrometeors is typically much shorter than that from ground objects. In Section 2.4, two ground clutter detection algorithms based on dual pol measurement are discussed. In this section, a test statistic obtained from the generalized likelihood ratio test (GLRT), and a SBC applied to the Dual-Pol discriminants (SBC-DP), are developed to detect ground clutter mixed with weather signals. In Section 2.5, the SBC-DPDS (Simple Bayesian Classifier applied to the Dual-Pol Dual-Scan discriminants) algorithm is introduced. In Section 2.6, the performances of the five clutter detection algorithms are evaluated using the radar data collected by the OU-PRIME (5-cm polarimetric radar) and PX-1000 (3-cm polarimetric radar).

2.1 The Background of Simple Bayesian Classifier

Simple Bayesian Classifiers assume that the effect of an attribute value on a given class is independent of the values of the other attributes and it is called class-conditional independence. It simplifies the computations involved and thus is considered "simple". The SBC works as follows (Han et al., 2011):

1. Suppose *D* is a training set of tuples and their associated class labels. Each tuple consists of an *n*-dimensional attribute vector $\boldsymbol{X} = (x_1, x_2, ..., x_n)$ and an *n*-dimensional observation vector made on *n* attributes $\boldsymbol{X}^{\mathrm{O}} = (x_1^{\mathrm{O}}, x_2^{\mathrm{O}}, ..., x_n^{\mathrm{O}})$ where the superscript 'O' signifies observation. The attribute is equivalent to discriminant in this dissertation. For example, the differential reflectivity can be an attribute for polarimetric radar ground clutter detection.

2. Suppose that there are m classes, C_1, C_2, … C_m. For example, ground clutter is a class that differs itself from weather signal which is another class. Given an observation of the attributes, the classifier will predict that $\boldsymbol{X} = \boldsymbol{X}^{\mathrm{O}}$ belongs to the class having the highest posterior probability, conditioned on $\boldsymbol{X} = \boldsymbol{X}^{\mathrm{O}}$. That is, the SBC predicts that $\boldsymbol{X} = \boldsymbol{X}^{\mathrm{O}}$ belongs to the class C_i if and only if $p(C_i | \boldsymbol{X} = \boldsymbol{X}^{\mathrm{O}}) > p(C_j | \boldsymbol{X} = \boldsymbol{X}^{\mathrm{O}})$ for $1 \le j \le m$ and $j \ne i$. According to Bayes' theorem (Papoulis, 1991, Chap. 7-3):

$$p(C_i \mid \boldsymbol{X} = \boldsymbol{X}^{\mathrm{O}}) = \frac{p(\boldsymbol{X} = \boldsymbol{X}^{\mathrm{O}} \mid C_i)\, p(C_i)}{p(\boldsymbol{X} = \boldsymbol{X}^{\mathrm{O}})} \tag{2-1}$$

3. As $p(\boldsymbol{X} = \boldsymbol{X}^{\mathrm{O}})$ is constant for all classes (Han et al., 2011, Chap. 8.3), from (2-1) we have:

$$p(C_i \mid \boldsymbol{X} = \boldsymbol{X}^{\mathrm{O}}) \propto p(\boldsymbol{X} = \boldsymbol{X}^{\mathrm{O}} \mid C_i)\, p(C_i) \tag{2-2}$$

4. Given data sets with many attributes, it would be computationally expensive to calculate $p(\boldsymbol{X} = \boldsymbol{X}^{\mathrm{O}} \mid C_i)$. To reduce computations involved, the simple assumption of class-conditional independence is made, which presumes that the attributes' values are conditionally independent of one another, given the class label. Thus,

$$p(\boldsymbol{X} = \boldsymbol{X}^{\mathrm{O}} \mid C_i) = p(x_1 = x_1^{\mathrm{O}} \mid C_i) \times p(x_2 = x_2^{\mathrm{O}} \mid C_i) \times \cdots \times p(x_n = x_n^{\mathrm{O}} \mid C_i) \tag{2-3}$$

The probabilities $p(x_1 = x_1^{\mathrm{O}} \mid C_i)$, $p(x_2 = x_2^{\mathrm{O}} \mid C_i)$,…, $p(x_n = x_n^{\mathrm{O}} \mid C_i)$ can be obtained from the training tuples.

5. To predict the class label of $\boldsymbol{X} = \boldsymbol{X}^{\mathrm{O}}$, $p(\boldsymbol{X} = \boldsymbol{X}^{\mathrm{O}} \mid C_i)$ is evaluated for each class. The classifier predicts that the class label of $\boldsymbol{X} = \boldsymbol{X}^{\mathrm{O}}$ is the class C_i if and only if

$$p(\boldsymbol{X} = \boldsymbol{X}^{\mathrm{O}} \mid C_i)\, p(C_i) > p(\boldsymbol{X} = \boldsymbol{X}^{\mathrm{O}} \mid C_j)\, p(C_j),\ 1 \le j \le m \text{ and } j \ne i \tag{2-4}$$

Thus, the predicted class is the class C_i for which $p(\boldsymbol{X} = \boldsymbol{X}^{O} \mid C_i)p(C_i)$ is the maximum. In the next section, the spectrum clutter identification algorithm will be discussed.

2.2 Spectrum Clutter Identification (SCI) Algorithm

Considering that the statistics of the phase and the power of weather signals in the spectral domain are different from those statistics for echoes from stationary objects, a spectrum clutter identification (SCI) algorithm has been developed to detect ground clutter using single polarization radars, but SCI can be extended for dual-pol radars, which will not be discussed in this dissertation. SCI examines both the power and phase in the spectral domain and uses a Simple Bayesian Classifier (SBC) to combine four discriminants: spectral power distribution (section 2.2.1), spectral phase fluctuation (section 2.2.2), spatial texture of echo power (section 2.2.3), and spatial texture of spectrum width (section 2.2.4). These discriminants are used to make decisions as to the presence of clutter that can corrupt weather measurements. This work is focused on detecting ground clutter mixed with weather signals, even if the Clutter power to Signal power Ratio (CSR) is low but can still significantly bias weather moments. The performance of the SCI algorithm is shown by applying it to radar data collected by OU-PRIME in Section 2.6.1.

2.2.1 Spectral Power Distribution (SPD)

In this section SPD is defined and examples of its properties are shown when it is applied to combined simulated clutter and weather signal spectra of various CSRs. The SPD is calculated using the power spectrum $P(v)$ (i.e., $A^2(v)$, where $A(v)$ is the amplitude spectrum). The SPD is an indicator of how much power exists in

the interval $2\sqrt{2}\Delta v_w$ centered on zero Doppler velocity and how significant this power is as compared to power outside the interval. SPD is defined as:

$$\mathrm{SPD} = \frac{\sum_{-\sqrt{2}\Delta v_w}^{\sqrt{2}\Delta v_w} P(v)}{\sum_{-v_N}^{v_N} P(v) - \sum_{-\sqrt{2}\Delta v_w}^{\sqrt{2}\Delta v_w} P(v)} \tag{2-5}$$

In (2-5) v_N is the Nyquist velocity; $(\Delta v_w)^2$ is the second central moment of the observed clutter power spectrum. $(\Delta v_w)^2$ is principally due to the window function which will be explained later in this section, and $\pm\sqrt{2}\Delta v_w$ is the interval wherein the spectral power and phase characteristics of clutter and weather are examined. The larger is SPD, the more is power located within $\pm\sqrt{2}\Delta v_w$ relative to the power outside this interval; therefore SPD is related to CSR (Clutter power to Signal power Ratio). SPD is similar to CRN (Clutter Ratio Narrow) introduced by Hubbert et al. (2009b). CRN is the ratio of power within ± 0.5 m s^{-1} to that outside ± 0.5 m s^{-1} but within ± 2 m s^{-1}. Thus, CRN examines the power distribution around zero velocity whereas SPD examines the distribution for the entire spectrum. The CRN is not used in CMD because, as stated in (Hubbert et al., 2009b), CPA (Clutter Phase Alignment, a discriminant used in CMD) better discriminates narrow weather and clutter spectra than does CRN.

If we take the ratio of the spectral power of the zero Doppler to the total spectral power of all other spectral bins, the discriminant Power Ratio (PR) can be defined:

$$\mathrm{PR} = \frac{P(0)}{\sum_{-v_N}^{v_N} P(v) - P(0)} = \frac{\left|\frac{1}{M}\sum_{m=1}^{M} y_m\right|^2}{\frac{1}{M}\sum_{m=1}^{M}|y_m|^2 - \left|\frac{1}{M}\sum_{m=1}^{M} y_m\right|^2} \tag{2-6}$$

In (2-6), y represents the I/Q time series, m signifies the pulse number, and M is the total number of pulses in a dwell. From (2-6), it can be inferred that the ratio of the spectral power of the zero Doppler to the total spectral power of all other spectral bins can be calculated from the time domain rather than spectral domain, which is more computationally efficient. PR is not used in the SCI algorithm but will be discussed later in Sections 2.3-2.5.

In Table 2-1, the qualitative expected values of SPD given different conditions of weather signals and clutter are summarized, and functions *g*, *h*, and *u* indicate SPD is a function of the specified arguments.

Table 2-1: Qualitative expected values of SPD given different spectra.

	Clutter only (Fig.2-1a)	Weather only $\lvert v_{rw}\rvert \le 1$ m s^{-1} (Fig.2-1b)	Weather only $\lvert v_{rw}\rvert > 1$ m s^{-1}	Weather & clutter (not overlapped) (Figs. 2-1c,d)	Weather& clutter (overlapped) (Figs. 2-1e, f)
SPD	Large	$g(\sigma_{vw})$	Small	h(CSR)	u(CSR,v_{rw}, σ_{vw}.)

A Monte Carlo simulation (Li et al., 2013a) is used to obtain representative power spectra of clutter mixed with weather signals (Fig. 2-1). The parameters of the simulation are in Table 2-2; these match those of OU-PRIME, the weather radar

used to collect data for the performance evaluation of SCI algorithm. Only the relative strength and the Doppler velocity of weather change in each panel of Fig. 2-1. A Blackman window is applied to the simulated time series data. The red portions of the curves in Fig. 2-1 are within $\pm\sqrt{2}\Delta v_w$. The CNR [Fig. 2-1(a)] or SNR [Fig. 2-1(b)] or Signal plus Clutter to Noise Ratio SCNR (i.e., (S+C)/N) [Figs. 2-1(c)-(f)] are all set to 60 dB. The CSR is equal to 20 dB in Figs. 2-1(c) and (e), and equal to -15 dB in Figs. 2-1(d) and (f). In the figure caption, v_{rc}, σ_{vc}, and σ_{vw} are the mean radial velocity and spectrum width of clutter and spectrum width of weather signals; the panel entry v_{rw} is the estimated mean radial velocity for the weather signals; likewise v_{rs} and σ_{vs} entries are estimates for the summed spectrum. The rms (root mean square) value of turbulent velocities is fixed at 1 m s^{-1}, and the mean power, mean radial velocity and spectrum width are calculated in the spectral domain using all the spectral coefficients (i.e., no thresholds are applied). The spectral interval Δv between adjacent bins is equal to 0.1 m s^{-1}. The discriminant Spectral Phase Fluctuation (SPF) is discussed in Section 2.2.2.

Table 2-2**:** Radar and meteorological parameters used in the simulation.

wavelength (λ)	5.44 cm
One-way 3dB Beamwidth (θ_1)	0.5°
Scan Rate (α)	16° s^{-1} (0.28 radians per second)
Pulse Repetition Frequency (PRF)	1180 Hz
Number of Samples (M)	38
SCNR [(S+C)/N)]	60 dB

Turbulence Intensity (σ_t)	1 m s^{-1}
Mean Wind Velocity	0
Number of Stationary Scatterers	1
Number of Moving Scatterers	1000

In Figs. 2-1(a) and (b) (pure clutter and pure narrow-band weather signal), the SPD is equal to 5.6 and 2.4, respectively. The difference between the two SPD values is caused by the fact that the clutter spectrum is still narrower than the spectrum of the weather signal; thus more clutter power is within the spectral interval $\pm\sqrt{2}\Delta v_w$. The relatively large SPD difference suggests SPD has the capability to distinguish clutter from narrow-band zero-velocity weather signals.

In Figs. 2-1(c) and (d), the spectra of weather signal and clutter are not overlapped, and the SPD is equal to 4.6 and 0, respectively. SPD in panel (c) is larger than that in (d) because SPD (related to CSR) measures the ratio of power within $\pm\sqrt{2}\ \Delta v_w$ (i.e., mostly clutter power) and those outside of it (i.e., mostly weather power). Fig. 2-1(c) shows the estimates of radial velocity (v_{rs} = -0.3) and spectrum width (σ_{vs} = 1.9) of the summed spectra are significantly different from the weather signal's radial velocity (v_{rw} = -10) and spectrum width (σ_{vw} = 1). Fig. 2-1(d) suggests insignificant velocity estimate error due to clutter (CSR = -15 dB), but spectrum width estimates with clutter (i.e., σ_{vs} =1.4) are larger than σ_{vw} = 1, consistent with results to be shown in Table 2-3.

According to Section 3.7.1.2.3.1 of NEXRAD Technical Requirements (1991), bias in the estimates of both mean radial velocity (v_{rw}) and spectrum width (σ_{vw}) of weather signals shall be no more than 1 m s^{-1}. The bias due to clutter assuming v_{rw} is at the Nyquist velocity (the worst case condition for σ_{vw} estimate bias) is numerically calculated for SNR = infinity, in which both clutter (σ_{vc} = 0.6 m s^{-1}) and weather spectra have Gaussian shape. The minimum CSRs that cause a 1dB bias in mean power P_w and 1 m s^{-1} bias in v_{rw} and σ_{vw} estimates are shown in Table 2-3.

Table 2-3: The minimum CSR (dB), as a function of weather signal spectrum width (σ_{vw}), that causes biases of 1 dB in mean power (P_w) and 1 m s^{-1} in radial velocity (v_{rw}) and σ_{vw} estimates of weather signals.

	σ_{vw}=1	σ_{vw}=2	σ_{vw}=3	σ_{vw}=4	σ_{vw}=5	σ_{vw}=6
CSR(P_w)	-5.9	-5.9	-5.9	-5.9	-5.9	-5.9
CSR(v_{rw})	-11.8	-11.8	-11.8	-11.8	-11.8	-11.8
CSR(σ_{vw})	-19.2	-16.9	-15.3	-14	-12.8	-11.7

If the mean radial velocity of weather signal (v_{rw}) is at the Nyquist velocity (i.e., 16.06 m s^{-1} for OU-PRIME), the CSR needs to be -5.9 dB to bias the mean power 1 dB, but it only needs to be -11.8 dB to bias v_{rw} by 1 m s^{-1}, independent of the spectrum width (σ_{vw}) of the weather signal. But if σ_{vw} equals 1 m s^{-1}, the CSR only needs to be -19.2 dB to bias σ_{vw} to 2 m s^{-1}. Thus, it is concluded detection of

clutter down to a CSR = -15 dB is important considering the bias it can bring to the estimates of Doppler velocity and spectrum width; these two spectral moments place more stringent detection requirements on the clutter detectors than the error specified (i.e., 1 dB) for power measurements. If all the clutter power is within the interval $\pm\sqrt{2}\Delta v_w$ while all the weather power is outside of it, SPD = 0.03 if CSR = -15 dB. Thus, SPD = 0.03 will be used as a preliminary threshold to distinguish clutter from weather signals in Section 2.2.5.

In Figs. 2-1(e) and (f), the spectra of weather signal and clutter are overlapped, and the SPD is equal to 3.9 and 2.1, respectively. SPD in Fig. 2-1(e) is larger than that in Fig. 2-1(f) because the CSR is 20 dB and thus the SPD, as well as σ_{vs}, is more strongly influenced by clutter, whereas in Fig. 2-1(f) CSR is -15 dB and the weather spectrum mostly controls SPD. From Fig. 2-1(f), it can be seen that all the three radar moments of weather signals are almost equal to those of the summed spectra if the spectra are overlapped and CSR is equal to -15 dB or smaller.

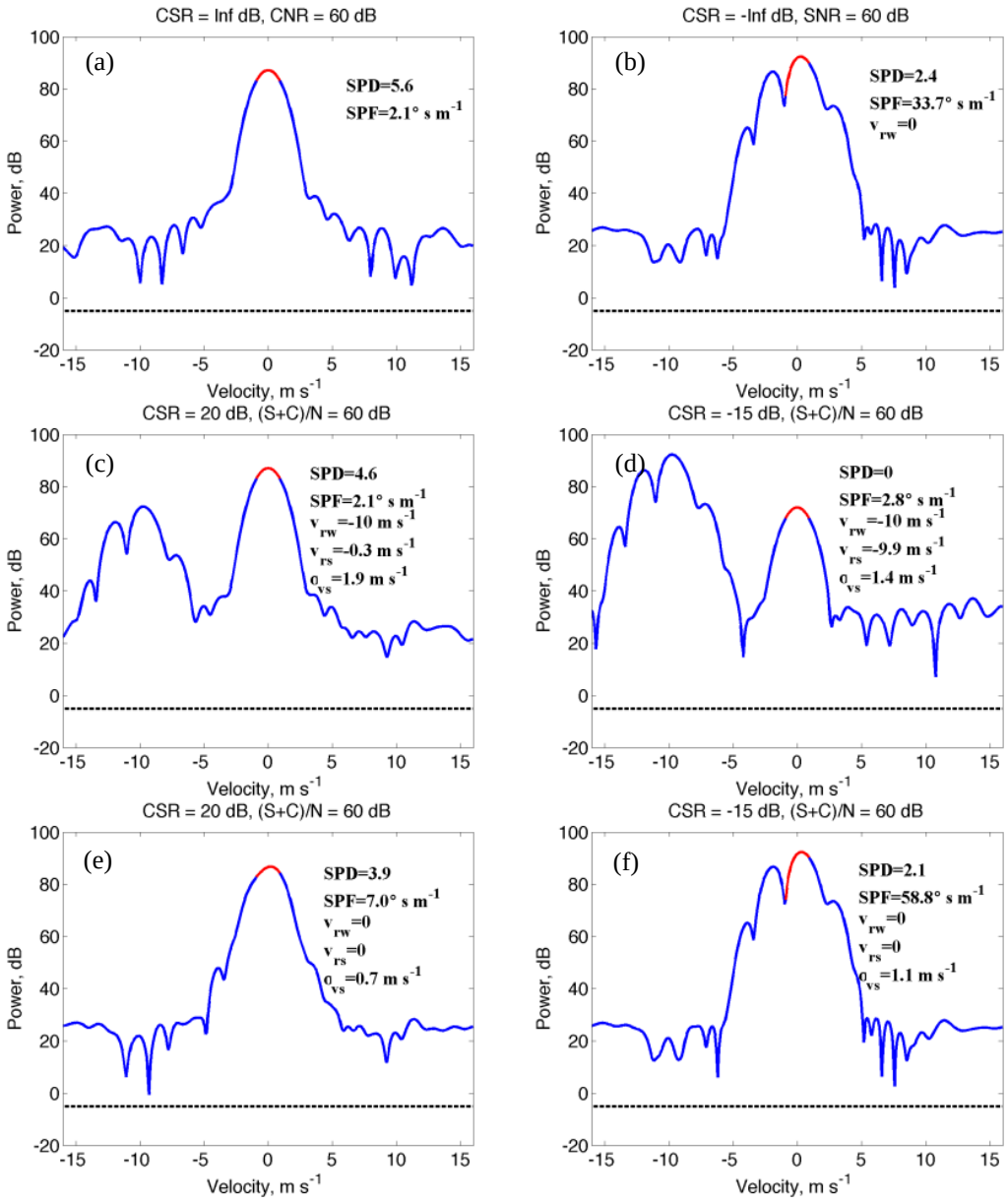

Figure 2-1: Spectra of simulated clutter mixed with a simulated narrow-band weather signal. The black dashed line is the noise floor and the red portions of the curves are within $\pm\sqrt{2}\,\Delta v_w$. $v_{rc} = 0$, $\sigma_{vc} = 0.6$ m s^{-1} and $\sigma_{vw} = 1.0$ m s^{-1}. This figure can also be found in Li et al., (2013a).

Approximation of the Observed Clutter Spectrum Width

The spectral interval $\pm \sqrt{2}\,\Delta v_w$ is determined wherein the spectral power and phase characteristics of clutter and weather are examined to detect the presence of significant clutter. Δv_w is determined by the beam's scan rate, the *intrinsic* spectrum width of the clutter, the dwell time, and the window weighting function. In order to reduce spectral leakage, a Blackman window with a maximum sidelobe level (SLL) of 58.1 dB is applied to the time-series data (Harris, 1978).

The *observed (measured)* clutter spectrum is broader than the *intrinsic* spectrum of clutter. The *intrinsic* clutter spectrum (i.e., the spectrum associated only with the physical characteristics of clutter) is the spectrum observed with asymptotic data collection parameters (i.e., T_s, the pulse repetition time, goes to zero and T_d, the dwell time, goes to infinity) when the beam is not scanning. The *intrinsic* spectra of clutter for urban, prairie, and wooded regions has been characterized, under conditions of full and light foliage and various intensities of wind, using a phased array radar and nearly asymptotic data collection parameters according to Curtis (2009). If the ground scatterers are fixed objects that do not move, nor have internal motions (henceforth these are called hard scatterers), the intrinsic clutter spectrum is a delta function centered on zero velocity. Billingsley (2002) states "… *Such a cell contains both fixed scatterers (ground, rocks, tree trunks) and moving scatterers (leaves, branches). The returned signal correspondingly contains both a constant (or steady) and a varying component.*" It can be calculated using the exponential model (Billingsley, 2002) that the *intrinsic spectrum width* of tree clutter is equal to

0.03, 0.08, 0.19, and 0.31 m s^{-1} respectively under light air (1-7 mph), breezy (7-15 mph), windy (15-30 mph), and gale force conditions (30-60 mph) for a 5-cm radar.

The *asymptotic* clutter spectrum is the one observed with asymptotic data collection parameters when the beam is scanning. The asymptotic spectrum can, at best, only be approximated because an infinite dwell time would require spatial homogeneity (in a statistical sense) of the ground scatterers as they are being scanned. If the scatterers are many and hard, the *asymptotic* spectrum has a finite width proportional to the antenna diameter D_a and the angular scan rate α. The square of the *asymptotic* clutter spectrum width caused by a Gaussian shaped beam pattern scanning at the angular rate α can be written as (Doviak and Zrnić, 2006, Appendix C):

$$\sigma_\alpha^2 = \left(\frac{\alpha \cos\theta_e D_a}{2.54\pi} \right)^2 \ln 2 = \left(\frac{\alpha\lambda \cos\theta_e}{2\pi\theta_1} \right)^2 \ln 2 = \frac{\alpha^2 \cos^2\theta_e}{16 k^2 \sigma_\theta^2} \qquad (2\text{-}7)$$

In (2-7), θ_e is the elevation angle (it will be assumed smaller than 5°; therefore $\cos\theta_e \approx 1$), θ_1 is the 3-dB one-way power pattern beamwidth, λ is the wavelength, $k = 2\pi/\lambda$ is the wave number, σ_θ^2 is the second central moment of the two-way power pattern and it is equal to $\theta_1^2 / 16\ln 2$ (Doviak and Zrnic, 2006, Section 5.3).

OU-PRIME had a beam scanning at a rate of 16° s^{-1} and processed 38 signal samples spaced at the PRT (Pulse Repetition Time) equal to 847 μs; thus the dwell time T_d=32.19 ms. Given the 3-dB one-way beamwidth θ_1 equals to 0.5°, $\theta_e \le 5°$, and λ=5.44 cm, σ_α is about 0.23 m s^{-1}. It will be assumed clutter is primarily from

hard scatterers on the ground; that is, the *intrinsic* clutter spectrum is a delta function, and the *asymptotic* clutter spectrum width is equal to σ_α. It can also be inferred that the spectrum width due solely to resolution volume displacement (0.23 m s^{-1}) dominates that due to physical motions of trees if it is under the light air and breezy conditions (0.03 and 0.08 m s^{-1}).

The *observed* clutter spectrum is the spectrum observed when the beam is scanning and actual data acquisition parameters are used. The *observed* clutter spectrum is the convolution of the *asymptotic* clutter spectrum and the spectrum associated with the Blackman window function. Thus, the expected width, Δv_w, of the observed clutter is $\Delta v_w = \sqrt{\sigma_B^2 + \sigma_\alpha^2}$. If the power spectrum of the Blackman window is W(v), the square root of the second central moment σ_B^2 of the power spectrum of Blackman window, numerically evaluated, can be approximated by:

$$\sigma_B = \sqrt{\frac{\int_{-v_N}^{v_N} v^2 W(v)\,dv}{\int_{-v_N}^{v_N} W(v)\,dv}} \approx \frac{0.34\lambda}{T_d} \approx 0.58 \text{ m s}^{-1} \qquad (2\text{-}8)$$

From (2-8), it is evident σ_B is inversely proportional to the dwell time T_d, and because $\sigma_\alpha = 0.23$, $\sigma_B \approx 2.5\sigma_\alpha$. Because T_d and α values in this work are those typically used operationally and are fixed, Δv_w is a constant. Thus, the broadening effect of the Blackman window dominates the broadening effect due to beam scanning so $\Delta v_w \approx \sigma_B$.

2.2.2 Spectral Phase Fluctuation (SPF)

In this section the discriminant SPF is defined. Numerical simulations and theory show the spectral phase $\xi(v)$ of clutter from a hard scatterer has a linear dependence on *v,* but the spectral phase of weather signal is a random function of *v*. Thus, the linearity of spectral phase in the spectral interval $\pm\sqrt{2}\,\Delta v_w$ could also be a good discriminant to distinguish clutter from weather signals.

In order to have more spectral phase data points within the interval $\pm\sqrt{2}\,\Delta v_w$ to compute SPF, zero padding to the time series data is applied after the window function. It is stated that zero padding in the time domain corresponds to *ideal interpolation* in the frequency domain according to Smith III (2007). The SPF was applied with and without zero padding and it was found the skill of SPF increased with zero padding because SPF can be more accurately estimated with more spectral lines within $\pm\sqrt{2}\,\Delta v_w$. Without zero padding only three spectral lines are within $\pm\sqrt{2}\,\Delta v_w$, but with zero padding there are 18 spectral lines. SPF calculates the standard deviation (SD) of the phase slope a(v) within the spectral interval. The SPF is defined as:

$$\mathrm{SPF} = \mathrm{SD}[\mathrm{a}(v)] = \mathrm{SD}\left[\frac{\xi(v)-\xi(v-\Delta v)}{\Delta v}\right],\ v \in \left[-\sqrt{2}\Delta v_w + \Delta v : \sqrt{2}\Delta v_w\right] \qquad (2\text{-}9)$$

The phase term $\xi(v)$ is unwrapped to avoid that the absolute jump between consecutive phase elements that is larger than or equal to $\pm\,\pi$. In (2-9), Δv is the spectral interval between adjacent bins and it is equal to 0.1 m s^{-1}. SPF measures how much the phase within the spectral interval $\pm\sqrt{2}\,\Delta v_w$ deviates from a straight

line. If all the phase elements within the spectral interval are on a straight line, SPF is equal to zero. SPF is small for clutter, but larger if the weather spectrum overlays the clutter spectrum within $\pm\sqrt{2}\,\Delta v_w$. Examples of the power spectrum $P(v)$ and spectral phase slope a(v) from real data collected by OU-PRIME are shown in Fig. 2-2.

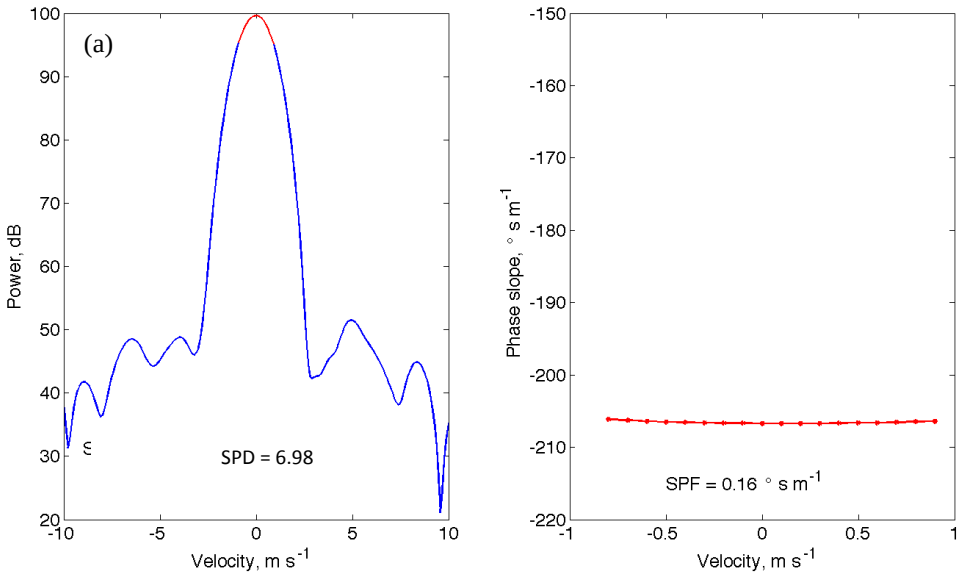

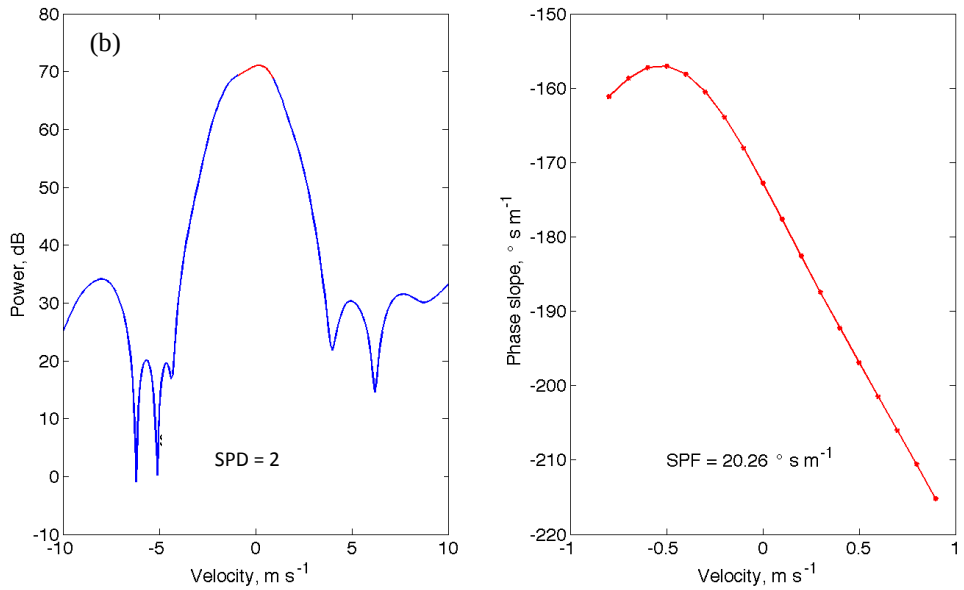

Figure 2-2: Power spectrum $P(v)$ and spectral phase slope a(v) within the spectral intervals ± 10 m s^{-1} and $\pm\sqrt{2}\Delta v_w$, respectively. (a) Clutter spectrum from clutter data: $v_{rc} = 0$, $\sigma_{vc} = 0.8$ m s^{-1}, and $\rho_{hv} = 0.58$; The clutter data were collected at 23:19 UTC on 01/13/2011 under clear condition with $\theta_e = 0$ by OU-PRIME; (b) Narrow-band zero-velocity weather signal spectrum from stratiform weather data: $v_{rw} = 0$, $\sigma_{vw} = 1.0$ m s^{-1}, and $\rho_{hv} = 0.997$; The weather data were collected at 05:51 UTC on 12/02/2009 under stratiform precipitation condition with $\theta_e = 3.5°$.

If the phase $\xi(v)$ in the spectral interval $\pm\sqrt{2}\,\Delta v_w$ lies on a straight line, the phase slope a(v) in this spectral interval should be a constant. As can be seen from Fig. 2-2(a), the spectral phase slope of clutter is almost a constant in the spectral interval but that of narrow-band zero- velocity weather signal is not. SPF is equal to 0.16° s m^{-1} in Fig. 2-2(a) and 20.26° s m^{-1} in Fig. 2-2(b). In addition, SPF is calculated for the simulated spectra shown in Fig. 2-1.

In Figs. 2-1(a) and (b), SPF is respectively equal to 2.1 and 33.7° s m^{-1} and these results suggest the SPF has the capability of distinguishing clutter from narrow-band zero-velocity weather signals. In Figs. 2-1(c) and (d), SPF is respectively equal to 2.1 and 2.8° s m^{-1}, both of which are small, which means SPF is almost not affected by CSR when v_{rw} is equal to -10 m s^{-1} (i.e., the spectral power of clutter is dominant in the spectral interval $\pm\sqrt{2}\,\Delta v_w$); In Figs. 2-1(e) and (f), SPF is respectively equal to 7.0 and 58.8° s m^{-1}, which means if the spectra of clutter and weather signal are overlapped and the weather power is dominant in the spectral interval $\pm\sqrt{2}\,\Delta v_w$, the phase of the spectral elements within $\pm\sqrt{2}\,\Delta v_w$ do not have a linear dependence on Doppler velocity.

2.2.3 Power Texture (PT)

In this section PT is defined. In this dissertation, the definition of texture is different from the one defined in Hubbert et al. (2009b). The texture in Hubbert et al. (2009b) is defined as the mean of the squared reflectivity difference between adjacent gates whereas the definition of texture in this dissertation is given by (2-10). The discriminant PT takes advantage of the fact that the mean power of weather signals is spatially more uniform than the mean power of clutter. PT is defined as:

$$\mathrm{PT}_{i,j} = \frac{\mathrm{SD}\left[P_{i,j-L:j+L}\right]}{\mathrm{MEAN}\left[P_{i,j-L:j+L}\right]} \tag{2-10}$$

$PT_{i,j}$ is the power texture at azimuth ϕ_i and range r_j. The standard deviation of power about its mean is calculated along the range for 9 gates (i.e., L = 4) centered on gate i,j.

2.2.4 Spectrum Width Texture (SWT)

In this section SWT is defined. Fang et al. (2004) pointed out that the spectrum width has significant error if the in-trip echo power is less than 20 dB stronger than the sum of out-of -trip echo powers. Applied to our case, it means that even if CSR is as small as -20 dB, the spectrum width of weather signal can have significant bias (Table 2-3). Ground clutter power is spatially variable compared to weather echo power and this is the reason why PT is an effective discriminant if the clutter power is dominant. However, if CSR is smaller than 0 dB, PT becomes less effective and clutter detection becomes difficult as noted by Hubbert et al. (2009b). On the other hand, estimated spectrum widths of weather signals can be significantly biased by clutter power, especially if the mean radial velocity of weather signal is far from zero. In this case SWT can be useful both when the CSR is low or high. However, when the radial velocity of weather signal is small and CSR is large, analysis has shown SWT is not as effective as PT.

For narrow-band weather signals and SNR > 15 dB, the APD (Absolute Power Differences) spectrum width estimator proposed by Melnikov and Doviak (2002) has better performance than the more commonly used estimators. The APD spectrum width estimator is:

$$\hat{\sigma}_v = \frac{\lambda}{4\pi T_s} \ln^{1/2} \frac{1}{\left\{1-\left[\Delta\hat{P}(T_s)/\hat{P}\right]^2\right\}\left\{1+\left[\overline{N}/(\hat{P}-\overline{N})\right]\right\}^2} \tag{2-11a}$$

$$\Delta\hat{P}(T_s) = \frac{1}{M-1}\sum_{k=1}^{M-1}\left|P_{k+1}-P_k\right| \tag{2-11b}$$

$$\hat{P} = \frac{1}{M}\sum_{k=1}^{M} P_k \tag{2-11c}$$

Where the diacritical hat $\wedge$ defines an estimate. M is the number of samples per dwell time T_d. The estimated power $\hat{P}$ is equal to the summation of signal power $\hat{S}$, clutter power $\hat{C}$, and average noise power $\overline{N}$. $\overline{N}$ is estimated with many more samples than that used to estimate $\hat{P}$ and is the reason for the overbar above N. The average noise power can be estimated by the gates (usually far from the radar) that only contain noise power. The definition of SWT is the same as PT shown in (2-10) except power P is changed to spectrum width σ_v.

The disadvantage of using PT or SWT is that it will increase the number of false positives (i.e., weather signals mistakenly identified as clutter). For example, if only one gate is contaminated by strong ground clutter, all nine range gates centered on the clutter gate could be tagged as having significant clutter even if there is no clutter. On the other hand because in the SCI algorithm, SPD discriminant is applied first (Section 2.2.5), and if SPD < 0.03, data from that gate will tagged as weather and thus data from this gate will not be falsely tagged by the PT or SWT discriminant as having significant clutter.

2.2.5 Implementation Procedures of the SCI Algorithm

In this dissertation, three classes are considered: ground clutter (class 'c'), weather signal I (class 'w0', narrow-band zero-velocity weather signals, $|\hat{v}| < 2$ m s^{-1} and $\hat{\sigma}_v < 2$ m s^{-1}), and weather signal II (class 'w', other weather signals).

$\boldsymbol{X}$ represents the 4-D attribute vector, $\boldsymbol{X}$ = (SPD, SPF, PT, SWT). For the current resolution volume, $\boldsymbol{X} = \boldsymbol{X}^{\mathrm{O}}$ (superscript 'O' represents the observed discriminants) and $\boldsymbol{X}^{\mathrm{O}} = \left(\mathrm{SPD}^{\mathrm{O}}, \mathrm{SPF}^{\mathrm{O}}, \mathrm{PT}^{\mathrm{O}}, \mathrm{SWT}^{\mathrm{O}}\right)$. The SBC predicts whether the $\boldsymbol{X} = \boldsymbol{X}^{\mathrm{O}}$ belongs to c, w0, or w. $\boldsymbol{X} = \boldsymbol{X}^{\mathrm{O}}$ belongs to c only if $p(\boldsymbol{X} = \boldsymbol{X}^{\mathrm{O}}|\mathrm{c})p(\mathrm{c}) > p(\boldsymbol{X} = \boldsymbol{X}^{\mathrm{O}}|\mathrm{w0})p(\mathrm{w0})$ and $p(\boldsymbol{X} = \boldsymbol{X}^{\mathrm{O}}|\mathrm{c})p(\mathrm{c}) > p(\boldsymbol{X} = \boldsymbol{X}^{\mathrm{O}}|\mathrm{w})p(\mathrm{w})$ according to (2-4).

Because the prior probabilities p(c), p(w0), and p(w) are not known a priori, all classes are assumed equally likely, which is $p(\mathrm{c}) = p(\mathrm{w0}) = p(\mathrm{w}) = 1/3$. Thus, we can infer that SBC assigns $\boldsymbol{X} = \boldsymbol{X}^{\mathrm{O}}$ to c only if $p(\boldsymbol{X} = \boldsymbol{X}^{\mathrm{O}}|\mathrm{c}) > p(\boldsymbol{X} = \boldsymbol{X}^{\mathrm{O}}|\mathrm{w0})$ and $p(\boldsymbol{X} = \boldsymbol{X}^{\mathrm{O}}|\mathrm{c}) > p(\boldsymbol{X} = \boldsymbol{X}^{\mathrm{O}}|\mathrm{w})$. $p(\boldsymbol{X} = \boldsymbol{X}^{\mathrm{O}} \mid i)$, i = c, w0, and w, is equal to:

$$p(\boldsymbol{X} = \boldsymbol{X}^{\mathrm{O}} \mid i) = p(\mathrm{SPD} = \mathrm{SPD}^{\mathrm{O}}, \mathrm{SPF} = \mathrm{SPF}^{\mathrm{O}}, \mathrm{PT} = \mathrm{PT}^{\mathrm{O}}, \mathrm{SWT} = \mathrm{SWT}^{\mathrm{O}} \mid i) \quad (2\text{-}12)$$

According to (2-3), (2-12) can be rewritten as:

$$\begin{aligned} p(\boldsymbol{X} = \boldsymbol{X}^{\mathrm{O}} \mid i) = {} & p(\mathrm{SPD} = \mathrm{SPD}^{\mathrm{O}} \mid i) \times p(\mathrm{SPF} = \mathrm{SPF}^{\mathrm{O}} \mid i) \\ & \times p(\mathrm{PT} = \mathrm{PT}^{\mathrm{O}} \mid i) \times p(\mathrm{SWT} = \mathrm{SWT}^{\mathrm{O}} \mid i) \end{aligned} \quad (2\text{-}13)$$

The conditional probability density functions of SPD SPF, SWT and PT, given different classes can be obtained from ground truth (i.e., clutter data obtained in clear air conditions and weather data obtained at high elevation angles), which is also the training data. Thus, the joint conditional probability density function

$p(\boldsymbol{X} \mid i)$ can be calculated for each class. One needs to be aware that $p(\boldsymbol{X} \mid i)$ is dependent on the radar sites, radar characteristics, scan strategies, and environmental conditions.

The SCI algorithm is divided in the following steps:

1) Calculate SCNR/SNR. If SCNR/SNR > 3 dB, go to step 2), otherwise the current gate is considered not to have significant weather; then compute SCNR/SNR for the next range gate.

2) Apply the Blackman window function and then add zeros to the time series data if necessary.

3) Compute SPD. If SPD>0.03, go to step 4), otherwise the current gate is considered not clutter contaminated. This SPD threshold reduces the number of false positives caused by the texture discriminants; the threshold of 0.03 corresponds to a CSR equal to -15 dB (Section 2.2.1).

4) Compute SPF, PT, and SWT. Look up the joint conditional PDF $p(\boldsymbol{X} \mid i)$ obtained from ground truth. Calculate $p(\boldsymbol{X} = \boldsymbol{X}^{\mathrm{O}} \mid \mathrm{c})$, $p(\boldsymbol{X} = \boldsymbol{X}^{\mathrm{O}} \mid \mathrm{w}\,0)$, and $p(\boldsymbol{X} = \boldsymbol{X}^{\mathrm{O}} \mid \mathrm{w})$.

5) If $p(\boldsymbol{X} = \boldsymbol{X}^{\mathrm{O}} \mid \mathrm{c}) > p(\boldsymbol{X} = \boldsymbol{X}^{\mathrm{O}} \mid \mathrm{w}\,0)$ and $p(\boldsymbol{X} = \boldsymbol{X}^{\mathrm{O}} \mid \mathrm{c}) > p(\boldsymbol{X} = \boldsymbol{X}^{\mathrm{O}} \mid \mathrm{w})$ for the current gate, data are clutter contaminated, otherwise, data are not contaminated; then return to step 1) for the next gate.

The performance evaluation of the SCI algorithm will be given in Section 2.6.1.

2.3 Simple Bayesian Classifier applied to the Dual-Scan Discriminants (SBC-DS)

The SBC-DS algorithm to discriminate weather signals from ground clutter, described in this dissertation, takes advantage of the fact the correlation time of radar echoes from hydrometeors is typically much shorter than that from ground objects. Because the typical correlation time of weather signals from 10-cm wavelength radar is less than 10 ms for most weather phenomena according to Fang et al. (2004), such signals generally do not correlate from one 360^{o} azimuthal scan to the next. Ground clutter observed both under NP and AP conditions should have correlation times much longer than that associated with weather signals, and thus the SBC-DS algorithm should apply as well to clutter received via AP conditions. Because much of the ground clutter has long correlation times, Fabry (2004) was able to use the scan-to-scan phase difference of clutter to measure changes in the field of refractive index of air near the surface. The focuses of this method are 1) clutter recognition gate by gate whereby reflectivity texture is not used and 2) distinguishing ground clutter from narrow-band zero-velocity weather signals.

In this method three discriminants are combined using SBC to distinguish ground clutter from weather signals: (1) Cross-correlation coefficient between two scans at zero lag $\left|\rho_{12}(0)\right|$ (SNR > 20 dB, the 20 dB threshold can be found in

Melnikov and Zrnic 2007) or first lag $|\rho_{12}(1)|$ (SNR ≤ 20 dB), (2) Power Ratio of the first scan (PR_1), and (3) Power Ratio of the second scan (PR_2). In Section 2.3.1, the definition of the discriminant $|\rho_{12}(l)|$ is given; In Section 2.3.2, the definitions of PR_1 and PR_2 are given. In Section 2.3.3, the implementation procedures of the SBC-DS algorithm are discussed.

2.3.1 Cross-Correlation Coefficient between Two Scans

A time-series of echo voltages from two scans need to be collected from the same location (i.e., the same azimuth and elevation angle). In the volume coverage patterns (VCPs) of the WSR-88D, two sequential azimuthal scans with different PRTs (Pulse Repetition Times) are used at each of two low elevation angles (i.e., 0.5° and 1.5°) to mitigate range-velocity ambiguities (Federal Handbook, 2006, Chap. 5.3.2). The first azimuthal scan collects voltage samples data using a long PRT (e.g., T_{s1} = 3.10 ms) and the second scan at the same elevation angles uses a short PRT (e.g., T_{s2} = 973 μs). To implement the SBC-DS algorithm, the short PRT data are non-uniformly down-sampled to nearly match the location of voltage samples collected with long PRT. Because the WSR-88D records the azimuth of each voltage sample, we were able to select those short PRT voltage samples that are nearest in azimuth to the long PRT voltage samples. The largest beam displacement for the two adjacent scans is about 0.02° for the WSR-88D.

Assuming the signals to be wide sense stationary, the cross correlation coefficient between two scans $|\rho_{12}(l)|$ for l = 0 or 1 is defined as:

$$\left|\rho_{12}(l)\right| = \frac{\left|E\left\{y_{1,m+l}y_{2,m}^{*}\right\}\right| + \left|E\left\{y_{1,m}y_{2,m+l}^{*}\right\}\right|}{2\sqrt{\left|E\left\{y_{1,m+l}y_{1,m}^{*}\right\}E\left\{y_{2,m+l}y_{2,m}^{*}\right\}\right|}}, \quad 0 \le m \le M - |l| - 1 \qquad (2\text{-}14)$$

M is the number of samples in the dwell time; y_1 is the time-series of voltage samples from the first scan, and y_2 is the down-sampled time-series of voltage samples from the second scan from the same volume but collected at a higher pulse repetition frequency (PRF); $E\{\mathrm{x}\}$ represents an ensemble average. Because y_1 and y_2 are assumed to be ergodic in the wide sense, the ensemble average can be approximated by a time average (Papoulis, 1991, Chap. 13-1). l = 1 only if SNR is less than 20 dB in order to avoid the bias caused by noise.

Because the correlation time of ground clutter is typically much longer than that for weather signals, $\left|\rho_{12}(l)\right|$ is expected to be larger for ground clutter than for both the weather signal I (narrow-band zero-velocity weather signals) and weather signal II (other weather signals). Weather signal I are echoes from resolution volumes where turbulence and mean wind shear are weak; thus these signals commonly have longer correlation time τ_c compared with weather signal II having no constraint on bandwidth. On the other hand, weather signal I have fewer independent samples ($M_I = T_d / \sqrt{\pi}\tau_c$, where M_I is the number of independent samples and T_d is the dwell time). Because estimate variance decreases as a function of the number of independent samples according to Marshall and Hitschfeld (1953), the variance of CPDF (Conditional Probability Density Function) of $\left|\rho_{12}(l)\right|$ estimates for weather signal I is typically larger than for weather signal II

having no constraint on bandwidth. This is likely the reason why the CPDF of weather signal I is broader than the CPDF for weather signal II which will be shown in Fig. 2-11 in the performance evaluation section. Ground clutter correlation time (as low as 44 ms from full foliage prairie for 10-cm wavelength echoes when the wind is about 13 mph according to Curtis 2009 Chap. 2.10) can be much smaller than the radar revisit time, but is still much larger than the correlation time for weather signals.

2.3.2 Power Ratio (PR)

The definition of PR is already given in (2-6), and it is rewritten here as:

$$\mathrm{PR}_i = 10\log 10\left[\frac{\left|\frac{1}{M}\sum_{m=1}^{M} y_{i,m}\right|^2}{\frac{1}{M}\sum_{m=1}^{M}\left|y_{i,m}\right|^2 - \left|\frac{1}{M}\sum_{m=1}^{M} y_{i,m}\right|^2}\right], \text{ where } i = 1 \text{ or } 2 \qquad (2\text{-}15)$$

It is expected that PR is larger for ground clutter than for both weather signal I and II considering that ground clutter has zero Doppler and narrow spectrum width.

2.3.3 Implementation Procedures of the SBC-DS Algorithm

In the SBC-DS algorithm, the 3-D attribute vector is $\boldsymbol{X} = (\left|\rho_{12}(l)\right|, \mathrm{PR}_1, \mathrm{PR}_2)$ and $p(\boldsymbol{X} = \boldsymbol{X}^{\mathrm{O}} \mid i) = p(\mid \rho_{12}(l) \mid = \mid \rho_{12}^{\mathrm{O}}(l) \mid \mid i) \times p(\mathrm{PR}_1 = \mathrm{PR}_1^{\mathrm{O}} \mid i) \times p(\mathrm{PR}_2 = \mathrm{PR}_2^{\mathrm{O}} \mid i)$.

The SBC-DS algorithm is divided in the following steps:

1) Calculate SCNR/SNR. If SCNR/SNR > 3 dB, go to step 2), otherwise the current gate is considered not to have significant weather; then compute SCNR/SNR for the next range gate.

2) Compute $\left|\rho_{12}(l)\right|$, PR_1, and PR_2. Look up the joint conditional PDF $p(\boldsymbol{X}\,|\,i)$ obtained from ground truth. Calculate $p(\boldsymbol{X}=\boldsymbol{X}^{\mathrm{O}}\,|\,\mathrm{c})$, $p(\boldsymbol{X}=\boldsymbol{X}^{\mathrm{O}}\,|\,\mathrm{w}\,0)$, and $p(\boldsymbol{X}=\boldsymbol{X}^{\mathrm{O}}\,|\,\mathrm{w})$.

3) If $p(\boldsymbol{X}=\boldsymbol{X}^{\mathrm{O}}\,|\,\mathrm{c}) > p(\boldsymbol{X}=\boldsymbol{X}^{\mathrm{O}}\,|\,\mathrm{w}\,0)$ and $p(\boldsymbol{X}=\boldsymbol{X}^{\mathrm{O}}\,|\,\mathrm{c}) > p(\boldsymbol{X}=\boldsymbol{X}^{\mathrm{O}}\,|\,\mathrm{w})$ for the current gate, data are clutter contaminated, otherwise, data are not contaminated; then return to step 1) for the next gate.

The performance evaluation of the SBC-DS algorithm will be given Section 2.6.3 with data collected by the PX-1000 3-cm polarimetric transportable radar.

2.4 Clutter Detection Algorithms based on Dual-Pol (DP) Measurement

Polarimetric weather radars provide additional measurements that allow better characterization of the targeted medium. Because ground clutter has different polarimetric characteristics from weather echoes, dual polarization measurements can be used to distinguish one from the other. Ground clutter and weather signals also have different statistical properties which can be utilized to distinguish one from the other. A test statistic, obtained from the Generalized Likelihood Ratio Test (GLRT), and a Simple Bayesian Classifier applied to the Dual-Pol discriminants (SBC-DP), are developed to detect ground clutter mixed with weather signals. It is

found that the test statistic produces false detections caused by weather signal I while the SBC-DP can effectively neutralize them. Both the test statistic and SBC-DP are aimed at detecting ground clutter based solely on data from each resolution volume.

For weather radar measurement tested for the presence of ground clutter, one of the two hypotheses, a) the measurement is the combined result of weather and noise (null hypothesis H_0), or b) the measurement is the combined result of ground clutter, weather, and noise (alternative hypothesis H_1), can be assumed to be true according to Richards (2005). The selected hypothesis should better account for the measurement than the other one. Because the weather radar signal is described statistically, the analysis starts with the modeling of the probability density function (PDF) that describes the measurement to be tested under each of the two hypotheses. The next step is to decide what the rule will be for deciding what constitutes an optimal choice between the two hypotheses. In the aviation radar community, the Neyman-Pearson criterion is commonly used according to Skolnik (2002) Chap. 5.3, which is designed to maximize the probability of detection P_{D} under the constraint that the probability of false alarm P_{FA} does not exceed a set constant. Kay (1993a) Theorem 3.1 stated that the Likelihood Ratio Test (LRT) is the optimal detector according to the Neyman-Pearson theorem because it provides maximum P_{D} given a specified P_{FA}. However, in real-world applications, we do not always have the knowledge of the values of the parameters describing the PDFs under the two hypotheses and a generalized likelihood ratio test (GLRT) is used instead in such conditions. In GLRT, the unknown parameters are replaced by their Maximum

Likelihood Estimates (MLEs). The test statistic obtained from the GLRT is used to detect ground clutter mixed with weather and noise.

Another approach to detect ground clutter is data classification. Data classification is a two-step process, consisting of a learning step, where a classification model is constructed from the training data, and a classification step, where the model is used to predict class labels in the testing data (Han et al., 2011, Chap. 8). In the learning step, the discriminants or attributes need to be defined which should have distinct statistical properties (PDFs) given different classes. A classification rule is needed to classify testing data. The commonly used classification rule in the weather radar community is fuzzy logic (Hubbert et al., 2009b)(Park et al., 2009)(Liu and Chandrasekar, 2000)(Wang et al., 2008). However, the membership functions of fuzzy logic classifiers are created based on experience. On the contrary, SBC is a statistical classifier based on Bayes' theorem. In the SBC-DP algorithm, a simple Bayesian classifier (SBC) is used to detect ground clutter with inputs derived from the mean and covariance of the received signals and these inputs can also be indicated from the test statistic.

In Section 2.4.1, the test statistic is derived; in Section 2.4.2, four discriminants are derived, which are the power ratio of the horizontal voltages, power ratio of the vertical voltages, differential reflectivity, and copolar correlation coefficient, and the four discriminants are combined by using the SBC to detect the presence of ground clutter.

2.4.1 Test Statistic

It is assumed that the received voltage (one sample of a time series) consists of either 1) ground clutter, weather signals, and noise, or 2) weather signals and noise. Thus, we have:

$$\vec{y}_m = \vec{c}_m + \vec{w}_m + \vec{n}_m \tag{2-16a}$$

$$\vec{y}_m = \vec{w}_m + \vec{n}_m \tag{2-16b}$$

In (2-16), $\vec{y}$ represents the received complex voltage vector and the arrow indicates a vector, $\vec{c}$ signifies clutter, $\vec{w}$ weather, and $\vec{n}$ noise. The subscript m signifies the m^{th} sample of an M sample time series. These complex voltage vectors, for a simultaneously transmit simultaneously receive (STSR) polarimetric radar, can be written as:

$$\vec{y}_m = \begin{bmatrix} y_{\text{h},m} & y_{\text{v},m} \end{bmatrix}^{\text{T}} \tag{2-17a}$$

$$\vec{c}_m = \begin{bmatrix} c_{\text{h},m} & c_{\text{v},m} \end{bmatrix}^{\text{T}} \tag{2-17b}$$

$$\vec{w}_m = \begin{bmatrix} w_{\text{h},m} & w_{\text{v},m} \end{bmatrix}^{\text{T}} \tag{2-17c}$$

$$\vec{n}_m = \begin{bmatrix} n_{\text{h},m} & n_{\text{v},m} \end{bmatrix}^{\text{T}} \tag{2-17d}$$

In (2-17) the subscripts h and v represent the horizontally and vertically polarized voltages. $y_{\text{h},m} = y_{\text{hh},m} + y_{\text{hv},m}$, where $y_{\text{hh},m}$ and $y_{\text{hv},m}$ are the received horizontally polarized voltages when transmitting simultaneously horizontal and vertical polarizations, respectively. The cross-polar signal $y_{\text{hv},m}$ is assumed to be principally

generated by the scatterers in a range cell of width r_6 (Doviak and Zrnic, 2006, Chap. 4.4.4), and not by coupling within the radar. Each complex voltage vector consists of two components: the complex voltages from horizontal and vertical receiving channels. Next the statistical models for $\vec{y}_m$, $\vec{c}_m$, $\vec{w}_m$, and $\vec{n}_m$ will be established. Before that, the following assumptions are made:

1. The clutter voltage vector $\vec{c}_m$ is complex and has a complex normal distribution with nonzero mean (the definition of complex normal distribution can be found in Kay, 1993b, Theorem 15.1) that can be expressed as $\vec{c}_m \sim CN(\vec{\mu}, \vec{\vec{C}}_c)$, where tilde signifies that $\vec{c}_m$ is complex and normally (CN) distributed with mean vector $\vec{\mu}$ equal to $\begin{bmatrix} \mu_h & \mu_v \end{bmatrix}^T$ and covariance matrix $\vec{\vec{C}}_c = E\left[\left(\vec{c}_m - \vec{\mu}\right)\left(\vec{c}_m - \vec{\mu}\right)^H\right]$ where $E[x]$ represents the ensemble average, and the superscript H the Hermitian or conjugate transpose. Vectors $[\vec{c}_1, \vec{c}_2, \ldots, \vec{c}_M]$ are identically distributed.

2. The weather voltage $\vec{w}_m$ is complex and has complex normal distribution with zero mean, and is expressed as $\vec{w}_m \sim CN(0, \vec{\vec{C}}_w)$ where $\vec{\vec{C}}_w$ is the covariance matrix of weather signals equal to $E\left[\vec{w}_m \vec{w}_m^H\right]$. Vectors $[\vec{w}_1, \vec{w}_2, \ldots, \vec{w}_M]$ are identically distributed.

3. The noise voltage $\vec{n}_m$ is assumed to be a complex white random vector with zero mean expressed as $\vec{n}_m \sim CN(0, N\vec{\vec{I}}_2)$ where N is the noise power and $\vec{\vec{I}}_2$ is a 2 by 2 identity matrix. Vectors $[\vec{n}_1, \vec{n}_2, \ldots, \vec{n}_M]$ are identically distributed.

4. The voltage vectors $\vec{c}_m$, $\vec{w}_m$, and $\vec{n}_m$ are independent of each other.

If assumptions 1 through 4 are true, the statistical model under the alternative hypothesis H_1 (2-16a) (i.e., the measurement is the combined result of ground clutter, weather, and noise) is (Kay, 1993b, Chap. 15.4):

$$\vec{y}_m \sim CN(\vec{\mu}, \ddot{C}_c + \ddot{C}_w + N\ddot{I}_2) = CN(\vec{\mu}, \ddot{C}_1) \tag{2-18a}$$

where $\ddot{C}_1 = E\left[\left(\vec{y}_m - \vec{\mu}\right)\left(\vec{y}_m - \vec{\mu}\right)^H\right]$. If ground clutter is not present, the statistical model under the null hypothesis H_0 (2-16b) can be written as:

$$\vec{y}_m \sim CN(0, \ddot{C}_w + N\ddot{I}_2) = CN(0, \ddot{C}_0) \tag{2-18b}$$

where $\ddot{C}_0 = E\left[\vec{y}_m \vec{y}_m^H\right]$.

Once a series of M samples of $\vec{y}_m$ (m = 1, 2, …, M) are measured, it is required to determine whether they fit better to the statistical model given by (2-18a) or (2-18b). A Likelihood Ratio Test (LRT) is often used to compare the fit of two models. The LRT is the optimal detector (Kay, 1993a, Theorem 3.1) according to the Neyman-Pearson theorem because it provides maximum probability of detection (P_D) given a specified probability of false alarm (P_{FA}).

The LRT test statistic L for M independent and identically distributed (iid) samples can be written as (Kay, 1993a, Theorem 3.1):

$$L = \frac{p(\vec{y}_1, \vec{y}_2, ..., \vec{y}_M \mid \vec{\mu}, \vec{\vec{C}}_1)}{p(\vec{y}_1, \vec{y}_2, ..., \vec{y}_M \mid \vec{\vec{C}}_0)} = \frac{\prod_{m=1}^{M} p(\vec{y}_m \mid \vec{\mu}, \vec{\vec{C}}_1)}{\prod_{m=1}^{M} p(\vec{y}_m \mid \vec{\vec{C}}_0)} \tag{2-19}$$

In (2-19) p represents the probability density function. For weather signals and clutter, vectors $\boldsymbol{y} = [\vec{y}_1, \vec{y}_2, \ldots, \vec{y}_M]$ are rarely independent, and thus the right side of (2-19) is at best an approximation. The larger is L (i.e., the distribution of the measurement follows more closely the distribution given in (2-18a)), the larger is the likelihood the weather signal is contaminated by ground clutter. When $\vec{\mu} = 0$, $L = 1$, i.e., the hypothesis H_1 and H_0 are equally likely.

Because $\vec{\mu}, \vec{\vec{C}}_1$, and $\vec{\vec{C}}_0$ are unknown for hypothesis H_1 and H_0 in the LRT, the generalized likelihood ratio test (GLRT) will be used instead. In the GLRT the unknown parameters are replaced by their Maximum Likelihood Estimations (MLEs) obtained using a finite number of M samples. These unknown parameter estimates are given in Hurtado and Nehorai (2008):

$$\hat{\vec{\mu}} = \frac{1}{M}\sum_{m=1}^{M} \vec{y}_m, \hat{\vec{\vec{C}}}_1 = \frac{1}{M}\sum_{m=1}^{M} \left(\vec{y}_m - \hat{\vec{\mu}}\right)\left(\vec{y}_m - \hat{\vec{\mu}}\right)^{\mathrm{H}} \tag{2-20a}$$

$$\hat{\vec{\vec{C}}}_0 = \frac{1}{M}\sum_{m=1}^{M} \vec{y}_m \vec{y}_m^{\mathrm{H}} \tag{2-20b}$$

In practice GLRT works quite well, although it is not associated with optimality (Kay, 1993a, Chap. 6.4.2). Thus, (2-19) can be rewritten as:

$$L_{\mathrm{G}} = \frac{p(\vec{y}_1, \vec{y}_2, ..., \vec{y}_M \,|\, \hat{\vec{\mu}}, \hat{\hat{C}}_1)}{p(\vec{y}_1, \vec{y}_2, ..., \vec{y}_M \,|\, \hat{\hat{C}}_0)} = \frac{\prod_{m=1}^{M} p(\vec{y}_m \,|\, \hat{\vec{\mu}}, \hat{\hat{C}}_1)}{\prod_{m=1}^{M} p(\vec{y}_m \,|\, \hat{\hat{C}}_0)} \tag{2-21}$$

Based on (Kay, 1993b, Chap. 15.4), the probability density functions $p(\vec{y}_m \,|\, \hat{\vec{\mu}}, \hat{\hat{C}}_1)$ and $p(\vec{y}_m \,|\, \hat{\hat{C}}_0)$ can be written as:

$$p(\vec{y}_m \,|\, \hat{\vec{\mu}}, \hat{\hat{C}}_1) = \frac{1}{\pi^2 \det\left(\hat{\hat{C}}_1\right)} \exp\left[-(\vec{y}_m - \hat{\vec{\mu}})^{\mathrm{H}} \hat{\hat{C}}_1^{-1} (\vec{y}_m - \hat{\vec{\mu}})\right] \tag{2-22a}$$

$$p(\vec{y}_m \,|\, \hat{\hat{C}}_0) = \frac{1}{\pi^2 \det\left(\hat{\hat{C}}_0\right)} \exp\left(-\vec{y}_m^{\mathrm{H}} \hat{\hat{C}}_0^{-1} \vec{y}_m\right) \tag{2-22b}$$

In (2-22a) and (2-22b), det represents the determinant of a matrix. Bring (2-22a) and (2-22b) into (2-21), we have:

$$L_G = \frac{\frac{1}{\pi^{2M} \det\left(\hat{\hat{C}}_1\right)^M} \exp\left[-\left(\sum_{m=1}^{M} (\vec{y}_m - \hat{\vec{\mu}})^H \hat{\hat{C}}_1^{-1} (\vec{y}_m - \hat{\vec{\mu}})\right)\right]}{\frac{1}{\pi^{2M} \det\left(\hat{\hat{C}}_0\right)^M} \exp\left[-\left(\sum_{m=1}^{M} \vec{y}_m^H \hat{\hat{C}}_0^{-1} \vec{y}_m\right)\right]} \tag{2-23}$$

Then take the logarithm on both sides of (2-23) we obtain that:

$$\ln L_G = M \ln \det\left(\hat{\hat{C}}_0\right) + M \,\mathrm{tr}(\hat{\hat{C}}_0^{-1} \hat{\hat{C}}_0) - M \ln \det\left(\hat{\hat{C}}_1\right) - M \,\mathrm{tr}(\hat{\hat{C}}_1^{-1} \hat{\hat{C}}_1) \tag{2-24}$$

In (2-24) tr represents the trace of a matrix, $\sum_{m=1}^{M} \vec{y}_m^H \hat{\hat{C}}_0^{-1} \vec{y}_m = M \,\mathrm{tr}(\hat{\hat{C}}_0^{-1}\hat{\hat{C}}_0)$ and $\sum_{m=1}^{M} (\vec{y}_m - \hat{\vec{\mu}})^H \hat{\hat{C}}_1^{-1} (\vec{y}_m - \hat{\vec{\mu}}) = M \,\mathrm{tr}(\hat{\hat{C}}_1^{-1}\hat{\hat{C}}_1)$. Because both $\mathrm{tr}(\hat{\hat{C}}_0^{-1}\hat{\hat{C}}_0)$ and $\mathrm{tr}(\hat{\hat{C}}_1^{-1}\hat{\hat{C}}_1)$ are equal to $\mathrm{tr}\left(\vec{I}_2\right) = 2$, (2-24) can be rewritten as:

$$\ln L_G = M \ln \frac{\det\left(\hat{\hat{C}}_0\right)}{\det\left(\hat{\hat{C}}_1\right)} \tag{2-25}$$

From (2-20a) and (2-20b), we know that $\hat{\hat{C}}_0 = \frac{1}{M}\sum_{m=1}^{M} \vec{y}_m \vec{y}_m^H$ and $\hat{\hat{C}}_1 = \frac{1}{M}\sum_{m=1}^{M} \left(\vec{y}_m - \hat{\vec{\mu}}\right)\left(\vec{y}_m - \hat{\vec{\mu}}\right)^H$. Thus we can obtain that:

$$\det\left(\hat{\hat{C}}_0\right) = \det\left(\hat{\hat{C}}_1 + \hat{\vec{\mu}}\hat{\vec{\mu}}^H\right) \tag{2-26}$$

According to Sylvester's determinant theorem given in Bareiss (1968), we know that:

$$\det\left(\hat{\hat{C}}_0\right) = \det\left(\hat{\hat{C}}_1\right)\left(1 + \hat{\vec{\mu}}^H \hat{\hat{C}}_1^{-1} \hat{\vec{\mu}}\right) \tag{2-27}$$

Bring (2-27) into (2-25) we can obtain that:

$$\ln L_G = M \ln\left(1 + \hat{\vec{\mu}}^H \hat{\hat{C}}_1^{-1} \hat{\vec{\mu}}\right) \tag{2-28}$$

Since ln(1+*x*) is monotonically increasing with increasing *x*, an equivalent test statistic is:

$$T = \hat{\hat{\mu}}^H \hat{\hat{C}}_1^{-1} \hat{\hat{\mu}} \tag{2-29}$$

In (2-29), $\hat{\hat{C}}_1$ can be written as:

$$\begin{aligned} \hat{\hat{C}}_1 &= \begin{bmatrix} \hat{C}_{1\mathrm{hh}} & \hat{C}_{1\mathrm{hv}} \\ \hat{C}_{1\mathrm{vh}} & \hat{C}_{1\mathrm{vv}} \end{bmatrix} \\ &= \begin{bmatrix} \dfrac{1}{M}\sum_{m=1}^{M}\left|y_{\mathrm{h},m} - \hat{\mu}_{\mathrm{h}}\right|^2 & \dfrac{1}{M}\sum_{m=1}^{M}\left(y_{\mathrm{h},m} - \hat{\mu}_{\mathrm{h}}\right)\left(y_{\mathrm{v},m} - \hat{\mu}_{\mathrm{v}}\right)^* \\ \dfrac{1}{M}\sum_{m=1}^{M}\left(y_{\mathrm{h},m} - \hat{\mu}_{\mathrm{h}}\right)^*\left(y_{\mathrm{v},m} - \hat{\mu}_{\mathrm{v}}\right) & \dfrac{1}{M}\sum_{m=1}^{M}\left|y_{\mathrm{v},m} - \hat{\mu}_{\mathrm{v}}\right|^2 \end{bmatrix} \end{aligned} \tag{2-30}$$

In (2-30) the star * represents conjugate. The inverse matrix $\hat{\hat{C}}_1^{-1}$ can be written as:

$$\hat{\hat{C}}_1^{-1} = \frac{1}{\hat{C}_{1\mathrm{hh}}\hat{C}_{1\mathrm{vv}} - \left|\hat{C}_{1\mathrm{hv}}\right|^2}\begin{bmatrix} \hat{C}_{1\mathrm{vv}} & -\hat{C}_{1\mathrm{hv}} \\ -\hat{C}_{1\mathrm{vh}} & \hat{C}_{1\mathrm{hh}} \end{bmatrix} \tag{2-31}$$

Substituting (2-31) into (2-29), *T* can be written as:

$$T = \frac{\left|\hat{\mu}_{\mathrm{h}}\right|^2 \hat{C}_{1\mathrm{vv}} + \left|\hat{\mu}_{\mathrm{v}}\right|^2 \hat{C}_{1\mathrm{hh}} - \hat{\mu}_{\mathrm{h}}\hat{\mu}_{\mathrm{v}}^* \hat{C}_{1\mathrm{vh}} - \hat{\mu}_{\mathrm{h}}^*\hat{\mu}_{\mathrm{v}}\hat{C}_{1\mathrm{hv}}}{\hat{C}_{1\mathrm{hh}}\hat{C}_{1\mathrm{vv}} - \left|\hat{C}_{1\mathrm{hv}}\right|^2} \tag{2-32}$$

If both the numerator and denominator are divided by $\hat{C}_{1\mathrm{hh}}\hat{C}_{1\mathrm{vv}}$, we have:

$$T = \frac{\dfrac{\left|\hat{\mu}_{\mathrm{h}}\right|^2}{\hat{C}_{1\mathrm{hh}}} + \dfrac{\left|\hat{\mu}_{\mathrm{v}}\right|^2}{\hat{C}_{1\mathrm{vv}}} - \dfrac{\hat{\mu}_{\mathrm{h}}\hat{\mu}_{\mathrm{v}}^*\hat{C}_{1\mathrm{vh}} + \hat{\mu}_{\mathrm{h}}^*\hat{\mu}_{\mathrm{v}}\hat{C}_{1\mathrm{hv}}}{\hat{C}_{1\mathrm{hh}}\hat{C}_{1\mathrm{vv}}}}{1 - \dfrac{\left|\hat{C}_{1\mathrm{hv}}\right|^2}{\hat{C}_{1\mathrm{hh}}\hat{C}_{1\mathrm{vv}}}} \tag{2-33}$$

In (2-33) terms $\left|\hat{\mu}_{\mathrm{h}}\right|^2 / \hat{C}_{1\mathrm{hh}}$ and $\left|\hat{\mu}_{\mathrm{v}}\right|^2 / \hat{C}_{1\mathrm{vv}}$ represent, for H and V channels, respectively, the ratio between the power at zero spectral line and the power summed from all other spectral lines. The power ratio is also shown in (2-6) and (2-15). The sum of these two terms will be defined as an alternative test statistic T_{a}**.** The reason that T_{a} is defined is because it is the sum of the two inputs $\mathrm{PR_h}$ and $\mathrm{PR_v}$ defined in Section 2.4.2.

$$T_{\mathrm{a}} = \frac{\left|\hat{\mu}_{\mathrm{h}}\right|^2}{\hat{C}_{1\mathrm{hh}}} + \frac{\left|\hat{\mu}_{\mathrm{v}}\right|^2}{\hat{C}_{1\mathrm{vv}}} \tag{2-34}$$

The performance evaluation of the test statistic will be given in Section 2.6.2.

2.4.2 Simple Bayesian Classifier applied to the Dual-Pol Discriminants (SBC-DP)

If the measurement is the combined result of ground clutter, weather, and noise, the estimated mean $\hat{\vec{\mu}}$ and covariance $\hat{\vec{\vec{C}}}_1$ of the received signal $\vec{y}$ is given in (2-20a), and they can be written as:

$$\hat{\vec{\mu}} = \begin{bmatrix} \hat{\mu}_{\mathrm{h}} & \hat{\mu}_{\mathrm{v}} \end{bmatrix}^{\mathrm{T}} \tag{2-35a}$$

$$\hat{\vec{\vec{C}}}_1 = \begin{bmatrix} \hat{C}_{1\mathrm{hh}} & \hat{C}_{1\mathrm{hv}} \\ \hat{C}_{1\mathrm{vh}} & \hat{C}_{1\mathrm{vv}} \end{bmatrix} \tag{2-35b}$$

From (2-35) the following four discriminants can be obtained:

$$\mathrm{PR_h} = 10\log_{10}\left(\frac{|\hat{\mu}_\mathrm{h}|^2}{\hat{C}_{1\mathrm{hh}}}\right) = 10\log 10\left[\frac{\left|\frac{1}{M}\sum_{m=1}^{M} y_{\mathrm{h},m}\right|^2}{\frac{1}{M}\sum_{m=1}^{M}|y_{\mathrm{h},m}|^2 - \left|\frac{1}{M}\sum_{m=1}^{M} y_{\mathrm{h},m}\right|^2}\right] \tag{2-36a}$$

$$\mathrm{PR_v} = 10\log_{10}\left(\frac{|\hat{\mu}_\mathrm{v}|^2}{\hat{C}_{1\mathrm{vv}}}\right) = 10\log 10\left[\frac{\left|\frac{1}{M}\sum_{m=1}^{M} y_{\mathrm{v},m}\right|^2}{\frac{1}{M}\sum_{m=1}^{M}|y_{\mathrm{v},m}|^2 - \left|\frac{1}{M}\sum_{m=1}^{M} y_{\mathrm{v},m}\right|^2}\right] \tag{2-36b}$$

$$Z_{\mathrm{DR}}(l) = 10\log_{10}\left(\frac{\left|\frac{1}{M-l}\sum_{m=1}^{M-l} y_{\mathrm{h},m} y^*_{\mathrm{h},m+l}\right|}{\left|\frac{1}{M-l}\sum_{m=1}^{M-l} y_{\mathrm{v},m} y^*_{\mathrm{v},m+l}\right|}\right), l = 0,1 \tag{2-36c}$$

$$|\rho_{\mathrm{hv}}(l)| = \frac{\left|\frac{1}{M-l}\sum_{m=1}^{M-l} y_{\mathrm{h},m+l} y^*_{\mathrm{v},m}\right| + \left|\frac{1}{M-l}\sum_{m=1}^{M-l} y_{\mathrm{h},m} y^*_{\mathrm{v},m+l}\right|}{2\sqrt{\left|\frac{1}{M-l}\sum_{m=1}^{M-l} y_{\mathrm{h},m+l} y^*_{\mathrm{h},m}\right|\left|\frac{1}{M-l}\sum_{m=1}^{M-l} y_{\mathrm{v},m+l} y^*_{\mathrm{v},m}\right|}}, l = 0,1 \tag{2-36d}$$

$\mathrm{PR_h}$ and $\mathrm{PR_v}$ are the ratios between the power at zero spectral line and the sum of powers at all other spectral lines of the horizontal and vertical channel, respectively; In (2-36c) and (2-36d), l = 0 (SNR > 20 dB) or 1 (SNR ≤ 20 dB). For the OU-PRIME data, l = 0 is chosen; while for the PX-1000 data without pulse compression, l = 1 is chosen to avoid the contamination of noise. (2-36a) and (2-36b) can also be obtained from T_a because T_a is the summation of $\mathrm{PR_h}$ and $\mathrm{PR_v}$.

In the SBC-DP algorithm, the 4-D attribute vector is $\boldsymbol{X}$ = ($\mathrm{PR_h}$, $\mathrm{PR_v}$, $Z_{\mathrm{DR}}(l)$, $|\rho_{\mathrm{hv}}(l)|$). (2-3) can be rewritten as:

$$\begin{aligned} p(\boldsymbol{X} = \boldsymbol{X}^{\mathrm{O}} \mid i) = {} & p(\mathrm{PR_h} = \mathrm{PR_h^O}, \mathrm{PR_v} = \mathrm{PR_v^O} \mid i) \times \\ & p(Z_{\mathrm{DR}}(l) = Z^{\mathrm{O}}_{\mathrm{DR}}(l) \mid i) \times p(|\rho_{\mathrm{hv}}(l)| = |\rho^{\mathrm{O}}_{\mathrm{hv}}(l)| \mid i) \end{aligned} \tag{2-37}$$

In (2-37) we use the joint probability $p(\mathrm{PR_h} = \mathrm{PR_h^O}, \mathrm{PR_v} = \mathrm{PR_v^O} \mid i)$ because $\mathrm{PR_h}$ and $\mathrm{PR_v}$ are highly correlated, especially for weather signals. By doing so, it is expected that the SBC would have better classification between classes.

The SBC-DP is divided in the following steps:

1) Calculate SCNR/SNR. If SCNR/SNR > 3 dB, go to step 2), otherwise the current gate is considered not to have significant weather; then compute SCNR/SNR for the next range gate.

2) Compute $\mathrm{PR_h}$, $\mathrm{PR_v}$, $Z_{\mathrm{DR}}(l)$, and $|\rho_{\mathrm{hv}}(l)|$. Look up the joint conditional PDF $p(\boldsymbol{X} \mid i)$ obtained from ground truth. Calculate $p(\boldsymbol{X} = \boldsymbol{X}^{\mathrm{O}} \mid \mathrm{c})$, $p(\boldsymbol{X} = \boldsymbol{X}^{\mathrm{O}} \mid \mathrm{w}0)$, and $p(\boldsymbol{X} = \boldsymbol{X}^{\mathrm{O}} \mid \mathrm{w})$.

3) If $p(\boldsymbol{X} = \boldsymbol{X}^{\mathrm{O}} \mid \mathrm{c}) > p(\boldsymbol{X} = \boldsymbol{X}^{\mathrm{O}} \mid \mathrm{w}0)$ and $p(\boldsymbol{X} = \boldsymbol{X}^{\mathrm{O}} \mid \mathrm{c}) > p(\boldsymbol{X} = \boldsymbol{X}^{\mathrm{O}} \mid \mathrm{w})$ for the current gate, data are clutter contaminated, otherwise, data are not contaminated; then return to step 1) for the next gate.

The performance evaluation of the SBC-DP algorithm will be given in Sections 2.6.2 and 2.6.3. In the next section, the SBC-DPDS (Simple Bayesian Classifier applied to the Dual Pol Dual Scan discriminants) algorithm will be discussed.

2.5 Simple Bayesian Classifier applied to the Dual-Pol Dual-Scan Discriminants (SBC-DPDS)

Both dual scan and dual pol measurements are proved to be effective in detecting ground clutter in the presence of weather signals (Li et al., 2013b). In this section, ten discriminants obtained from the dual pol dual scan measurement are combined using SBC to make decisions as to the presence of ground clutter.

The following ten discriminants can be derived based on the dual pol dual scan measurement:

$$\mathrm{PR}_{\mathrm{h1}} = 10\log_{10}\left(\frac{\left|\hat{\mu}_{\mathrm{h1}}\right|^2}{\hat{C}_{\mathrm{h1h1}}}\right) \tag{2-38a}$$

$$\mathrm{PR}_{\mathrm{v1}} = 10\log_{10}\left(\frac{\left|\hat{\mu}_{\mathrm{v1}}\right|^2}{\hat{C}_{\mathrm{v1v1}}}\right) \tag{2-38b}$$

$$\mathrm{PR}_{\mathrm{h2}} = 10\log_{10}\left(\frac{\left|\hat{\mu}_{\mathrm{h2}}\right|^2}{\hat{C}_{\mathrm{h2h2}}}\right) \tag{2-38c}$$

$$\mathrm{PR}_{\mathrm{v2}} = 10\log_{10}\left(\frac{\left|\hat{\mu}_{\mathrm{v2}}\right|^2}{\hat{C}_{\mathrm{v2v2}}}\right) \tag{2-38d}$$

$$Z_{\mathrm{DR1}}(l) = 10\log_{10}\left(\frac{\left|\frac{1}{M-l}\sum_{m=1}^{M-l} y_{\mathrm{h1},m}\, y^{*}_{\mathrm{h1},m+l}\right|}{\left|\frac{1}{M-l}\sum_{m=1}^{M-l} y_{\mathrm{v1},m}\, y^{*}_{\mathrm{v1},m+l}\right|}\right), l = 0,1 \tag{2-38e}$$

$$Z_{\mathrm{DR2}}(l) = 10\log_{10}\left(\frac{\left|\frac{1}{M-l}\sum_{m=1}^{M-l} y_{\mathrm{h2},m}\, y^{*}_{\mathrm{h2},m+l}\right|}{\left|\frac{1}{M-l}\sum_{m=1}^{M-l} y_{\mathrm{v2},m}\, y^{*}_{\mathrm{v2},m+l}\right|}\right), l = 0,1 \tag{2-38f}$$

$$\left|\rho_{\mathrm{hv1}}(l)\right| = \frac{\left|\frac{1}{M-l}\sum_{m=1}^{M-l} y_{\mathrm{h1},m+l} y_{\mathrm{v1},m}^{*}\right| + \left|\frac{1}{M-l}\sum_{m=1}^{M-l} y_{\mathrm{h1},m} y_{\mathrm{v1},m+l}^{*}\right|}{2\sqrt{\left|\frac{1}{M-l}\sum_{m=1}^{M-l} y_{\mathrm{h1},m+l} y_{\mathrm{h1},m}^{*}\right|\left|\frac{1}{M-l}\sum_{m=1}^{M-l} y_{\mathrm{v1},m+l} y_{\mathrm{v1},m}^{*}\right|}}, l = 0,1 \qquad \text{(2-38g)}$$

$$\left|\rho_{\mathrm{hv2}}(l)\right| = \frac{\left|\frac{1}{M-l}\sum_{m=1}^{M-l} y_{\mathrm{h2},m+l} y_{\mathrm{v2},m}^{*}\right| + \left|\frac{1}{M-l}\sum_{m=1}^{M-l} y_{\mathrm{h2},m} y_{\mathrm{v2},m+l}^{*}\right|}{2\sqrt{\left|\frac{1}{M-l}\sum_{m=1}^{M-l} y_{\mathrm{h2},m+l} y_{\mathrm{h2},m}^{*}\right|\left|\frac{1}{M-l}\sum_{m=1}^{M-l} y_{\mathrm{v2},m+l} y_{\mathrm{v2},m}^{*}\right|}}, l = 0,1 \qquad \text{(2-38h)}$$

$$\left|\rho_{\mathrm{12h}}(l)\right| = \frac{\left|\frac{1}{M-l}\sum_{m=1}^{M-l} y_{\mathrm{h1},m+l} y_{\mathrm{h2},m}^{*}\right| + \left|\frac{1}{M-l}\sum_{m=1}^{M-l} y_{\mathrm{h1},m} y_{\mathrm{h2},m+l}^{*}\right|}{2\sqrt{\left|\frac{1}{M-l}\sum_{m=1}^{M-l} y_{\mathrm{h1},m+l} y_{\mathrm{h1},m}^{*}\right|\left|\frac{1}{M-l}\sum_{m=1}^{M-l} y_{\mathrm{h2},m+l} y_{\mathrm{h2},m}^{*}\right|}}, l = 0,1 \qquad \text{(2-38i)}$$

$$\left|\rho_{\mathrm{12v}}(l)\right| = \frac{\left|\frac{1}{M-l}\sum_{m=1}^{M-l} y_{\mathrm{v1},m+l} y_{\mathrm{v2},m}^{*}\right| + \left|\frac{1}{M-l}\sum_{m=1}^{M-l} y_{\mathrm{v1},m} y_{\mathrm{v2},m+l}^{*}\right|}{2\sqrt{\left|\frac{1}{M-l}\sum_{m=1}^{M-l} y_{\mathrm{v1},m+l} y_{\mathrm{v1},m}^{*}\right|\left|\frac{1}{M-l}\sum_{m=1}^{M-l} y_{\mathrm{v2},m+l} y_{\mathrm{v2},m}^{*}\right|}}, l = 0,1 \qquad \text{(2-38j)}$$

(2-38a)-(2-38d) represent the dc-ac power ratios calculated from voltages from horizontally and vertically polarized waves collected on the first and second scans. The power ratios are expected to be large for ground clutter and small for most weather signals except for the weather signal I (narrow-band zero-velocity weather signals) for which most power components are around zero Doppler. (2-38e) and (2-38f) represent the differential reflectivities of the first and second scan. As stated earlier, l = 1 is only used when SNR < 20 dB. It is expected that Z_{DR1} and Z_{DR2} for ground clutter would have a larger spread compared with weather signals. (2-38g) and (2-38h) signify the copolar correlation coefficients of the first and

second scan using lag 0 or 1 depending on the SNR. $|\rho_{\mathrm{hv1}}(l)|$ and $|\rho_{\mathrm{hv2}}(l)|$ for ground clutter are expected to have a larger spread compared with weather signals. (2-38i) and (2-38j) represent the correlation coefficient between two scans of H and V channels. $|\rho_{12\mathrm{h}}(l)|$ and $|\rho_{12\mathrm{v}}(l)|$ for ground clutter is expected to be larger compared with weather signals.

In the SBC-DPDS algorithm, the 10-D attribute vector is $\boldsymbol{X}$ = ($\mathrm{PR_{h1}}$, $\mathrm{PR_{v1}}$, $\mathrm{PR_{h2}}$, $\mathrm{PR_{v2}}$, $Z_{\mathrm{DR1}}(l)$, $Z_{\mathrm{DR2}}(l)$, $|\rho_{\mathrm{hv1}}(l)|$, $|\rho_{\mathrm{hv2}}(l)|$, $|\rho_{12\mathrm{h}}(l)|$, $|\rho_{12\mathrm{v}}(l)|$). (2-3) can be rewritten as:

$$
\begin{aligned}
p(\boldsymbol{X} = \boldsymbol{X}^{\mathrm{O}} \mid i) = {} & p(\mathrm{PR_h} = \mathrm{PR}^{\mathrm{O}}_{\mathrm{h1}}, \mathrm{PR_v} = \mathrm{PR}^{\mathrm{O}}_{\mathrm{v1}} \mid i) \times \\
& p(\mathrm{PR_h} = \mathrm{PR}^{\mathrm{O}}_{\mathrm{h2}}, \mathrm{PR_v} = \mathrm{PR}^{\mathrm{O}}_{\mathrm{v2}} \mid i) \times \\
& p(Z_{\mathrm{DR}}(l) = Z^{\mathrm{O}}_{\mathrm{DR1}}(l) \mid i) \times p(Z_{\mathrm{DR}}(l) = Z^{\mathrm{O}}_{\mathrm{DR2}}(l) \mid i) \times \\
& p(|\rho_{\mathrm{hv}}(l)| = |\rho^{\mathrm{O}}_{\mathrm{hv1}}(l)| \mid i) \times p(|\rho_{\mathrm{hv}}(l)| = |\rho^{\mathrm{O}}_{\mathrm{hv2}}(l)| \mid i) \times \\
& p(|\rho_{12\mathrm{h}}(l)| = |\rho^{\mathrm{O}}_{12\mathrm{h}}(l)|, |\rho_{12\mathrm{v}}(l)| = |\rho^{\mathrm{O}}_{12\mathrm{v}}(l)| \mid i)
\end{aligned}
\tag{2-39}
$$

In (2-39) we use the joint probabilities $p(\mathrm{PR_h} = \mathrm{PR}^{\mathrm{O}}_{\mathrm{h1}}, \mathrm{PR_v} = \mathrm{PR}^{\mathrm{O}}_{\mathrm{v1}} \mid i)$, $p(\mathrm{PR_h} = \mathrm{PR}^{\mathrm{O}}_{\mathrm{h2}}, \mathrm{PR_v} = \mathrm{PR}^{\mathrm{O}}_{\mathrm{v2}} \mid i)$, and $p(|\rho_{12\mathrm{h}}(l)| = |\rho^{\mathrm{O}}_{12\mathrm{h}}(l)|, |\rho_{12\mathrm{v}}(l)| = |\rho^{\mathrm{O}}_{12\mathrm{v}}(l)| \mid i)$ because $\mathrm{PR_h}$ and $\mathrm{PR_v}$, $|\rho_{12\mathrm{h}}(l)|$ and $|\rho_{12\mathrm{v}}(l)|$ are highly correlated for weather signals. By doing so, it is expected that the SBC would have better classification between classes.

The SBC-DPDS algorithm is divided in the following steps:

1) Calculate SCNR/SNR. If SCNR/SNR > 3 dB, go to step 2), otherwise the current gate is considered not to have significant weather; then compute SCNR/SNR for the next range gate.

2) Compute PR_{h1}, PR_{v1}, PR_{h2}, PR_{v2}, $Z_{DR1}(l)$, $Z_{DR2}(l)$, $|\rho_{hv1}(l)|$, $|\rho_{hv2}(l)|$, $|\rho_{12h}(l)|$, and $|\rho_{12v}(l)|$. Look up the joint conditional PDF $p(\boldsymbol{X} \mid i)$ obtained from ground truth. Calculate $p(\boldsymbol{X} = \boldsymbol{X}^{O} \mid \mathrm{c})$, $p(\boldsymbol{X} = \boldsymbol{X}^{O} \mid \mathrm{w}\,0)$, and $p(\boldsymbol{X} = \boldsymbol{X}^{O} \mid \mathrm{w})$.

3) If $p(\boldsymbol{X} = \boldsymbol{X}^{O} \mid \mathrm{c}) > p(\boldsymbol{X} = \boldsymbol{X}^{O} \mid \mathrm{w}\,0)$ and $p(\boldsymbol{X} = \boldsymbol{X}^{O} \mid \mathrm{c}) > p(\boldsymbol{X} = \boldsymbol{X}^{O} \mid \mathrm{w})$ for the current gate, data are clutter contaminated, otherwise, data are not contaminated; then return to step 1) for the next gate.

The performance evaluation of the SBC-DPDS algorithm will be given in Section 2.6.3.

2.6 Performance Evaluation of Clutter Detection Methods

In Section 2.6.1 the performance of the SCI algorithm will be tested using the data collected by the OU-PRIME; in Section 2.6.2, the performances of the test statistic and SBC-DP are evaluated with the same data used in Section 2.6.1; in Section 2.6.3 the performances of the SBC-DS and SBC-DPDS algorithms are evaluated and compared with the SBC-DP with the data collected by the PX-1000.

2.6.1 Evaluation of the SCI Algorithm

The controlled data sets are obtained by adding clutter data, obtained at low elevation angles under cold clear air conditions, to the stratiform weather data obtained at high elevation angles where ground clutter can be neglected (Li et al., 2013a)(Melnikov et al., 2008). A field of clutter data were collected at 23:19 UTC on 01/13/2011 with the elevation angle fixed at 0° and while the beam was scanned over 360^{o} of azimuth. Ground clutter I/Q data were edited by deleting those few resolution volumes showing mean Doppler velocities $|v| \geq 1$ m s^{-1} and SNR < 3 dB. This deletion provides a clutter field not contaminated from moving objects on the ground or airborne (e.g., birds and aircraft). The 3 dB SNR threshold appears to produce data in which noise effects are not obvious and it is commonly used for the WSR-88D weather radars according to Ivic et al. (2009). Weather data were collected on seven days (04:55 UTC 04/18/2010, 12:33 UTC 05/14/2010, 21:49 UTC 09/08/2010, 07:04 UTC 04/12/2009, 18:02 UTC 10/21/2009, 13:08 UTC 04/17/2010, and 09:07 UTC 05/13/2010) with the elevation angle fixed 3.5°. The first three weather data are used for testing and the last four are used for training. Because the one-way 3-dB beamwidth of OU-PRIME is 0.5°, there is practically no clutter present in the weather data. Stratiform weather was selected because there are many gates containing weather signal I (narrow-band zero-velocity weather signals) which are the most difficult to distinguish from ground clutter (Hubbert et al., 2009b)(Li et al., 2013a). The ground truth of a field of weather significantly contaminated by clutter is obtained as follows:

All the gates where ground clutter can bias weather power by more than 1 dB or weather signal's mean radial velocity or its spectrum width by more than 1 m s^{-1} are considered as significantly contaminated by ground clutter (NEXRAD Technical Requirements, 1991, Sec. 3.7.1.2.3.1). Otherwise, even if ground clutter does exist in the resolution volume, it is considered as weather signal because its effect on weather estimates can be neglected.

By using the above conditions, not only CSR but also the mean radial velocity and spectrum width of weather signal, and the spectrum width of ground clutter are considered. For example, if CSR = -7 dB, noise power is negligible, mean radial velocity and spectrum width of the weather signal is 0 and 1 m s^{-1} respectively, and spectrum width of ground clutter is 0.6 m s^{-1}, the weather moments will not be significantly biased by clutter according to Li et al. (2013a); therefore weather data under these conditions is considered to be uncontaminated by clutter and clutter should not be detected. On the other hand, if CSR = -15 dB, mean radial velocity and spectrum width of weather signal is v_N and 1 m s^{-1} respectively (v_N is the Nyquist velocity = 16.06 m s^{-1} for OU-PRIME), and spectrum width of ground clutter is 0.6 m s^{-1}, weather signal spectrum widths can be biased more than 1 m s^{-1} by clutter Li et al. (2013a); in this case, weather signals are considered to be contaminated by clutter and clutter needs to be detected. In conclusion, CSR is not the only criterion to judge whether clutter needs to be detected or not.

In Fig. 2-3, the CPDFs (Conditional Probability Density Functions) of the four discriminants SPD, SPF, PT, and SWT obtained from training data are shown given the three classes, c, w0, and w. The training data are obtained by adding

clutter data, collected at 23:19 UTC on 01/13/2011 with θ_e = 0° under clear air condition, to weather data collected on four days with stratiform precipitations, which are 07:04 UTC 04/12/2009, 18:02 UTC 10/21/2009, 13:08 UTC 04/17/2010, and 09:07 UTC 05/13/2010 with θ_e = 3.5°.

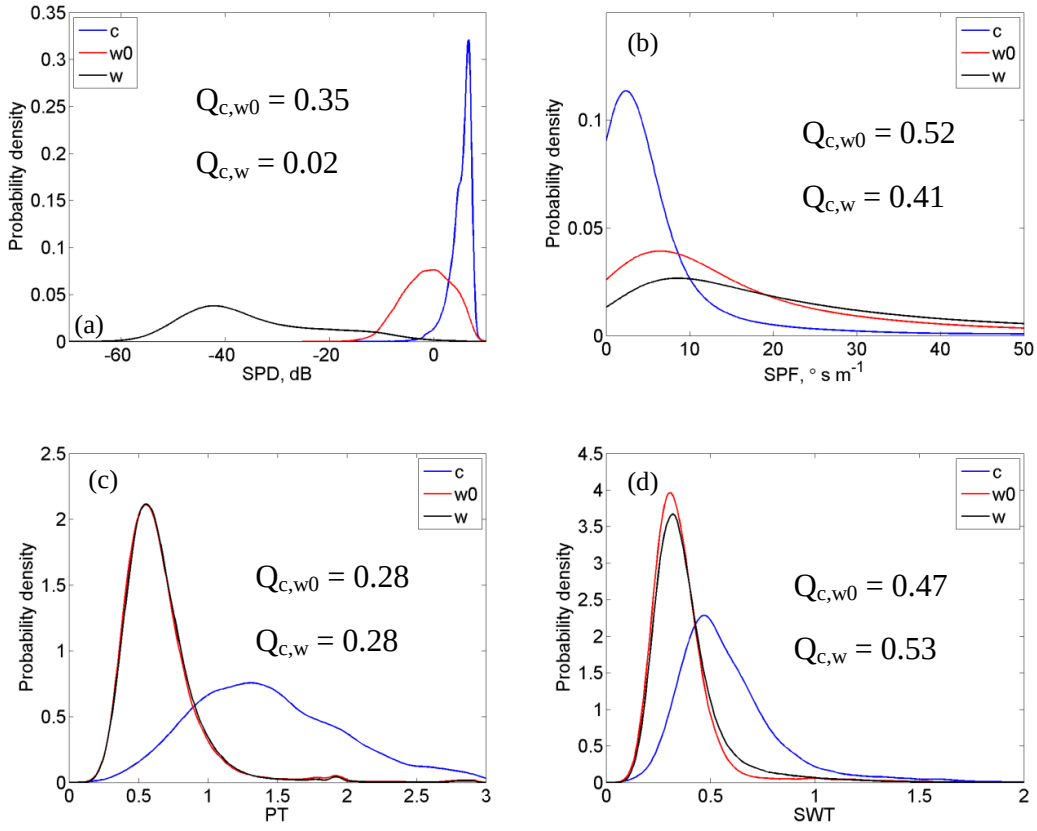

Figure 2-3: The conditional probability density functions (CPDFs) of (a) SPD in dB scale, (b) SPF, (c) PT, and (d) SWT given three classes c, w0, and w using controlled training data sets.

The CPDFs shown in Fig. 2-3 are smoothed by the Gaussian kernel introduced by Gourley et al. (2007). The numerical entries, $Q_{c,w0}$ etc. in Fig. 2-3, represent the common area (i.e., the area under the minimum of the two curves)

between the CPDFs given the various classes. A smaller common area indicates a better discrimination. It can be concluded that PT (power texture) outperforms the other three in distinguishing c from w0; on the other hand, SPD outperforms the other three in distinguishing c from w.

From Fig. 2-3(b), it can be seen that the CPDF given weather signals has long tails, which is related to the fact that spectral phase in the interval $\pm\sqrt{2}\Delta v_w$ fluctuates randomly. On the other hand, the CPDF given clutter would be almost a delta function centered at zero if there is only one hard scatterer in the resolution volume (i.e., the phase within the interval $\pm\sqrt{2}\Delta v_w$ would almost be linear). The reason that the CPDF is far away from a delta function can be explained by the fact that there are multiple hard scatterers being scanned by the radar.

One thing to notice is that unlike the SPD and SPF, the CPDFs of PT p(PT|w0) and p(PT|w) are almost the same. The disadvantage of using PT or SWT is that it will increase the number of false detections (i.e., weather signals mistakenly identified as clutter).

After the CPDFs shown in Fig. 2-3 are obtained from controlled training data, they are used on testing data to make decisions as to the presence of clutter. In Fig. 2-4, the moment data for the three testing cases, collected on 04:55 UTC 04/18/2010, 12:33 UTC 05/14/2010, and 21:49 UTC 09/08/2010, are shown. In Fig. 2-5, clutter maps obtained using the SCI algorithm are compared with the ground truth for the three testing data.

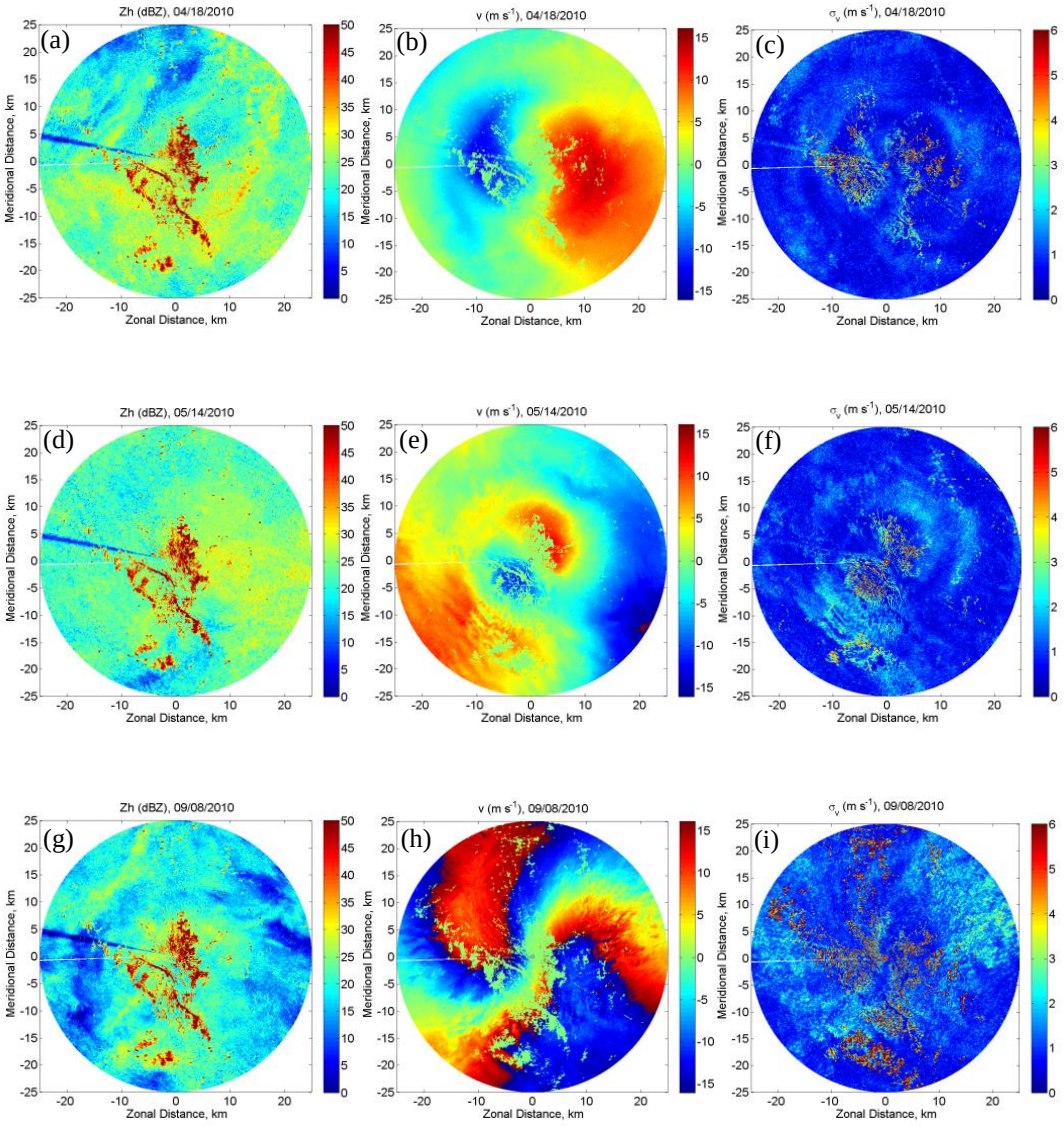

Figure 2-4: Mean powers (a, d, g), mean radial velocities, (b, e, h), and spectrum widths (c, f, i), of three controlled testing data sets.

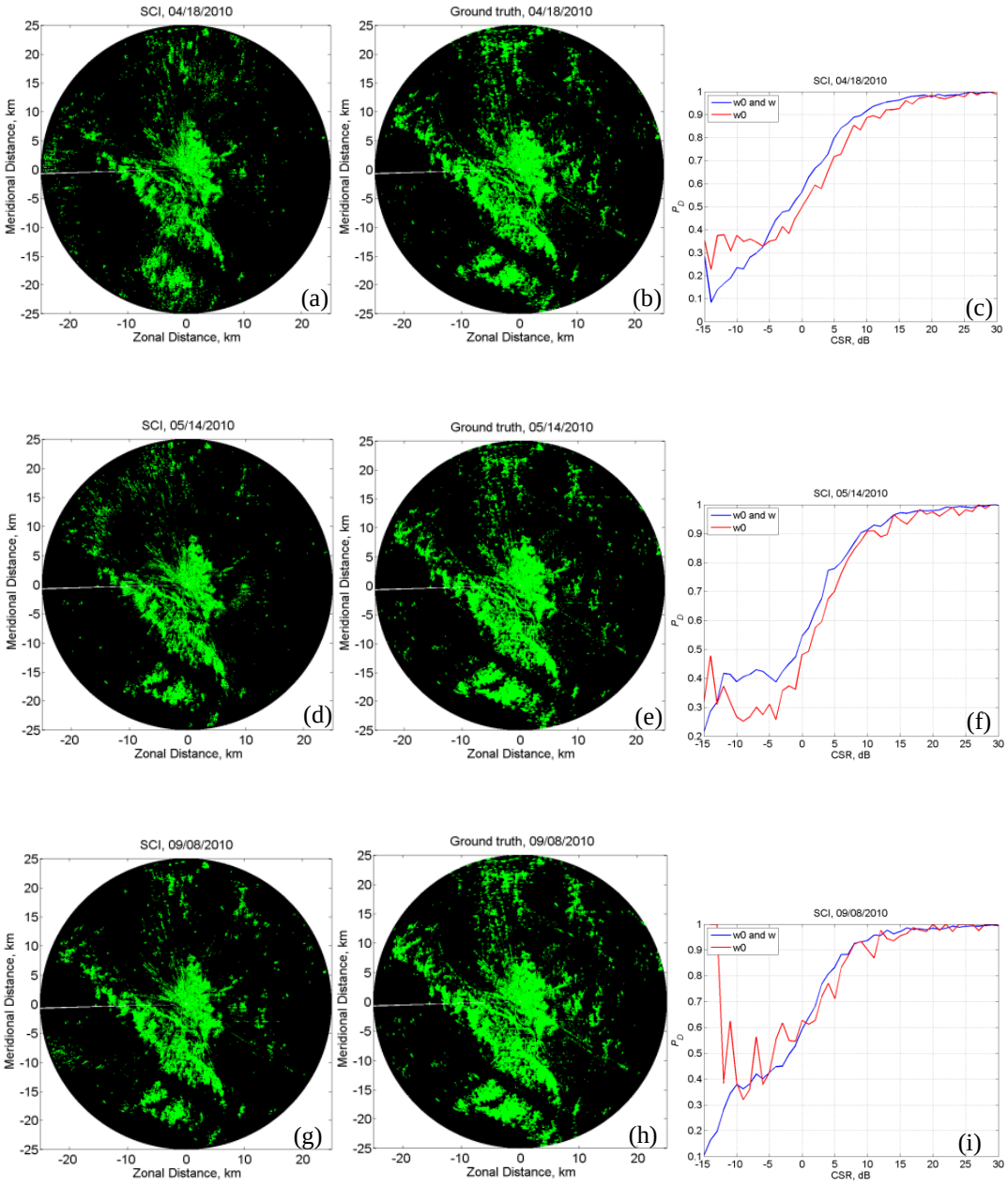

Figure 2-5: SCI clutter maps (a, d, g) compared with the ground truth (b, e, h) for the three testing data. P_D as a function of CSR (dB) is shown in (c, f, i). The blue line represents the performance of the SCI detecting ground clutter in the presence of both w and w0 while the red line represents that in the presence of only w0.

In Fig. 2-5(c)(f)(i), red curves are noisier because there are fewer numbers of narrow-band zero-velocity weather signals (weather signal I) compared with other weather signals (weather signal II). In Table 2-4 we list the probability of detection P_D, probability of false alarm P_{FA}, and critical success index (CSI) introduced by Schaefer (1990) for the three controlled testing data sets.

Table 2-4. P_D, P_{FA}, and CSI for the three testing data by using the SCI algorithm.

	P_D	P_{FA}	CSI
04/18/2010	74.17%	2.53%	0.70
05/14/2010	73.89%	2.04%	0.70
09/08/2010	75.55%	0.86%	0.74

Terms in In Table 2-4, are defined as follows (Li et al., 2013a; Schaefer, 1990):

$$P_D = \frac{TP}{TP + FN} \tag{2-40a}$$

$$P_{FA} = \frac{FP}{FP + TN} \tag{2-40b}$$

$$CSI = \frac{TP}{TP + FN + FP} \tag{2-40c}$$

In (2-40), TP signifies true positive, FN false negative, FP false positive, and TN true negative (TN). “Positive” labels the location that the detector judges as clutter contaminated, and “Negative” labels the location that the detector judges as weather; “True Positives” labels the location that 1) the detector judges as clutter

contaminated and 2) weather moments are significantly biased by clutter; "False Negative" denotes the location that 1) the detector judges as weather and 2) weather moments are significantly biased by clutter; "False Positive" denotes the location that 1) the detector judges as clutter and 2) weather moments are not significantly biased by clutter; "True Negative" denotes the location that 1) the detector judges as weather and 2) weather moments are not significantly biased by clutter. For an ideal detector, we have $P_D = 100\%$, $P_{FA} = 0$, and CSI = 1.

In the next Section, the performance of the clutter detection algorithms based on dual pol measurement will be evaluated using the same data used in this Section.

2.6.2 Evaluation of the Test Statistic and SBC-DP Algorithm

In this Section, we will first evaluate the performance of the test statistic T (2-33) and its alternative form T_a (2-34). Then, the SBC-DP algorithm will be evaluated.

Evaluation of the Test Statistic

In Fig. 2-6 the Receiver Operating Characteristics (ROC) curves discussed in Fawcett (2003) and Kharin and Zwiers (2003) and CSI vs P_{FA} curves of T and T_a for three controlled testing data sets are shown.

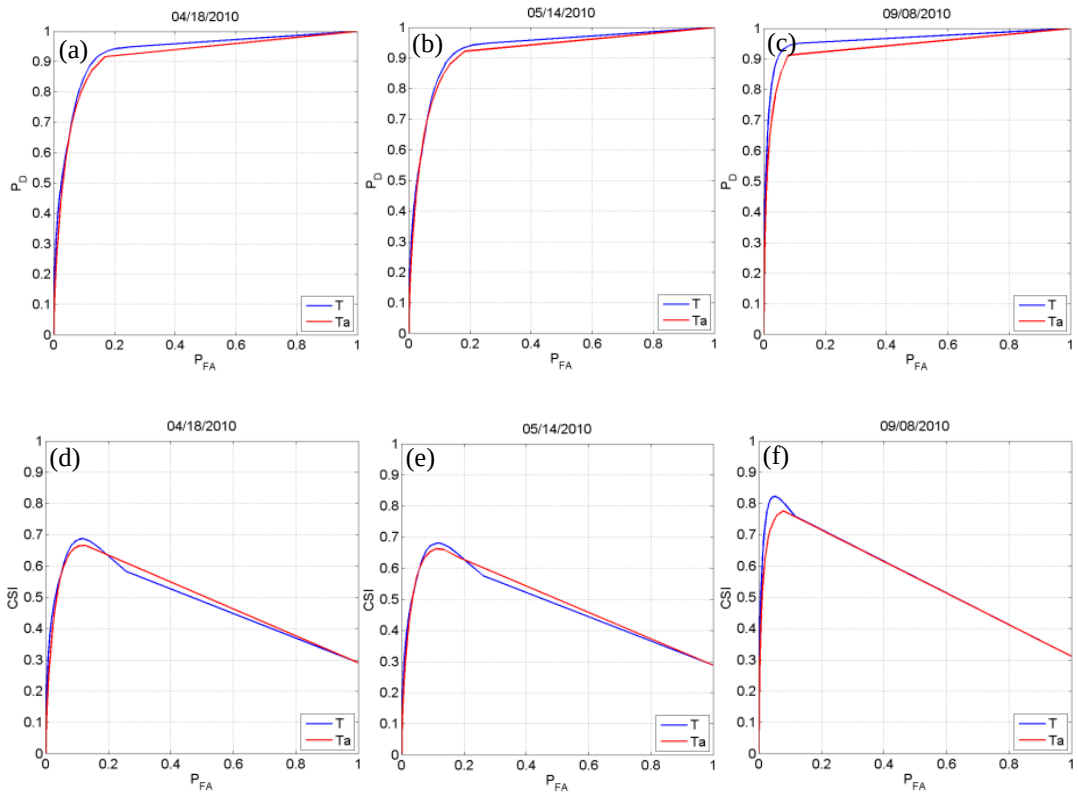

Figure 2-6: The Radar Operation Curves (a, b, c) and the CSI vs P_{FA} curves (d, e, f) of T (blue) and T_a (red) for the same testing data sets shown in Fig. 2-4.

From Fig. 2-6, it can be concluded that T performs better than T_a because T not only includes T_a but also polarimetric measurements shown in (2-33) while T_a is the summation of power ratios from horizontal and vertical voltages. In Table 2-5 we list the probability of detection P_D, probability of false alarm P_{FA}, and critical success index (CSI) for the three controlled tesing data sets by using T and T_a. In Table 2-5 we intentionally chose the same P_{FA} shown in Table 2-4 for the purpose of comparison.

Table 2-5. P_D, P_{FA}, and CSI for the three testing data by using $T(T_a)$.

	P_D	P_{FA}	CSI
04/18/2010	50%(46%)	2.53%	0.47(0.43)
05/14/2010	45.14%(41.6%)	2.04%	0.43(0.40)
09/08/2010	58.39%(48.61%)	0.86%	0.57(0.48)

In Table 2-5, the numbers in brackets are obtained by using T_a. By comparing Table 2-5 with 2-4, it can be concluded that the performance of the test statistic is not very effective when there are many narrow-band zero-velocity weather signals. In Fig. 2-7, $10\log_{10}(T)$ and $10\log_{10}(T_a)$ fields are shown for three testing data sets.

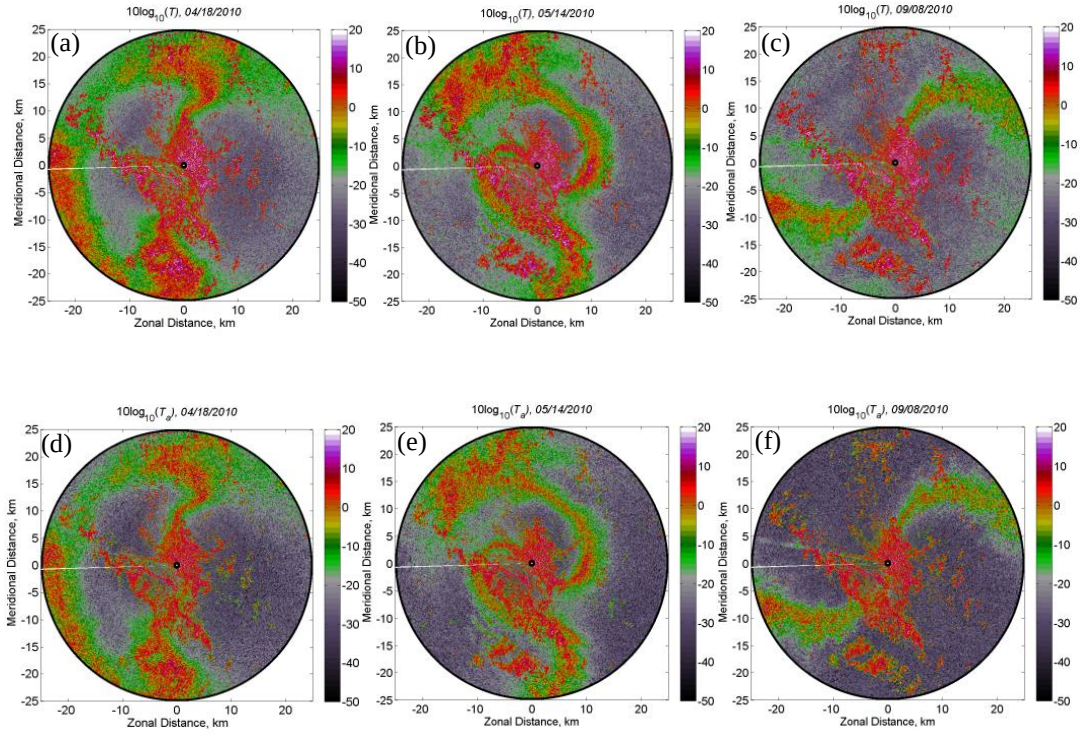

Figure 2-7: $10\log_{10}(T)$ field for three testing data sets (a, b, c); $10\log_{10}(T_a)$ field for three testing data sets (d, e, f).

From Fig. 2-7, it can be concluded that both T and T_a have difficulties in distinguishing ground clutter from weather signal I, which can cause false detections. In Fig. 2-8, the CPDFs of $10\log_{10}(T)$ and $10\log_{10}(T_a)$ are shown for the four training data sets.

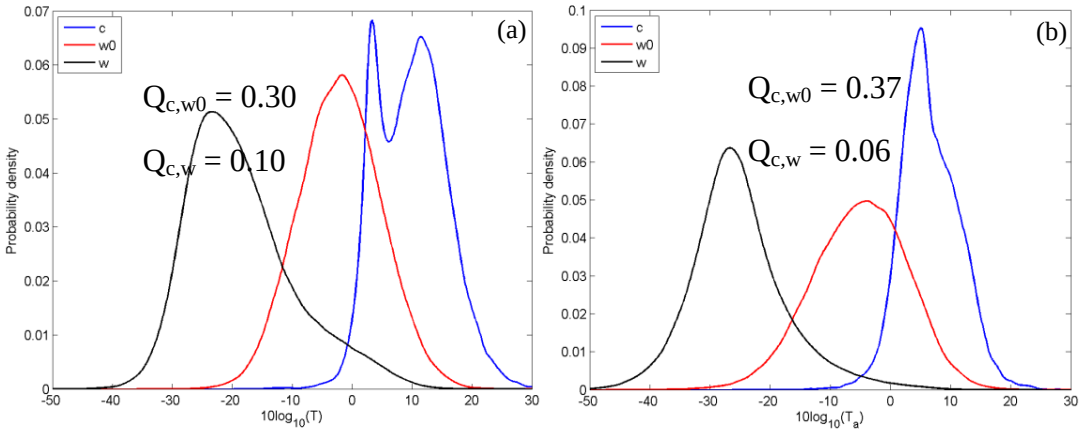

Figure 2-8: The conditional probability density functions (CPDFs) of (a) T and (b) T_a given three classes c, w0, and w. The training data are the same as the one shown in Fig. 2-3.

In the next section, we will evaluate the performance of the SBC-DP algorithm, which can effectively neutralize the false detections caused by narrow-band zero-velocity weather signals when using the test statistic.

Evaluation of the SBC-DP Algorithm

As described in Section 2.4.2, four discriminants will be used, which are PR_H, PR_V, $Z_{DR}(0)$, and $|\rho_{hv}(0)|$ shown in (2-36a)-(2-36d). In Fig. 2-9, the CPDFs of the four discriminants obtained from training data are shown.

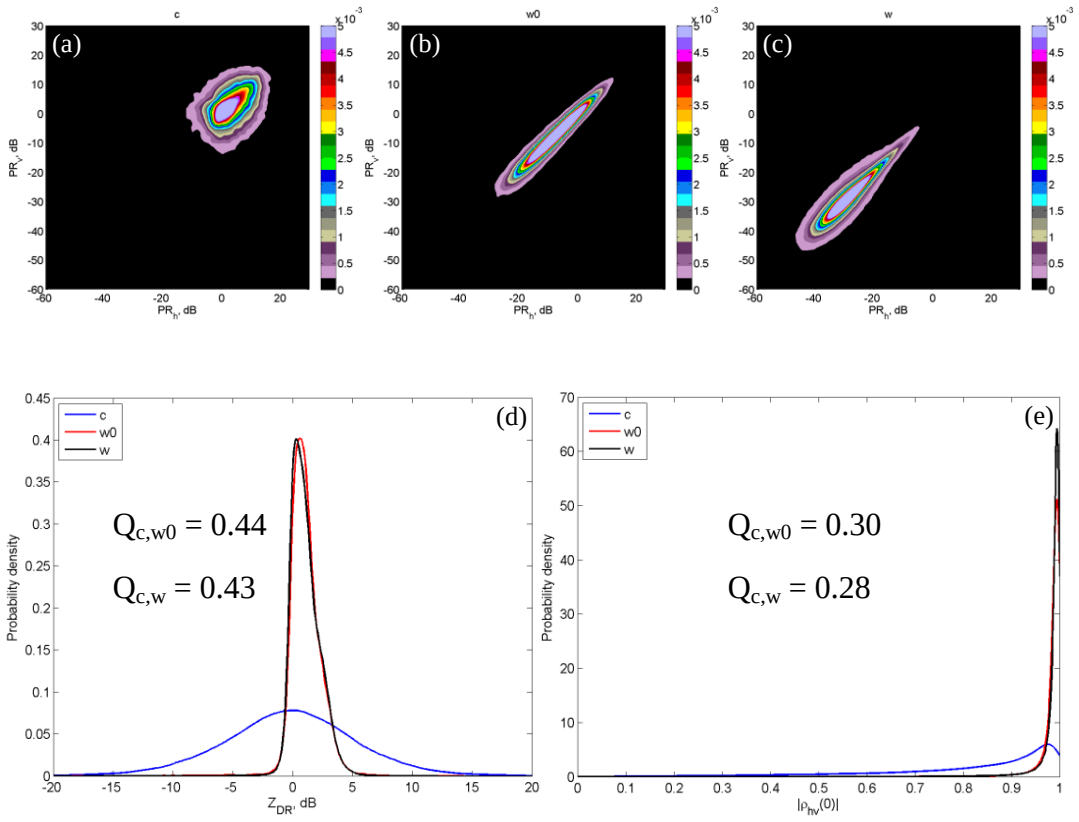

Figure 2-9: $p(PR_h, PR_v \mid i)$ given (a) i = c, (b) i = w0, and (c) i = w; The CPDFs of (d) $Z_{DR}(0)$ and (e) $|\rho_{hv}(0)|$ given three classes c, w0, and w. The training data are the same as the one shown in Fig. 2-3.

From Fig. 2-9 (a)-(c) it can be concluded that (1) generally, c has larger PR than both w and w0; (2) PR_h and PR_v are most correlated for w0, then w, and then c; (3) it is more difficult to distinguish c from w0 than w. In Fig. 2-9(d), the CPDFs of $Z_{DR}(0)$ and $|\rho_{hv}(0)|$ for w and w0 are almost the same. The conditional

probabilities $p(Z_{DR}(0)|w)$ and $p(Z_{DR}(0)|w0)$ are almost equal to zero when $Z_{DR}(0)$ is less than -2 dB or larger than 5 dB; $Z_{DR}(0)$ has a much larger spread for c than w and w0. In Fig. 2-9(e), the conditional probabilities $p(|\rho_{hv}(0)||w)$ and $p(|\rho_{hv}(0)||w0)$ are almost equal to zero when $|\rho_{hv}(0)|$ is less than 0.85 and the peak is located at $|\rho_{hv}(0)| = 0.995$; $|\rho_{hv}(0)|$ has a much larger spread for c and the peak of $p(|\rho_{hv}(0)||c)$ is located at $|\rho_{hv}(0)| = 0.96$.

In Fig. 2-10, the clutter maps obtained by using the SBC-DP algorithm are compared with the ground truth for the three testing data.

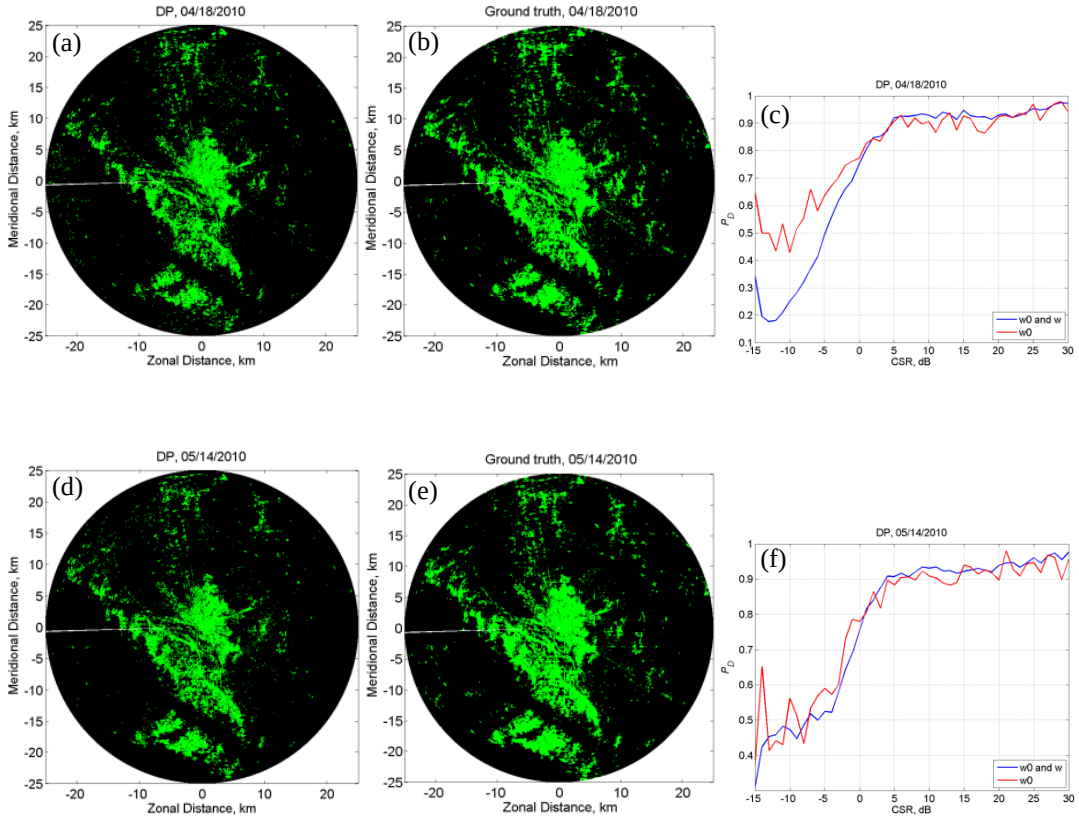

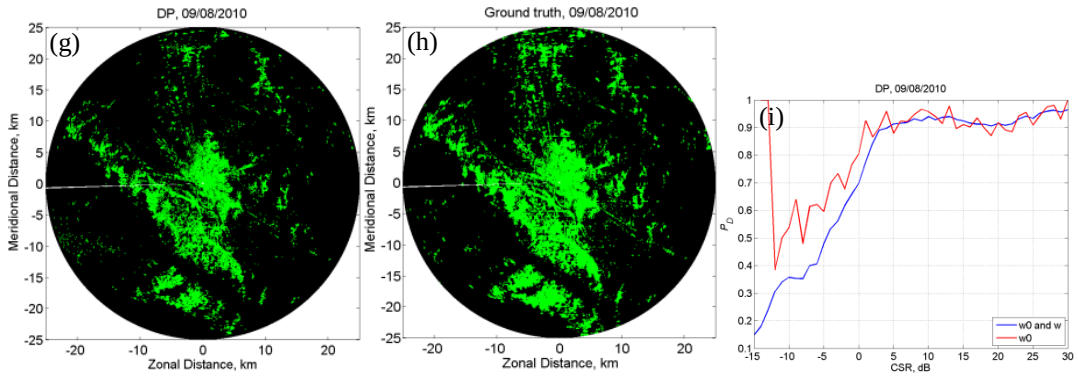

Figure 2-10: SBC-DP clutter maps (a, d, g) compared with the ground truth (b, e, h) for the three testing data. P_D as a function of CSR (dB) is shown in (c, f, i) for the three testing data. The blue line represents the performance of the SBC-DP in detecting ground clutter in the presence of both w and w0 while the red line in the presence of only w0.

From Fig. 2-10, we find that the SBC-DP algorithm has better detection performance when clutter is mixed with w0 than mixed with w and w0. The reason is that PR is larger when clutter is mixed with w0 than mixed with w. Larger PR means a higher probability that the gate is contaminated by ground clutter according to Fig. 2-9. In Table 2-6 we list the probability of detection P_D, probability of false alarm P_{FA}, and critical success index (CSI) for the three testing data sets by using the SBC-DP algorithm.

Table 2-6. P_D, P_{FA}, and CSI for the three testing data by using the SBC-DP algorithm.

	P_D	P_{FA}	CSI
04/18/2010	86.27%	1.67%	0.83

05/14/2010	85.29%	1.11%	0.83
09/08/2010	84.86%	0.65%	0.84

Compared with the SCI algorithm, the SBC-DP algorithm significantly reduces the number of false detections which can be inferred by comparing Fig. 2-5 to 2-10 and Table 2-4 to 2-6. The SBC-DP algorithm also has higher P_D compared with the SCI especially when CSR > -6 dB (the CSR needs to be -5.9 dB to bias the mean power 1 dB from Table 2-3). Compared with the SCI, the SBC-DP algorithm is based solely on data from each resolution volume because spatial texture increases false alarms and unnecessary filtering (Torres et al., 2012). In the next section, the SBC-DS and SBC-DPDS algorithms will be evaluated and compared with the SBC-DP using the data collected by PX-1000, a 3-cm polarimetric transportable radar.

2.6.3 Evaluation of the SBC-DS and SBC-DPDS Algorithms

The training weather data were collected at 02:47, 02:52, 02:59, 03:04, and 03:08 UTC on Dec 15th 2012 by the PX-1000 radar (the details of the radar are discussed in Cheong et al. (2013)), with two scans at the same elevation angle (3°) separated by about 25 s. The clutter data were collected at 14:35 UTC on Feb 28th 2013 with two scans at the same elevation angle (1°) separated by about 25 s. We combined the weather and clutter the same way described in Section 2.6.1.

As described in Sections 2.3 and 2.5, three discriminants are used in the SBC-DS algorithm and ten discriminants are used in the SBC-DPDS algorithm. In Fig. 2-11, the CPDFs $p(\mathrm{PR_h}, \mathrm{PR_v} \mid i)$, $p(Z_{\mathrm{DR}}(1) \mid i)$, $p(|\rho_{\mathrm{hv}}(1)| \mid i)$, and $p(|\rho_{12\mathrm{h}}(1)|, |\rho_{12\mathrm{v}}(1)| \mid i)$ obtained from training data are shown.

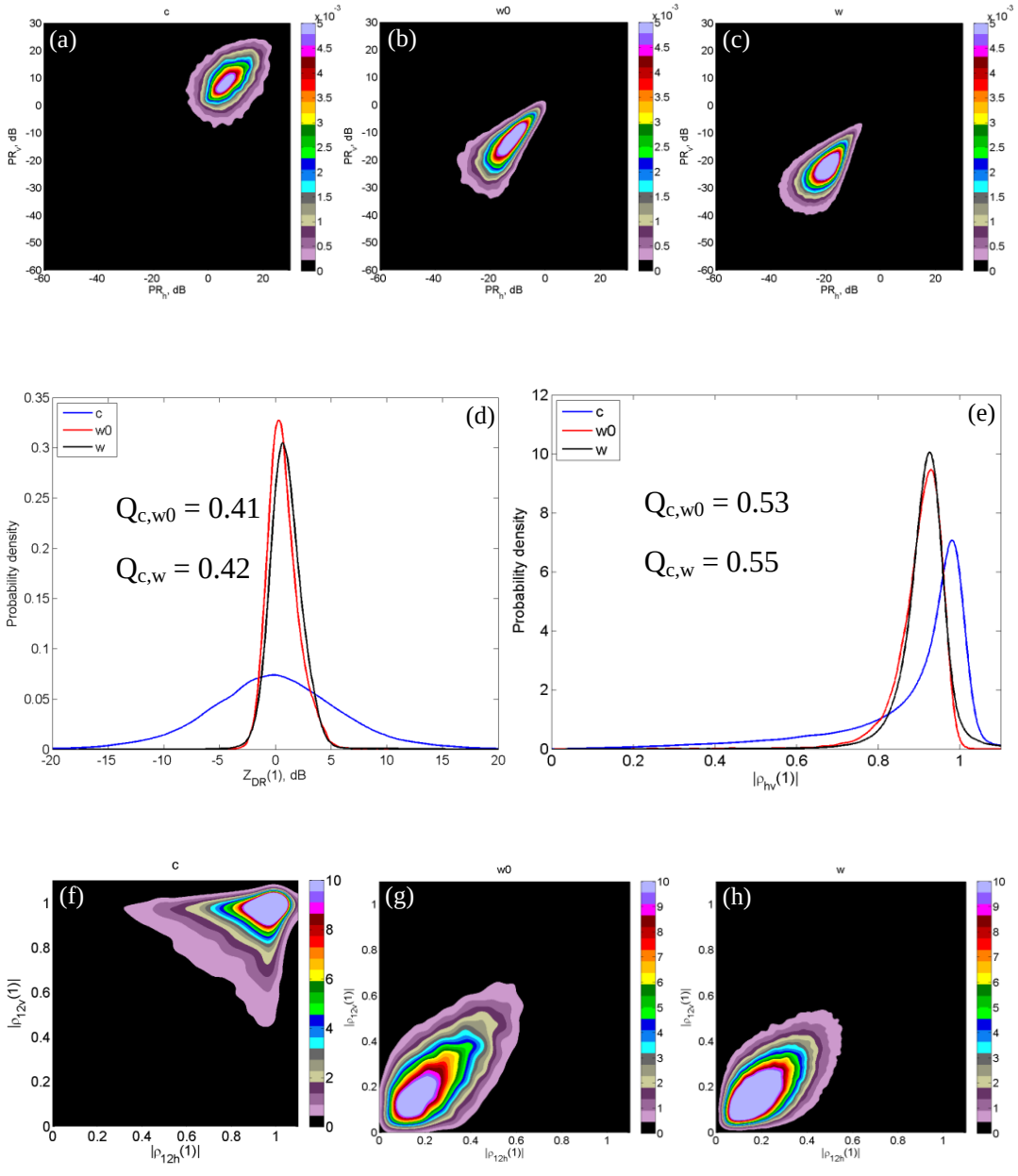

Figure 2-11: $p(\mathrm{PR_h}, \mathrm{PR_v} \mid i)$ given (a) i = c, (b) i = w0, and (c) i = w; (d) $p(Z_{\mathrm{DR}}(1) \mid i)$ given i = c, w0, and w; (e) $p(\left|\rho_{\mathrm{hv}}(1)\right| \mid i)$ given i = c, w0, and w; $p(\left|\rho_{12\mathrm{h}}(1)\right|, \left|\rho_{12\mathrm{v}}(1)\right| \mid i)$ given (f) i = c, (g) i = w0, and (h) i = w.

From Fig. 2-11, we can conclude that the Power Ratio (PR) is generally larger for clutter than weather signals; $Z_{\mathrm{DR}}(1)$ has a much larger spread for c; $\left|\rho_{\mathrm{hv}}(1)\right|$ has a larger spread for c and in contrast to Fig. 2-9(e), the peak of $p(\left|\rho_{\mathrm{hv}}(1)\right| \mid \mathrm{c})$ is to the right of those of $p(\left|\rho_{\mathrm{hv}}(1)\right| \mid \mathrm{w})$ and $p(\left|\rho_{\mathrm{hv}}(1)\right| \mid \mathrm{w}\,0)$. The reason is still unknown. One possible explanation is the PX-1000 receiver is saturated for ground clutter echoes. When the receiver is saturated for each pulse received, the received voltages would be a constant for both H and V channels, thus the correlation coefficient would be equal to 1.

After the CPDFs shown in Fig. 2-11 are obtained from training data, they will be used on testing data to make decisions as to the presence of clutter. In Fig. 2-12, the reflectivity, Doppler velocity, spectrum width, power ratio, differential reflectivity, copolar correlation coefficient, and cross-correlation coefficient between two scans for the testing data, collected on 03:12 UTC 12/15/2012, are shown.

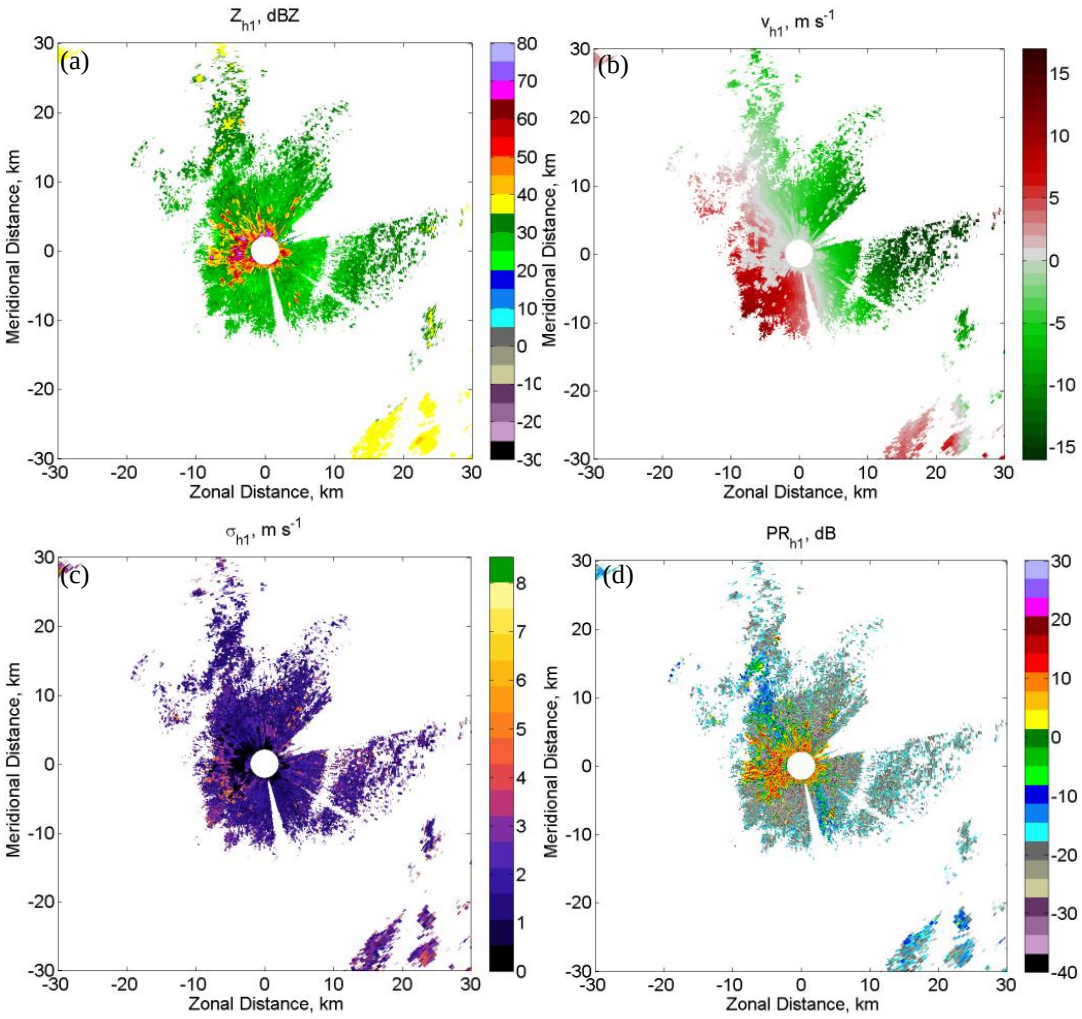
Z_{h1}, dBZ
(a)
v_{h1}, m s^{-1}
(b)
σ_{h1}, m s^{-1}
(c)
PR_{h1}, dB
(d)
Meridional Distance, km
Zonal Distance, km

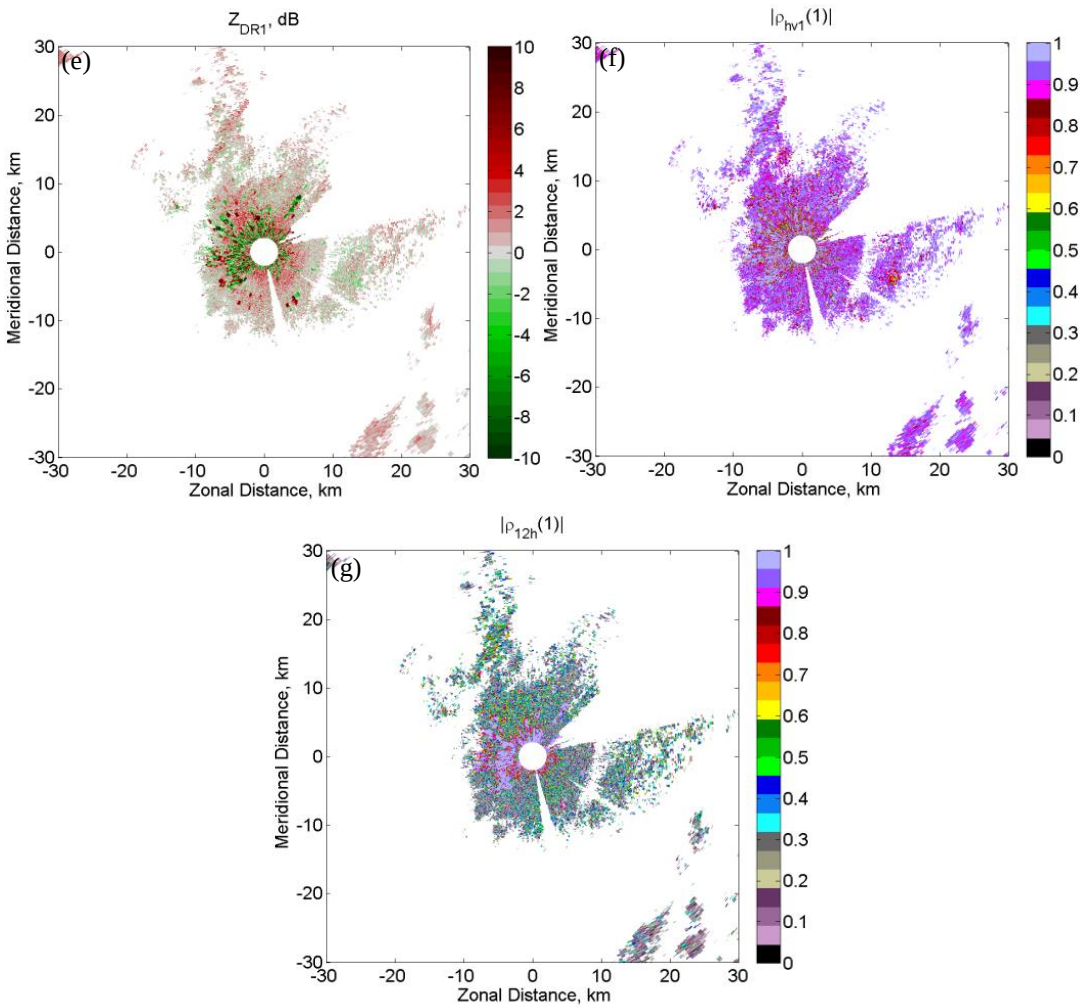

Figure 2-12: Weather signals (03:12 UTC 12/15/2012) mixed with ground clutter (14:35 UTC on 12/28/2013). (a) Horizontal reflectivity of the first scan; (b) Horizontal Doppler velocity of the first scan; (c) Horizontal spectrum width of the first scan; (d) Horizontal power ratio of the first scan; (e) Differential reflectivity of the first scan using 1-lag estimator; (f) Copolar correlation coefficient of the first scan using 1-lag estimator; (g) cross-correlation coefficient between two scans of horizontal voltages using 1-lag estimator.

From Fig. 2-12 we can conclude that compared with weather signals, clutter generally has higher reflectivity, near-zero Doppler, narrower spectrum width, higher power ratio (PR), larger spread of $Z_{\mathrm{DR}}(1)$, larger spread of $\left|\rho_{\mathrm{hv}}(1)\right|$, and higher $\left|\rho_{12}(1)\right|$. In Fig. 2-13, clutter maps obtained using SBC-DPDS, SBC-DP, and SBC-DS algorithms are compared with the ground truth, and P_{D} vs. CSR are shown for the same data shown in Fig. 2-12.

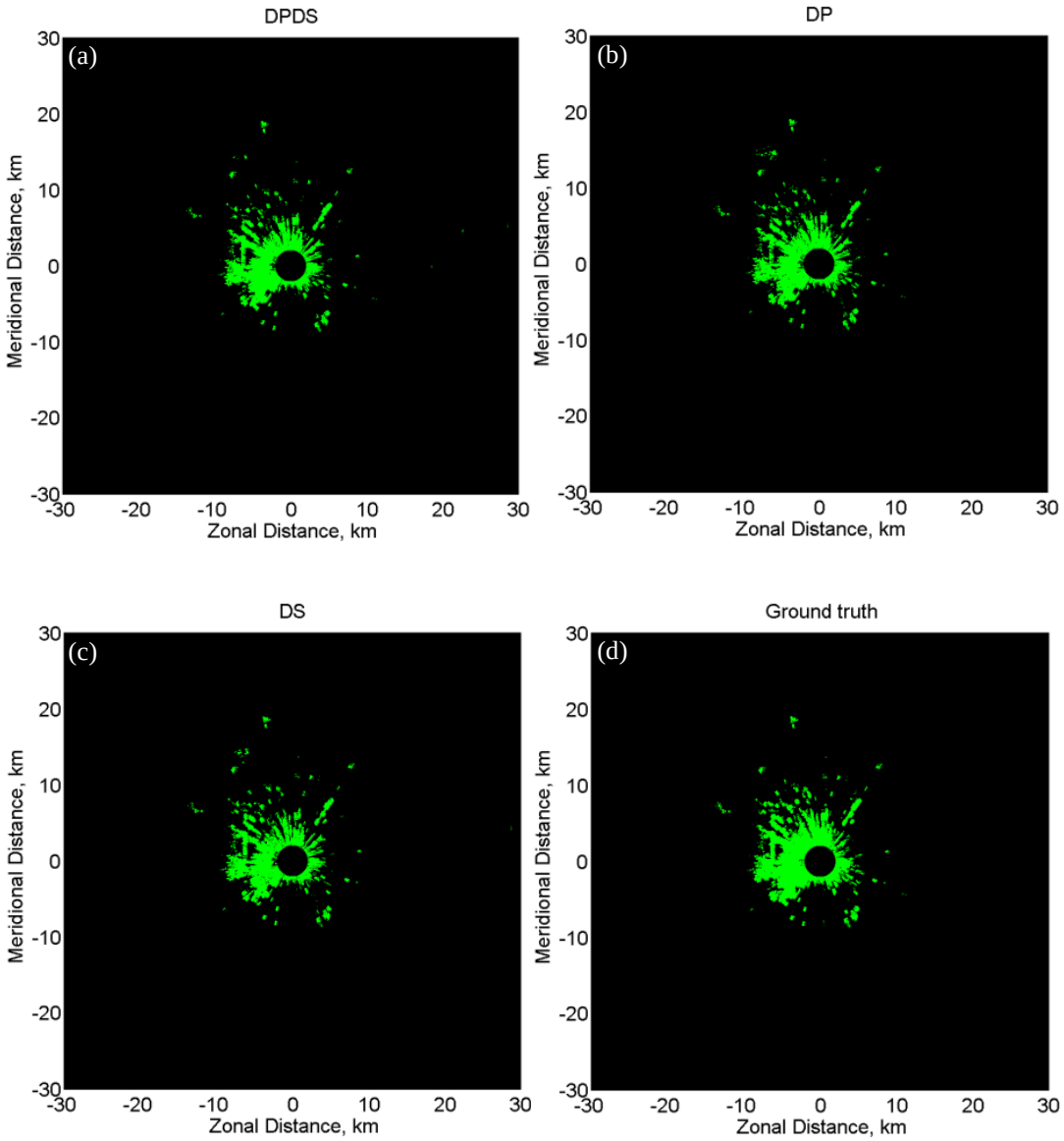

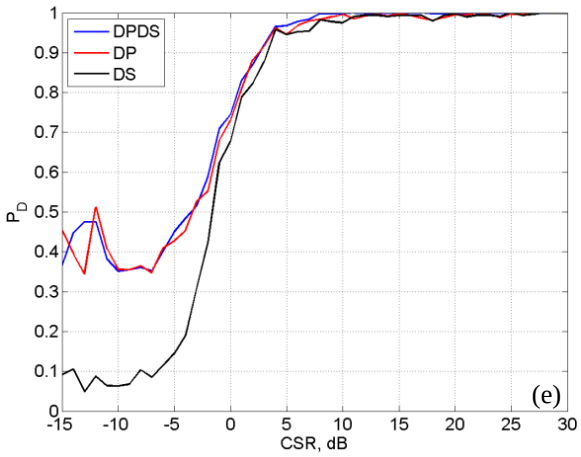

Figure 2-13: Clutter maps obtained using (a) SBC-DPDS, (b) SBC-DP, and (c) SBC-DS; (d) Ground truth; (e) P_D as a function of CSR. The data are the same as the one shown in Fig. 2-12.

For the SBC-DS algorithm, the CPDFs $p(PR_1 \mid i)$, $p(PR_2 \mid i)$, and $p(|\rho_{12}(1)| \mid i)$ are used; For the SBC-DP algorithm, the CPDFs $p(PR_h, PR_v \mid i)$, $p(Z_{DR}(1) \mid i)$, and $p(|\rho_{hv}(1)| \mid i)$ are used. From Fig. 2-13 we can conclude that the SBC-DP algorithm has comparable detection performance with the SBC-DPDS algorithm. The SBC-DS algorithm performs equally well with the other two when CSR is larger than 5 dB but it performs poorer when CSR is smaller than 5 dB.

In Table 2-7 we list the probability of detection P_D, probability of false alarm P_{FA}, and critical success index (CSI) for the three testing data sets.

Table 2-7. P_D, P_{FA}, and CSI for the three testing data by using the SBC-DPDS, SBC-DP, and SBC-DS algorithms. All the testing weather data were collected at different times on 12/15/2012.

	P_D DPDS	P_D DP	P_D DS	P_{FA} DPDS	P_{FA} DP	P_{FA} DS	CSI DPDS	CSI DP	CSI DS
03:12	86.06%	85.25%	79.31%	3.42e-4	4.22e-4	3.61e-4	0.85	0.84	0.78
03:18	95.53%	94.62%	91.20%	1.68e-4	1.92e-4	1.71e-4	0.95	0.94	0.90
03:22	97.30%	96.32%	93.92%	1.94e-4	2.18e-4	1.92e-4	0.95	0.94	0.92

From Table 2-7, we can see that all three methods produce low P_{FA}, the reason is that there are not as many narrow-band zero-velocity weather signals as shown in Fig. 2-4. However, if there are many narrow-band zero-velocity weather signals, it is expected that the SBC-DPDS algorithm will produce the lowest P_{FA} with the highest P_D.

Chapter 3: Bi-Gaussian Model Adaptive Processing (BGMAP)

In this Chapter, a ground clutter filter implemented in the spectral domain based on the Bi-Gaussian model is discussed. In Section 3.1, a cost function based on Bayes' theorem is derived and by minimizing it the weather moments can be estimated; In Section 3.2, a noise floor estimation method is introduced and the selection of window function based on the estimated CSR is discussed; In Section 3.3, the Bi-Gaussian fitting of the weather and clutter spectra by minimizing the cost function are discussed; In Section 3.4, the BGMAP algorithm is applied to the same data as shown in Fig. 2-4 to evaluate its performance.

3.1 Derivation of the Cost Functions based on the Maximum A Posteriori and Least Squares Approaches

The Power Spectral Density (PSD) of time-series voltages $y_{x,m} = c_{x,m} + w_{x,m} + n_{x,m}$ (x = h or v; m = 1, 2, …, M) consists of a weather spectrum centered at the mean Doppler velocity of weather signal (v_{rw}), a clutter spectrum centered at the mean Doppler velocity of ground clutter (v_{rc}), and a noise floor. Both the I (in-phase) and Q (quadrature) voltages of weather and noise have Gaussian statistics according to the Central-Limit Theorem (Doviak and Zrnic, 2006, Sec. 4.3), and thus the amplitude is Rayleigh distributed and power is exponential distributed. According to Billingsley (2002), the distribution of ground clutter amplitude is commonly described by Weibull distribution, which has no physical basis but is simply curve fitting tool to better describe the data. In this dissertation, it is assumed that each spectral line of the observed spectrum, which is the convolution of the intrinsic spectrum and the spectrum of window function, is independently exponential distributed and the Doppler spectra of weather and clutter are Gaussian. The expected observed spectra can be written as:

$$S(v) = \frac{P_w}{\sigma_{vw}\sqrt{2\pi}} \exp\left[-\frac{(v - v_{rw})^2}{2\sigma_{vw}^2} \right] + \frac{P_c}{\sigma_{vc}\sqrt{2\pi}} \exp\left[-\frac{(v - v_{rc})^2}{2\sigma_{vc}^2} \right] + \frac{P_n}{2v_N} \qquad (3\text{-}1)$$

In (3-1), P_w is the weather power, v_{rw} is the mean Doppler velocity of weather, and σ_{vw} is the spectrum width of weather; P_c is the clutter power, v_{rc} is the mean Doppler velocity of clutter, and σ_{vc} is the spectrum width of clutter and it is

assumed that $\sigma_{vc} < \sigma_{vw}$; P_n is the noise power and v_N is the Nyquist velocity. v_{rc} can only be -Δv, 0, or Δv, where Δv is the spectral line spacing. Because of the window function, the seven parameters in (3-1), P_w, v_{rw}, σ_{vw}, P_c, v_{rc}, σ_{vc}, and P_n, are the biased estimates of the intrinsic parameters.

3.1.1 The Maximum A Posteriori (MAP) Approach

If the power of each spectral line is exponentially distributed as assumed, we have:

$$p(\hat{S}_m \mid S_m) = \frac{1}{S_m} \exp\left(-\frac{\hat{S}_m}{S_m} \right) \tag{3-2}$$

In (3-2), $\hat{S}_m$ is the measured power corresponding to the m^{th} spectral line and S_m is equal to $S(v_m)$ given in (3-1). Instead of the measured value $\hat{S}_m$, one would like to know the expected value S_m, which is determined by seven variables: P_w, v_{rw}, σ_{vw}, P_c, v_{rc}, σ_{vc}, and P_n. It is possible for us to find S_m that maximize $p(S_m \mid \hat{S}_m)$ by using Bayes' theorem (Papoulis, 1991, Chap. 7-3):

$$p(S_m \mid \hat{S}_m) = \frac{p(\hat{S}_m \mid S_m) p(S_m)}{p(\hat{S}_m)} = \frac{p(\hat{S}_m \mid S_m) p(S_m)}{\int_{P_n / 2v_N}^{+\infty} p(\hat{S}_m \mid S_m) p(S_m) \, \mathrm{d} S_m} \tag{3-3}$$

In (3-3) $p(S_m)$ is a prior probability for S_m, which is unknown. In the absence of other information, it is assumed that $p(S_m)$ is uniform over the range $\left[P_n / 2v_N \quad +\infty \right)$. Thus (3-3) can be rewritten as:

$$p(S_m \mid \hat{S}_m) = \frac{p(\hat{S}_m \mid S_m)}{\int_{P_n/2v_N}^{+\infty} p(\hat{S}_m \mid S_m)\,\mathrm{d}\,S_m} \tag{3-4}$$

Bring (3-2) into (3-4), we obtain:

$$p(S_m \mid \hat{S}_m) = \frac{\frac{1}{S_m}\exp\left(-\frac{\hat{S}_m}{S_m}\right)}{\int_{P_n/2v_N}^{+\infty} \frac{1}{S_m}\exp\left(-\frac{\hat{S}_m}{S_m}\right)\mathrm{d}\,S_m} \tag{3-5}$$

In this dissertation, the noise level $P_n / 2v_N$ is predetermined before the optimization by using the method described in Hildebrand and Sekhon (1974) which will be discussed in Section 3.2. Thus, searching for S_m is equivalent to search for the set of parameters P_w, v_{rw}, σ_{vw}, P_c, v_{rc}, and σ_{vc} that can maximize $p(S_m \mid \hat{S}_m)$. The denominator of (3-5) does not depend on the set of parameters and therefore plays no role in the optimization process (Kay, 1993b, Chap. 11.5). Thus, maximizing $p(S_m \mid \hat{S}_m)$ is equivalent to maximizing $\frac{1}{S_m}\exp\left(-\frac{\hat{S}_m}{S_m}\right)$. (3-5) can be rewritten as:

$$p(S_m \mid \hat{S}_m) = \frac{1}{g(\hat{S}_m, P_n / 2v_N)S_m}\exp\left(-\frac{\hat{S}_m}{S_m}\right) \tag{3-6}$$

In (3-6), g represents a function of $\hat{S}_m$ and $P_n / 2v_N$. In this dissertation, it is assumed that the spectral power distribution of each spectral line is independent. In this case, the joint probability can be written as a product:

$$p(S_1, S_2, ..., S_m \mid \hat{S}_1, \hat{S}_2, ..., \hat{S}_m) = \prod_{m=1}^{M} \frac{1}{g(\hat{S}_m, P_{\mathrm{n}} / 2v_{\mathrm{N}}) S_m} \exp\left(-\frac{\hat{S}_m}{S_m} \right) \tag{3-7}$$

If we take the logarithm of both sides of (3-7), we obtain:

$$\ln p(S_1, S_2, ..., S_m \mid \hat{S}_1, \hat{S}_2, ..., \hat{S}_m) = \sum_{m=1}^{M} \left(-\ln g(\hat{S}_m, P_{\mathrm{n}} / 2v_{\mathrm{N}}) \right) + \sum_{m=1}^{M} \left(-\ln S_m - \frac{\hat{S}_m}{S_m} \right) \tag{3-8}$$

Thus, in order to maximize $p(S_1, S_2, ..., S_m \mid \hat{S}_1, \hat{S}_2, ..., \hat{S}_m)$, we only need to minimize the cost function:

$$J_{\mathrm{MAP}} = \sum_{m=1}^{M} \left(\ln S_m + \frac{\hat{S}_m}{S_m} \right) \tag{3-9}$$

The subscript MAP signifies Maximum A Posteriori. Thus, we need to find the six variables P_{w}, v_{rw}, σ_{vw}, P_{c}, v_{rc}, and σ_{vc}, that minimizes $\sum_{m=1}^{M} \left(\ln S_m + \frac{\hat{S}_m}{S_m} \right)$.

3.1.2 The Least Squares (LS) Approach

Another way to derive the cost function is the Least Squares (LS) approach. A salient feature of the method is that no probabilistic assumptions are made about the data. The cost function derived from the LS approach in the log scale is:

$$J_{\mathrm{LS}} = \sum_{m=1}^{M} \left(\ln S_m - \ln \hat{S}_m \right)^2 \tag{3-10}$$

3.1.3 Comparisons between the MAP and LS

In order to compare the performance of (3-9) and (3-10), the following simulation is proposed:

1. Create the expected observed weather and clutter spectra using (3-1).

2. Randomize each spectral line with an exponential distribution with mean equal to S_m. Assume the distribution of each spectral line is independent from another.

3. Using interior point methods (Byrd et al., 2000) to search for the set of six unknown parameters P_w, v_{rw}, σ_{vw}, P_c, v_{rc}, and σ_{vc}, that minimizes (3-9) and (3-10), respectively.

4. Repeat steps 2 and 3 1000 times with different random seeds.

In this simulation, it is assumed that SNR = 30 dB, P_c = 40 dB, P_w = 20 dB, CSR = 20 dB, λ = 5.44 cm, PRT = 800 μs, M = 33, σ_{vw} = 2 m s^{-1}, v_{rc} = 0, v_{rw} = 0 and 8 m s^{-1}, and σ_{vc} = 0.5 m s^{-1}. In Table 3-1, the performances of the MAP and LS approaches are compared.

Table 3-1: Comparison between MAP and LS approaches if each spectral line is independently exponential distributed. The numbers out of the brackets represent means and those in the brackets represent standard deviations.

	v_{rw} = 0		v_{rw} = 8	
	MAP	LS	MAP	LS
$\hat{P}_w$	19.29(2.31)	17.67(2.78)	19.89(1.62)	17.91(1.96)

$\hat{v}_{rw}$	0(0.25)	0(0.29)	8(0.40)	7.96(0.45)
$\hat{\sigma}_{vw}$	2.02(0.14)	1.98(0.17)	1.98(0.19)	1.99(0.20)

From Table 3-1, we can conclude that MAP outperforms LS under the circumstances that each spectral line is independently exponential distributed. In Fig. 3-1, the simulated spectra using the procedures given above are shown. The blue line signifies the expected observed spectra obtained from (3-1), blue dash line the observed spectra with random variations using the simulation procedures given above, red line the fitted spectra using the MAP approach, and black line the fitted spectra using the LS approach. From Fig. 3-1, we can conclude that the LS approach is more affected by outliers (large fluctuations) than the MAP approach. Thus, in this dissertation, the cost function given in (3-9) will be used. In the next section, the window function selection and estimation of noise floor will be discussed.

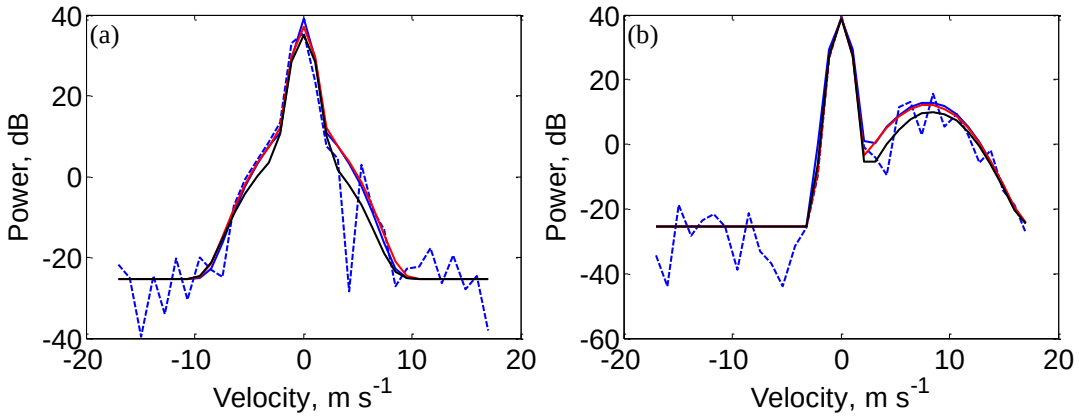

Figure 3-1: Simulated spectra using the procedures given in Section 3.1.3. v_{rw} is equal to (a) 0 and (b) 8 m s^{-1}. The blue line signifies the expected observed spectra, blue dash line the observed spectra with random variations, red line the fitted spectra using the MAP approach, and black line the fitted spectra using the LS approach.

3.2 Window Function Selection and Estimation of Noise Floor

Considering the spectral leakage due to limited number of samples, the selection of window function is very important to the reconstruction process (Siggia and Passarelli, 2004) in order to minimize the bias of weather spectra moments. In this dissertation, a similar window selection method with the one described in Siggia and Passarelli [9] will be used, which is shown below:

First a Hamming window weighting function is applied to the IQ data and then the BGMAP algorithm is implemented.

If the estimated CSR > 40 dB, repeat BGMAP using a Blackman window.

If the estimated CSR > 20 dB, repeat BGMAP using a Blackman window; Then if CSR > 25 dB Blackman results are used.

If CSR < 2.5 dB, repeat BGMAP using rectangular window; Then if CSR < 1 dB rectangular results are used.

ELSE, accept the Hamming window results.

In this dissertation we used the method described in Hildebrand and Sekhon (1974) to determine the noise floor and the boundary between the noise and signal/clutter region. The radar system noise power is exponentially distributed and it has a white spectrum. Because the noise spectral components are independent and according to the properties of exponential distribution, we have:

$$\mathrm{var}(S_n) = \langle S_n \rangle^2 \tag{3-11a}$$

$$\mathrm{var}(S_n) = \langle S_n^2 \rangle - \langle S_n \rangle^2 \tag{3-11b}$$

In (3-11), S_n corresponds to the noise spectral component. (3-11a) is obtained from the properties of exponential distribution while (3-11b) is obtained from the definition of variance. For white noise, the ensemble average $\langle S_n \rangle$ can be estimated from one realization of the process, by averaging all the noise spectral components in the power spectrum. Thus, we can define a parameter, which is the ratio between (3-11a) and (3-11b):

$$R = \frac{\langle S_n \rangle^2}{\langle S_n^2 \rangle - \langle S_n \rangle^2} \tag{3-12}$$

According to (Hildebra and Sekhon, 1974), for white noise, the ratio *R* should be unity because the mean is equal to the standard deviation of noise spectral components. For a spectrum containing weather/clutter, it is expected that *R* should be less than 1 because weather/clutter spectrum is not white and thus the ensemble average cannot be computed from one realization of the process. Thus, we can select the boundary between noise and weather/clutter by using (3-12). The ratio *R*, calculated from all the spectral components under the boundary, should be equal to 1. In Fig. 3-2, simulated power spectra containing weather, clutter, and noise are

shown. The power spectra are obtained by using the spectral simulator given in Zrnic (1975). In Fig. 3-2, P_c = 40 dB, CSR = 20 dB, v_{rw} = 5 m s^{-1}, σ_{vw} = 2 m s^{-1}, v_{rc} = 0, σ_{vc} = 0.5 m s^{-1}, and M = 64.

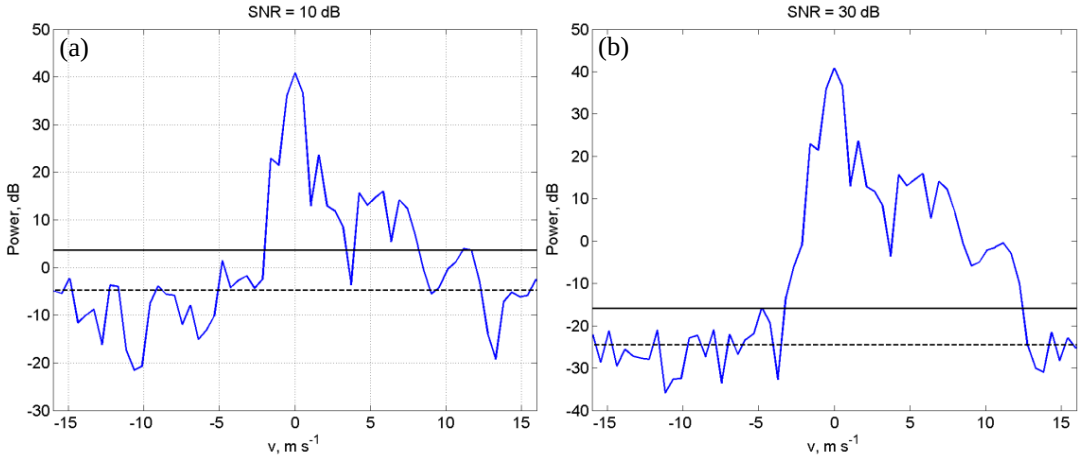

Figure 3-2: Simulated spectra containing weather, clutter, and noise. The black line is the boundary between noise and weather/clutter region (R = 1) and the black dash line is the noise floor. (a) SNR = 10 dB and (b) SNR = 30 dB.

In Fig. 3-3 the ratio R given in (3-12) as a function of threshold (dB below the peak) is shown for the simulated spectra given in Fig. 3-2. The ratio R is calculated with all the spectral components under every arbitrarily assigned threshold (blue curve). The noise and signal/clutter boundary corresponds to the threshold with R = 1 (black line).

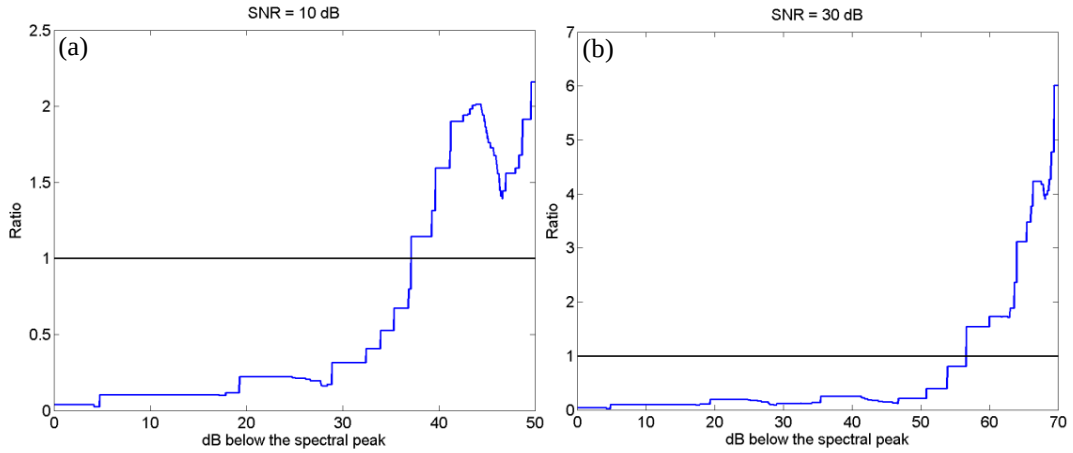

Figure 3-3: The blue curve represents the ratio (3-12) as a function of threshold and the black line corresponds to R = 1. The threshold is dB below the spectral peak and the ratio is calculated with all the spectral components under the threshold. (a) SNR = 10 dB and (b) SNR = 30 dB.

After the boundary is calculated in Fig. 3-3, all the spectral components under the boundary are averaged to obtain the noise floor, which are the black dash lines shown in Fig. 3-2. If there are few number of samples in a dwell (e.g., M = 10), the boundary cannot be accurately estimated. In this case, zero padding to time series data after the window function is applied because zero padding corresponds to ideal interpolation in the spectral domain according to Smith III (2007). In the next section, the Bi-Gaussian fitting of weather and clutter spectra by minimizing the cost function J_{MAP} given in (3-9) will be discussed.

3.3 Bi-Gaussian Fitting of the Weather and Clutter Spectra

After the noise floor P_{n} is determined, all the spectral components are used to fit the Bi-Gaussian model given in (3-1) by searching for the optimal unknown

parameters $P_w, v_{rw}, \sigma_{vw}, P_c, v_{rc}, \sigma_{vc}$ that can minimize J_{MAP}. Interior point methods (Byrd et al., 2000) will be used in the optimization process which will not be discussed because it is not a focus of this dissertation. One thing to notice is that if v_{rw} is close to the Nyquist velocity, the Bi-Gaussian assumption does not hold because the weather spectrum would be divided into two parts on the two ends of the spectrum. In this case, we need to shift the spectral interval of $[-v_N \; v_N]$ to $[-v_N + \Delta v_s \; v_N + \Delta v_s]$ to obtain a complete weather spectrum. Δv_s represents a shifted velocity and it can be determined from the following steps:

1. All the noise spectral components (identified by Section 3.2) are set to zero.
2. All the spectral components within ±4 m s^{-1} are set to zero.
3. Find the radial velocity v_{max} corresponding to the maximum spectral component.
4. If $v_{max} - v_N/2$ is less than $-v_N$, Δv_s is equal to $v_N/2 + v_{max}$.
5. If $v_{max} + v_N/2$ is larger than v_N, Δv_s is equal to $-v_N/2 + v_{max}$.
6. Otherwise Δv_s is equal to zero.

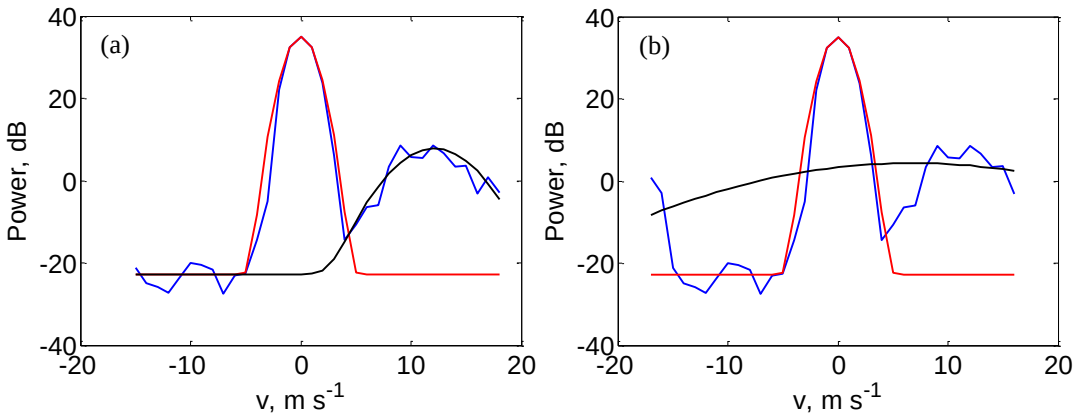

Figure 3-4: The blue line is the observed spectra, and it consists of clutter, weather, and noise. The red line represents the fitted clutter+noise spectrum and the black line represents the fitted weather+noise spectrum by minimizing J_{MAP}. In (a), the spectral interval $[-v_N\ v_N]$ is shifted to $[-v_N + \Delta v_s\ v_N + \Delta v_s]$; In (b), the spectral interval is not shifted.

In Fig. 3-4, P_c = 40 dB, CSR = 20 dB, SNR = 30 dB, v_{rw} = 12 m s^{-1}, σ_{vw} = 2 m s^{-1}, v_{rc} = 0, σ_{vc} = 0.5 m s^{-1}, M = 33, and PRT = 800 μs. We can conclude that when the mean radial velocity of weather spectrum is close to the ambiguity velocity, the Bi-Gaussian model fails (Fig. 3-4b) when fitting the spectra from $-v_N$ to v_N. In Fig. 3-4a, $\hat{P}_w$ = 19.48 dB (-0.52 dB error), $\hat{v}_{rw}$ = 12.11 m s^{-1} (0.11 m s^{-1} error) and $\hat{\sigma}_w$ = 2.47 m s^{-1} (0.47 m s^{-1} error); in Fig. 3-4b, $\hat{P}_w$ = 18.28 dB (-1.72), $\hat{v}_{rw}$ = 0.47 m s^{-1} (-11.53) and $\hat{\sigma}_w$ = 9.82 m s^{-1} (7.82). After the Bi-Gaussian fitting, all the six unknown parameters $P_w, v_{rw}, \sigma_{vw}, P_c, v_{rc}, \sigma_{vc}$ can be estimated.

The implementation procedure of the BGMAP clutter filter is described in the flowchart shown in Fig. 3-5.

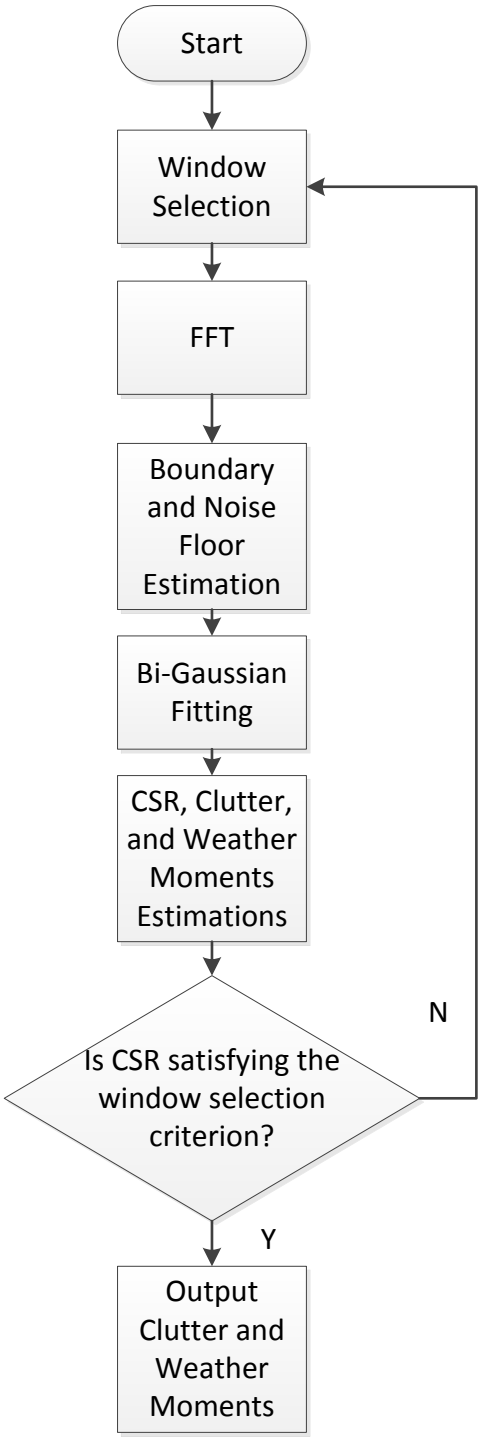

Figure 3-5: Flowchart of the Bi-Gaussian Model Adaptive Processing (BGMAP) algorithm.

In Fig. 3-5, the Hamming window is used for the first attempt and based on the estimated CSR we will decide whether other window functions (i.e., rectangular or Blackman) will be used or not. The window selection rule is discussed in Section 3.2.

In Fig. 3-6, some examples of simulated spectra and their BGMAP fittings based on the MAP approach are shown. CSR = 0 dB, SNR = 30 dB, M = 33, P_w = P_c = 40 dB, v_{rc} = 0, σ_{vc} = 0.5 m s^{-1}, σ_{vw} = 2 m s^{-1}.

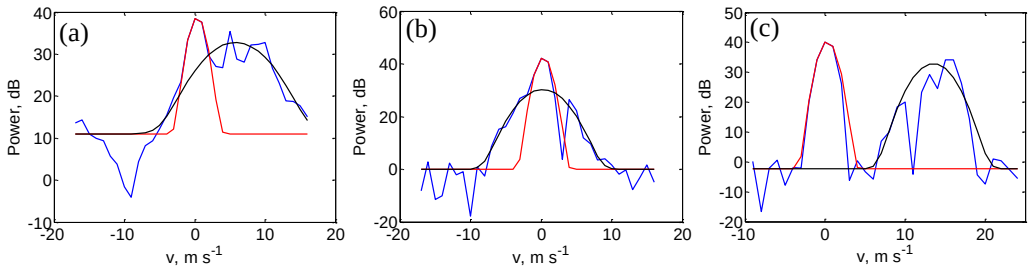

Figure 3-6: The blue line is the simulated observed spectra, the red line is the fitted clutter+noise Gaussian spectrum, and the black line is the fitted weather+noise Gaussian spectrum. v_{rw} is equal to (a) 6, (b) 0, and (c) 15 m s^{-1}.

In Fig. 3-6(a), the estimated weather power, radial velocity, and spectrum width is equal to 41.9 dB (1.9 dB error), 5.8 m s^{-1} (-0.2 m s^{-1} error), and 3.3 m s^{-1} (1.3 m s^{-1} error); In Fig. 3-6(b), the estimated weather moments are 37.7 dB (-2.3), 0.2 m s^{-1} (0.2), and 2.2 m s^{-1} (0.2); In Fig. 3-6(c), the estimated weather moments are 39.2 dB (-0.8), 13. 5 m s^{-1} (1.5), and 1.7 m s^{-1} (-0.3).

In the next section, the performance of the BGMAP will be compared with GMAP using the same data shown in Fig. 2-4.

3.4 Performance Evaluation of the BGMAP Algorithm using the Real Data

In this section the BGMAP algorithm will be applied to the three testing data shown in Fig. 2-4. In Figs. 3-7, 3-8, and 3-9, the ground truth (weather moments), clutter contaminated moments, and filtered weather moments using BGMAP and GMAP algorithms are shown for the three testing data. In these figures, BGMAP and GMAP algorithms will be only applied to the gates detected by the SBC-DP algorithm (Section 2.4.2).

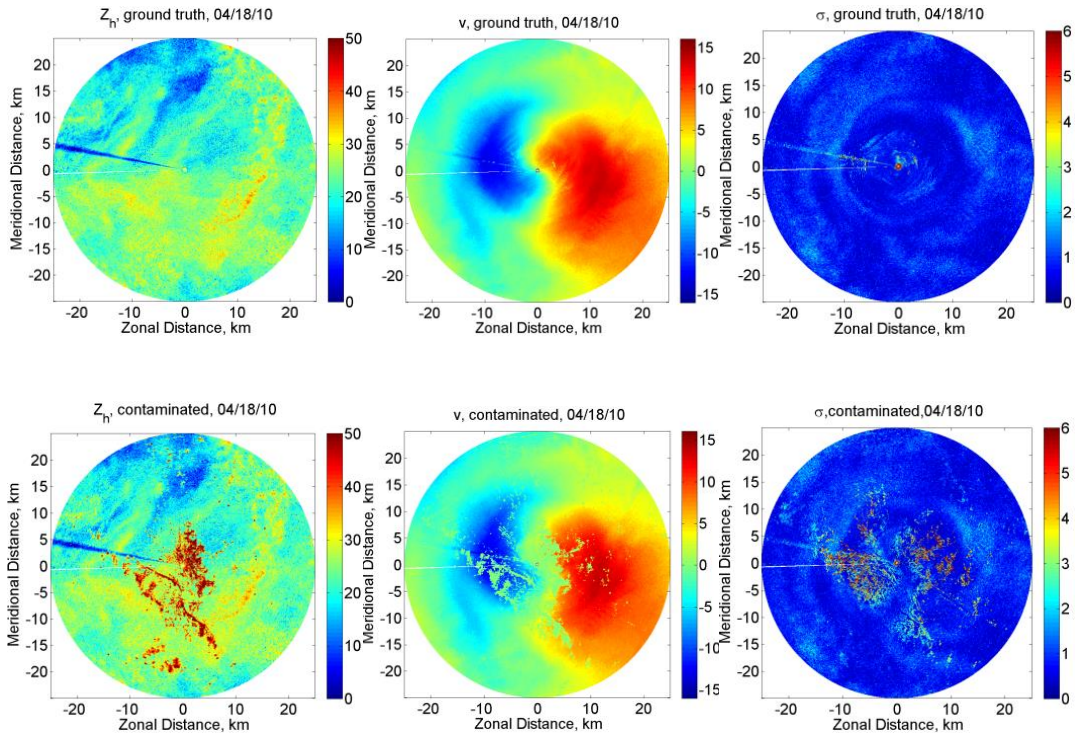

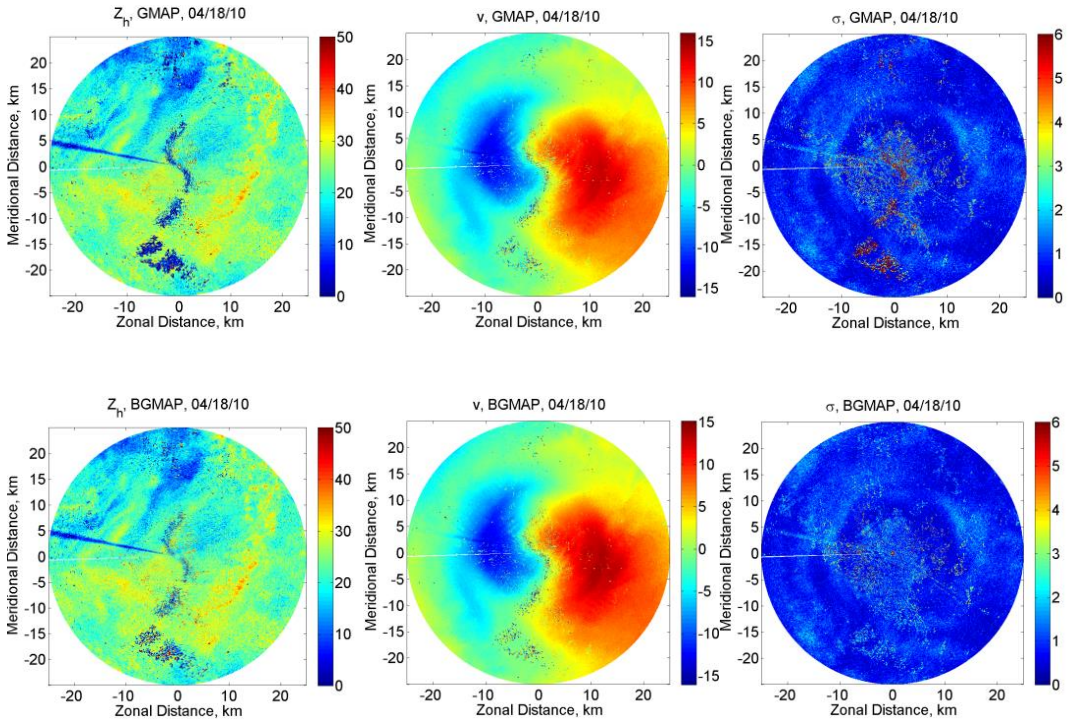

Figure 3-7: First row: weather data collected on 04/18/2010 at θ_e = 3.5°; Second row: weather data collected on 04/18/2010 combined with clutter data collected on 01/13/2011 at θ_e = 0; Third row: Filtered weather data using GMAP algorithm; Fourth row: Filtered weather data using BGMAP algorithm.

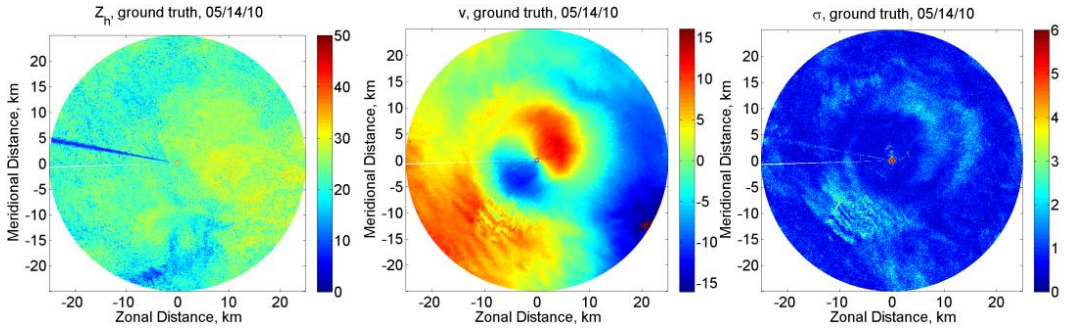

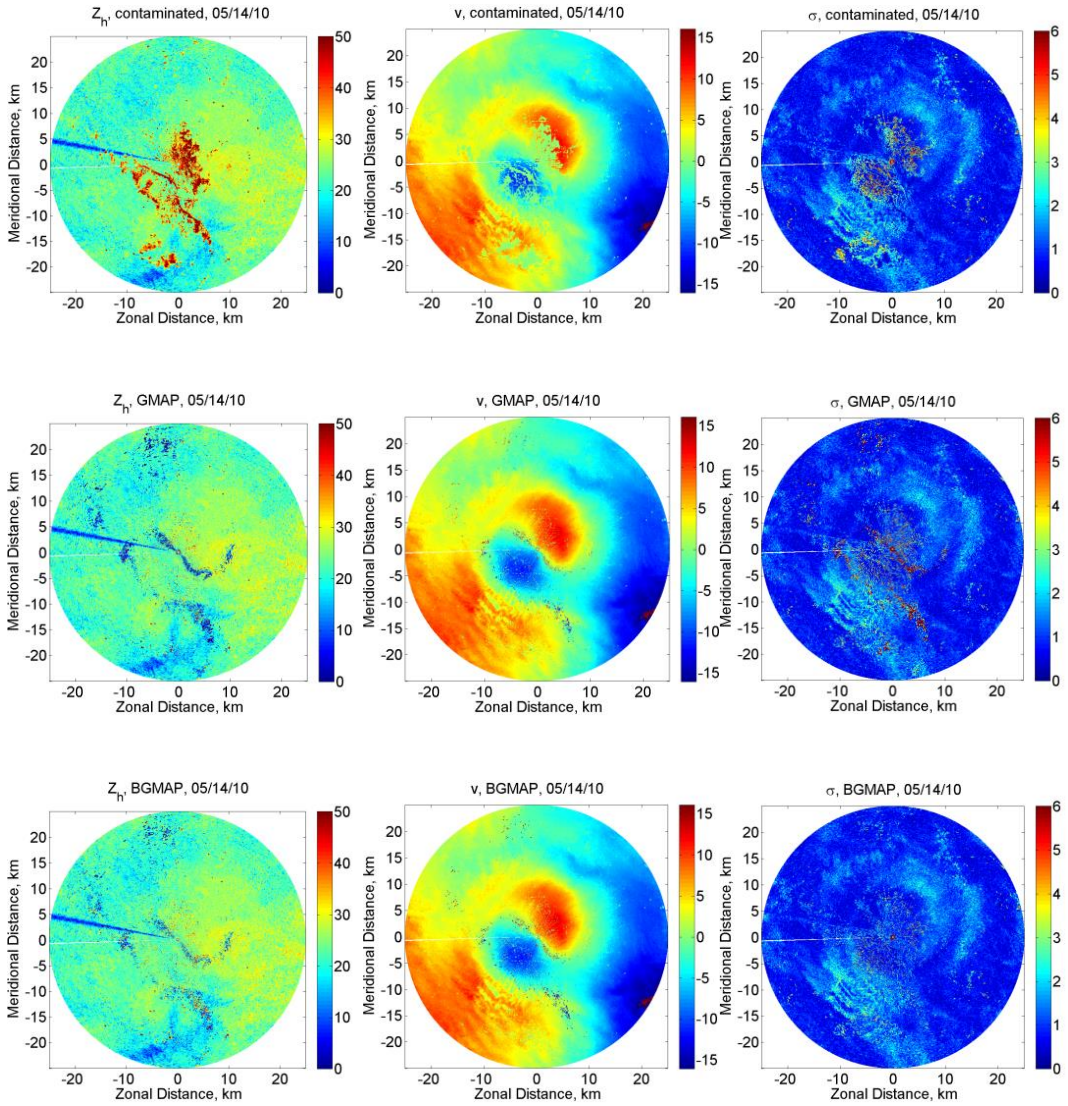

Figure 3-8: The only difference between Fig. 3-8 and 3-7 is that the weather data were collected on 05/14/2010.

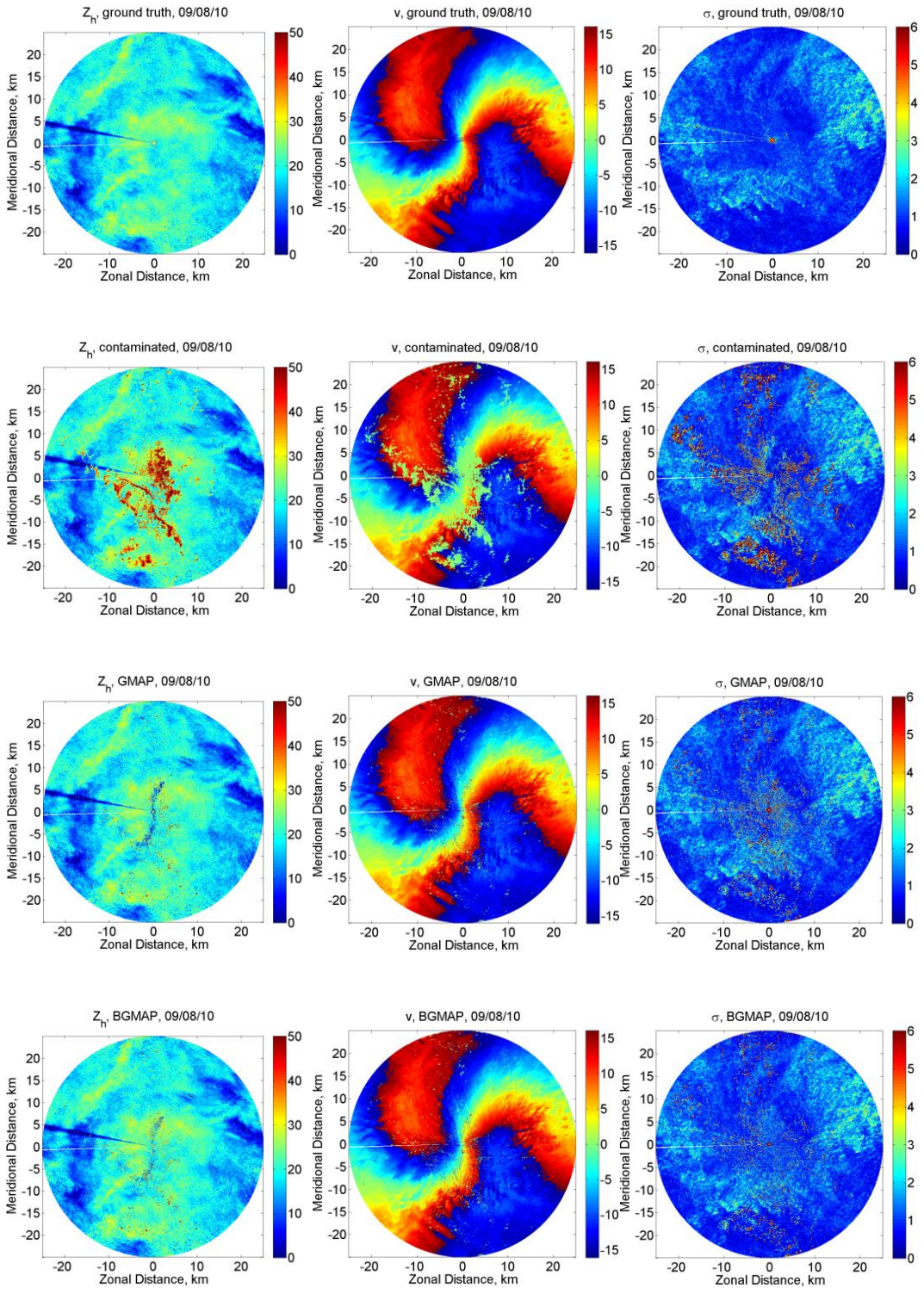

Figure 3-9: The only difference between Fig. 3-9 and 3-7 is that the weather data were collected on 09/08/2010.

From Figs. 3-7 to 3-9, a subjective comparison between BGMAP and GMAP shows that BGMAP slightly outperforms GMAP in estimating weather power, but significantly outperforms GMAP in estimating spectrum width; BGMAP and GMAP have comparable performance in estimating weather Doppler velocity. Both BGMAP and GMAP perform poorly on the clutter contaminated gates where weather signals have near-zero Doppler and narrow spectrum width, because weather and clutter spectra are heavily overlapped and it is the most difficult to distinguish them in the spectral domain.

In Table 3-2, Mean Absolute Errors (MAEs) are calculated at those locations identified as having ground clutter by the SBC-DP algorithm, and these are the locations where the GMAP and BGMAP algorithms are applied; for reference MAEs are also calculated if no filter is applied for the three cases shown in Figs. 3-7 to 3-9.

Table 3-2: MAEs at clutter locations identified by the SBC-DP algorithm if GMAP and BGMAP filters are applied, and if no filter is applied.

	GMAP			BGMAP			No Filter		
	Z_w dBZ	v_{rw} m s^{-1}	σ_{vw} m s^{-1}	Z_w dBZ	v_{rw} m s^{-1}	σ_{vw} m s^{-1}	Z_w dBZ	v_{rw} m s^{-1}	σ_{vw} m s^{-1}
04/18/10	5.13	1.68	1.53	4.48	1.90	0.92	13.03	3.90	1.42
05/14/10	4.02	1.60	1.38	3.27	1.89	0.83	12.73	4.34	1.25
09/08/10	2.87	2.05	1.20	2.75	2.10	0.80	13.89	7.48	2.32

The inputs in Table 3-2 represent the MAEs of weather moments. From the quantitative evaluation shown in Table 3-2, we can find that BGMAP outperforms GMAP in estimating weather reflectivity and and spectrum width while GMAP has slightly better performance than BGMAP in estimating weather Doppler velocity. For the case 1 and 2, the MAE of weather reflectivity and spectrum width is reduced respectively by around 0.7 dBZ and 0.7 m s^{-1} if BGMAP is used instead of GMAP. As can be seen from Figs. 3-7, 3-8, and 3-9, for both GMAP and BGMAP algorithms, the bias of reflectivity and Doppler velocity estimation becomes more significant when the weather signals have near zero Doppler velocities. For the first two cases shown in Table 3-3, the error becomes even larger when the GMAP algorithm is used to estimate spectrum width than the case when no filter is applied.

Chapter 4: Conclusions

Considering the significant bias caused by ground clutter on the estimations of weather moments, polarimetric parameters, rainfall rate, hydrometeor classification, five new clutter detection algorithms and one new clutter filtering algorithm are discussed in this dissertation. The five different clutter detection algorithms are the Spectrum Clutter Identification (SCI), SBC applied to the Dual-Scan discriminants (SBC-DS), test statistic, SBC applied to the Dual-Pol discriminants (SBC-DP), and SBC applied to the Dual-Pol Dual-Scan discriminants (SBC-DPDS). The clutter filtering algorithm is the Bi-Gaussian Model Adaptive Processing (BGMAP).

The SCI clutter detection algorithm is designed for single pol radars to detect ground clutter mixed with weather signals, even if the Clutter to Signal power Ratio (CSR) is low but clutter can significantly bias weather spectral moment estimates. SCI combines the discriminants Spectral Power Distribution (SPD), Spectral Phase Fluctuations (SPF), Power Texture (PT), and Spectrum Width Texture (SWT) using a Simple Bayesian Classifier (SBC) to detect clutter mixed with weather signals.

The Conditional Probability Density Functions, CPDFs, versus the levels of the various discriminants for practically pure ground clutter and pure narrow-band zero-velocity and non-zero velocity weather signals are obtained from clutter and stratiform weather data collected by OU-PRIME. It is shown (Fig. 2-3a) that the common area $Q_{c,w}$ between the minimum of the CPDF curves for clutter and non-zero velocity weather signals is about 0.02 for the SPD discriminant. The common area is a measure of the discriminant's capability to distinguish various classes of clutter and weather. This small $Q_{c,w}$ (ideally $Q_{c,w} = 0$) suggests SPD is effective in detecting clutter mixed with non-zero velocity weather signals. But the common area, $Q_{c,w0}$, for narrow-band zero-velocity weather signals is significantly larger (Fig.2-3a) demonstrating the difficulty to distinguish this class of weather signals from clutter.

If a single fixed scatterer generates clutter, the spectral phase is linear in the spectral interval $\pm\sqrt{2}\Delta v_w$ independent of the position of the scatterer within the radar's resolution volume. Departure from linearity is the basis to use spectral phase to detect stratiform weather signals mixed with clutter. However, it is found that the SPF discriminant improves the P_D by only a few percent. This small improvement is

due to clutter not typically being from a collection of scatterers where one scatterer is dominant.

The texture discriminants PT and SWT are both used in the SCI algorithm. PT effectively recognizes clutter when CSR is high (e.g., > 0 dB) whereas SWT recognizes clutter when CSR is low (e.g., -15 to 0 dB). Because the SWT is most effective if the Doppler velocity is at the Nyquist velocity, and because evaluation of the SCI algorithm were made using data collected by OU-PRIME, a 5-cm radar, it is expected the SWT discriminant will be more effective for 10-cm radars that have twice as large a Nyquist velocity.

One problem in evaluating the performance of clutter detectors is having reliable ground truth. To provide this ground truth, practically pure stratiform weather and clutter data were synthesized to obtain a data field of clutter mixed with weather as also suggested by (Melnikov et al., 2008); in this case CSR is precisely known. This synthesis procedure provides quantitative estimates of CSRs to evaluate P_D and P_{FA}, and it was applied to three cases of stratiform weather and the performance is given in Fig. 2-5 and Table 2-4. We consider weather signals from a resolution volume are contaminated by ground clutter only if ground clutter can bias weather signal power by more than 1 dB or its mean radial velocity and spectrum width by more than 1 m s^{-1} (NEXRAD Technical Requirements, 1991, Sec. 3.7.1.2.3.1). Otherwise, even if ground clutter does exist in the resolution volume it is considered as weather signal because its effect on weather estimates can be neglected. By doing so, we not only considered CSR but also the mean radial

velocity and spectrum width of weather signals and the spectrum width of ground clutter.

The simple Bayesian classifier applied to the dual-scan discriminants (SBC-DS) presents clutter locations with higher spatial resolution and thus less false detections (Torres et al., 2012). Higher spatial resolution is obtained because the SBC-DS algorithm is based solely on data from each resolution volume. This method is especially useful if clutter is from fixed scatterers being scanned by the weather radar's beam. Narrow-band zero-velocity weather signals and clutter from fixed scatterers scanned by the radar beam have similar spectral characteristics and thus it is difficult to distinguish them from single scan data, especially when using the short dwell times typical for weather radar having rapidly scanning beams. Scan-to-scan clutter detection offers a complementary method to existing clutter detection methods.

Furthermore, the SBC-DS algorithm might be applied to WSR-88Ds because all WSR-88Ds use Volume Coverage Patterns (VCPs) that contain two 360^{o} azimuthal scans each with different PRTs at the two lowest elevation angles (0.5 and 1.5^{o}) where clutter matters the most. The SBC-DS might also be applied to phased array radar (PAR) when it is performing beam multiplexing introduced by Yu et al. (2007), not only to detect ground clutter but also to suppress it.

A polarimetric test statistic T and its alternate form T_a are derived from the statistical properties of the received signals. It is difficult to distinguish ground clutter from narrow-band zero-velocity weather signals by using T or T_a. It is expected that T alone would produce satisfactory results if there are few narrow-

band zero-velocity weather signals because more than 90% of false detections are caused by narrow-band zero-velocity weather signals if T is used.

In order to reduce the false detections caused by narrow-band zero-velocity weather signals using test statistic, a simple Bayesian classifier applied to the dual-pol discriminants (SBC-DP) with inputs derived from the mean and covariance of the received signals, is introduced. It is found that the SBC-DP algorithm greatly reduces the false alarms caused by narrow-band zero-velocity weather signals. From Fig. 2-10, we can infer that the SBC-DP outperforms the single pol SCI algorithm (Fig. 2-5) at larger CSRs (i.e., $0 < \text{CSR} < 10$ dB).

SBC-DP is based solely on data from each resolution volume because spatial texture increases false alarms and unnecessary filtering (Torres et al., 2012). In and above the bright band, the CPDFs given weather signals I and II are different from those shown in Fig. 2-9 because Fig. 2-9 is obtained from stratiform rain under the bright band. Thus, the bright band needs to be located before implementing SBC-DP algorithm, especially when the bright band is close to the ground during the winter season. Alternatively, we can use different CPDFs for weather signals from above, in, and below the melting layer. This needs to be explored and tested in future work.

SBC applied to the Dual-Pol Dual-Scan discriminants (SBC-DPDS) combines ten discriminants to make decisions as to the presence of clutter. It is expected that the SBC-DPDS will produce the lowest P_{FA} with the highest P_{D} compared with the SBC-DS and SBC-DP algorithms as can be inferred from Fig. 2-13 and Table 2-7.

The clutter detection algorithms introduced in this dissertation should be evaluated using other types of weather other than stratiform rain, which will be left for future work. On the other hand, detecting clutter in stratiform weather signals is the most challenging and thus it is anticipated that the clutter detection algorithms introduced in this dissertation should work as well, if not better, for other types of weather. Furthermore, future study should address the performance of clutter detection algorithms to detect clutter from heavily foliage woods under different wind conditions.

A Bi-Gaussian Model Adaptive Processing (BGMAP) algorithm for clutter filtering is discussed in this dissertation. The cost function obtained by using Maximum A Posterior (MAP) approach is compared with the Least Squares (LS) approach using simulations and it is found that MAP outperforms LS under the circumstance that each spectral line is independently exponential distributed. From Figs. 3-7 to 3-9, we can conclude that the accurate estimation of weather moments (especially reflectivity) is still challenging with the BGMAP algorithm when weather signals have near zero Doppler. In order to mitigate this problem, the clutter-free gates surrounding the clutter contaminated gate should be used as a priori information to help with the clutter filtering. This is the topic we will investigate in the future. In addition, the estimate of polarimetric parameters for clutter contaminated gates will also be studied in the future.

References

Bareiss, E. H., "Sylvester's identity and multistep integer preserving Gaussian elimination", *Math. Comput.,* **22(103)**, 565-578, 1968.

Billingsley, J. B., *Low angle radar clutter: measurement and empirical models*, William Andrew Publishing, 703 pp, 2002.

Byrd, R. H., J. C. Gilbert, and J. Nocedal, "A trust region method based on interior point techniques for nonlinear programming," *Math. Program.,* **89(1)**, 149-185, 2000.

Cao, Q., G. Zhang, R. D. Palmer, M. Knight, R. May, and R. J. Stafford, "Spectrum-time estimation and processing (STEP) for improving weather radar data quality," *IEEE Trans. Geosci. Remote Sens.*, **55(11)**, 4670-4683, 2012.

Cheong, B. L., R. Kelly, R. D. Palmer, Y. Zhang, M. Yeary, and T. Y. Yu, "A solid-state polarimetric X-band weather radar and time-frequency multiplexed waveform for blind range mitigation," *IEEE Trans. Instrum. Meas.*, accepted.

Clark, P. and T. Niblett, "The CN2 induction algorithm," *Machine learning*, **3(4)**, 261-283, 1989.

Curtis, C. D., "Exploring the capabilities of the agile beam phased array weather radar", Ph. D. dissertation, Dept. Elect. Eng., University of Oklahoma, Norman, OK, 2009.

Doviak, R. J. and D. S. Zrnić, *Doppler Radar and Weather Observations,* 2nd ed., Dover, 562pp, 2006.

Fabry, F., "Meteorological value of ground target measurements by radar", *J. Atmos. Ocean. Technol.,* **21(4)**, 560-573, 2004.

Fang, M., R. J. Doviak, and V. Melnikov, "Spectrum width measured by WSR-88D: Error sources and statistics of various weather phenomena," *J. Atmos. Ocean. Technol.*, **21(6)**, 888-904, 2004.

Fawcett, T., "ROC graphs: Notes and Practical Considerations for Data Mining Researchers," Technical Report HPL-2003-4, HP Labs, 2003.

Federal Handbook, *Federal Meteorological Handbook No. 11, Doppler Radar Meteorological Observations*, Part C, 390 pp, 2006. Available at: http://www.ofcm.gov/fmh11/fmh11partc/pdf/FMH-11-PartC-April2006.pdf

Gourley, J. J., P. Tabary, and J. P. D. Chatelet, "A fuzzy logic algorithm for the separation of precipitating from nonprecipitating echoes using polarimetric radar observations," *J. Atmos. Oceanic Technol.*, **24(8)**, 1439-1451, 2007.

Groginsky H. L. and K. M. Glover, "Weather radar canceller design," *Proc. 19th Conf. Radar Meteorol.*, Miami Beach, FL, Amer. Meteor. Soc., April 15-18, 1980.

Han, J., M. Kamber, and J. Pei, *Data Mining Concepts and Techniques*, 3rd ed., MA: MK, 703 pp, 2011.

Harris, F. J., "On the use of windows for harmonic analysis with the discrete Fourier transform", *Proc. IEEE*, **66(1)**, 51-83, 1978.

Hildebrand, P. H. and R. S. Sekhon, "Objective determination of noise-level in Doppler spectra," *J. Appl. Meteorol.*, **13(7)**, 808-811, 1974.

Hubbert, J. C., Dixon, M., Ellis, S. M., and Meymaris, G., "Weather radar ground clutter. Part I: Identification, Modeling, and Simulation," *J. Atmos. Oceanic Technol.*, **26**, 1165-1180, 2009a.

Hubbert, J. C., Dixon, M., and Ellis, S. M., "Weather radar ground clutter. Part II: Real-time identification and filtering," *J. Atmos. Oceanic Technol.*, **26**, 1181-1197, 2009b.

Hurtado, M. and A. Nehorai, "Polarimetric detection of targets in heavy inhomogeneous clutter", *IEEE Trans. Signal Process.,* **56(4)**, 1349-1361, 2008.

Ice, R. L., Rhoton, R. D., Krause, J. C., Saxion, D. S., Boydstun, O. E., Heck, A. K., Chrisman, J. N., Berkowitz, D. S., and Zittel, W. D., "Automatic clutter mitigation in the WSR-88D, design, evaluation, and implementation," *34th Conference on Radar Meteorology,* Williamsburg, VA, Amer. Meteor. Soc., Paper 5.3, 2009.

Ivic, I. R., D. S. Zrnic, and T. Y. Yu, "The Use of Coherency to Improve Signal Detection in Dual-Polarization Weather Radars," *J. Atmos. Oceanic Technol.*, **26(11)**, 2474-2487, 2009.

Kay, S. M., *Fundamentals of Statistical Signal Processing: Detection Theory*, Englewood Cliffs, NJ: Prentice Hall, 1993a.

Kay, S. M., *Fundamentals of Statistical Signal Processing: Estimation Theory*, Englewood Cliffs, NJ: Prentice Hall, 1993b.

Kessinger, C., S. Ellis, and J. V. Andel, "The radar echo classifier: A fuzzy logic algorithm for the WSR-88D," *Proc. Third Conf. on Artificial Intelligence Applications to the Environmental Science*, Long Beach, CA, Amer. Meteor. Soc., P 1.6, 2003.

Kharin, W., and F. W. Zwiers, "On the ROC score of probability forecasts", *J. Climate*, **16(24)**, 4145-4150, 2003.

Lee, R., G. Deruna, and J. Joss, "Intensity of ground clutter and of echoes of anomalous propagation and its elimination," *Proc. 27th Conf. Radar Meteorol.,* Vail, CO, Amer. Meteor. Soc., pp. 651-652, 1995.

Li, Y., G. Zhang, R. J. Doviak, Q. Cao, and L. Lei, "A new approach to detect ground clutter mixed with weather signals," *IEEE Trans. Geosci. Remote Sens*., **51(4)**, 2373-2387, 2013a.

Li, Y., G. Zhang, R. J. Doviak, and D. S. Saxion, "Scan-to-scan correlation of weather radar signals to identify ground clutter," *IEEE Geosci. Remote Sens. Letters,* **10(4),** 855-859, 2013b.

Liu, H. and V. Chandrasekar, "Classification of hydrometeors based on polarimetric radar measurements: development of fuzzy logic and neuro-fuzzy systems, and in situ verification," *J. Atmos. Oceanic Technol.*, **17**, 140-164, 2000.

Marshall, J. S. and W. Hitschfeld, "Interpretation of the fluctuating echo from randomly distributed scatterers. 1," *Can. J. Phys*., **31(6)**, 962-994, 1953.

Meischner, M., *Weather Radar Principles and Advanced Applications*, Springer, 337 pp, 2002.

Melnikov, V. M., P. Zhang, D. S. Zrnić, and A. Ryzhkov, (2008). Recombination of super resolution data and ground clutter recognition on the polarimetric WSR-88D. NSSL, Norman, OK. Available at: http://publications.nssl.noaa.gov/wsr88d_reports/Super_Res_and_CLutterRPT2.pdf/

Melnikov, V. M. and R. J. Doviak, "Spectrum widths from echo power differences reveal meteorological features", *J. Atmos. Oceanic Technol.,* **19(11)**, 1793-1810, 2002.

Melnikov, V. M. and D. S. Zrnić, "Autocorrelation and cross-correlation estimators of polarimetric variables," *J. Atmos. Oceanic Technol.*, **24**, 1337-1350, 2007.

NEXRAD Technical Requirements, NEXRAD Joint System Program Office (SPO1), Silver Spring, MD, 1991.

Nguyen, C. M., D. N. Moisseev, and V. Chandrasekar, "A parametric time domain method for spectral moment estimation and clutter mitigation for weather radars," *J. Atmos. Oceanic Technol.,* **25(1)**, 83-92, 2008.

Palmer, R.D., D. Bodine, M. Kumjian, B. Cheong, G. Zhang, Q. Cao, H. B. Bluestein, A. Ryzhkov, T. Y. Yu, and Y. Wang, "Observations of the 10 May 2010

tornado outbreak using OU-PRIME: Potential for new science with high-resolution polarimetric radar," *Bull. Amer. Meteorol. Soc.*, **92(7)**, 871-891, 2011.

Park, H., A. V. Ryzhkov, D. S. Zrnić, and K. E. Kim, "The hydrometeor classification algorithm for the polarimetric WSR-88D: description and application to an MCS," *Weather and Forecasting,* **24(3)**, 730-748, 2009.

Papoulis, A., *Probability, Random Variables, and Stochastic Processes,* Mcgraw Hill College, 666 pp, 1991.

Richards, M. A., *Fundamentals of Radar Signal Processing*, McGraw-Hill, 513pp, 2005.

Rico-Ramirez, M. A. and Cluckie, I. D., "Classification of ground clutter and anomalous propagation using dual-polarization weather radar," *IEEE Trans. Geosci. Remote Sens.*, **46(7)**, 1892-1904, 2008.

Schaefer, J. T., "The critical success index as an indicator of warning skill," *Weather and Forecasting*, **5(4)**, 570-575, 1990.

Schuur, T., A. Ryzhkov, and P. Heinselman, (2003). Observations and Classification of echoes with the polarimetric WSR-88D radar. NSSL, Norman, OK. Available at: http://arrc.ou.edu/~guzhang/Polarimetry/img/class/Schuur2003.pdf

Siggia, A. D. and R. E. Passarelli, "Gaussian model adaptive processing (GMAP) for improved ground clutter cancellation and moment calculation", *Proc. Third European Conf. on Radar in Meteorology and Hydrology*, Visby, Sweden, ERAD, 67-73, 2004.

Skolnik, M. I., *Introduction to Radar Systems*, 3rd ed., McGraw-Hill, 772pp, 2002.

Smith III, J. O., *Mathematics of the Discrete Fourier Transform (DFT): with Audio Applications*, 2nd ed., W3K, 322 pp, 2007.

Steiner, M., and Smith, J. A., "Use of three-dimensional reflectivity structure for automated detection and removal of nonprecipitating echoes in radar data," *J. Atmos. Oceanic Technol.,* vol. 19, no. 5, pp. 673-686, May 2002.

Torres, S., D. Warde, and D. S. Zrnić, (2012). Signal design and processing techniques for WSR-88D ambiguity resolution: part 15, the CLEAN-AP filter. NSSL, Norman, OK. Available at: http://cimms.ou.edu/rvamb/Documents/Report_15.pdf

Taylor, T. T., "Design of circular apertures for narrow beamwidths and low sidelobes," *IRE Trans. Antennas Propag.*, **8**, 17-22, 1960.

Waldteufel, (1976). An analysis of weather spectra variance in a tornadic storm. NOAA Technical Memorandum ERL-NSSL-76.

Warde, D. and S. Torres, "A novel ground-clutter-contamination mitigation solution for the NEXRAD network: the CLEAN-AP filter," Preprints, *26th International Conference on Interactive Information and Processing Systems (IIPS) for Meteorology, Oceanography, and Hydrology*, Atlanta, GA, Amer. Meteor. Soc., Paper 8.6, 2010.

Wang, Y., T. Yu, M. Yeary, A. Shapiro, M. Foster, D. L. Andra Jr., and M. Jain, "Tornado detection using a neuro-fuzzy system to integrate shear and spectral signatures," *J. Atmos. Oceanic Technol.,* **25(7)**, 1136-1148, 2008.

Yu, T., M. B. Orescanin, C. D. Curtis, D. S. Zrnić, and D. E. Forsyth, "Beam multiplexing using the phased-array weather radar", *J. Atmos. Oceanic Technol.,* **24(4)**, 616-626, 2007.

Zhang, G., Li, Y., Doviak, R. J., Priegnitz, D., Carter J., and Curtis, C. D., "Multipatterns of the National Weather Radar Testbed mitigate clutter received via sidelobes," *J. Atmos. Oceanic Technol.*, **28(3)**, 401-409, 2011.

Zrnic, D. S., "Simulation of weatherlike Doppler spectra and signals," *J. Appl. Meteorol.*, **14(4)**, 619-620, 1975.